

BLEJSKE DELAVNICE IZ FIZIKE

BLED WORKSHOPS IN PHYSICS

LETNIK 20, ŠT. 1

VOL. 20, NO. 1

ISSN 1580-4992

Proceedings of the Mini-Workshop
**Electroweak Processes
of Hadrons**

Bled, Slovenia, July 15–19, 2019

Edited by

Bojan Golli

Mitja Rosina

Simon Širca

University of Ljubljana and Jožef Stefan Institute

DMFA – ZALOŽNIŠTVO
LJUBLJANA, NOVEMBER 2019

The Mini-Workshop *Electroweak Processes of Hadrons*

was organized by

*Society of Mathematicians, Physicists and Astronomers of Slovenia
Department of Physics, Faculty of Mathematics and Physics, University of Ljubljana*

and sponsored by

*Department of Physics, Faculty of Mathematics and Physics, University of Ljubljana
Jožef Stefan Institute, Ljubljana
Society of Mathematicians, Physicists and Astronomers of Slovenia
Partially Supported by University of Graz*

Organizing Committee

Mitja Rosina, Bojan Golli, Simon Širca

List of participants

*Roelof Bijker, Ciudad de México, bijker@nucleares.unam.mx
Marko Bračko, Ljubljana, marko.bracko@ijs.si
Gernot Eichmann, Lisbon, gernot.eichmann@tecnico.ulisboa.pt
Harald Fritzschn, Munich, fritzch@mpp.mpg.de
Bojan Golli, Ljubljana, bojan.golli@ijs.si
Marek Karliner, Tel Aviv, marek@tauex.tau.ac.il
Hyun-Chul Kim, Incheon, South Korea, hchkim@inha.ac.kr
June-Young Kim, Incheon, South Korea, juneyoung.ghim@gmail.com
Raquel Molina Peralta, Madrid, raquemoli@ucm.es
Willi Plessas, Graz, williballd.plessas@uni-graz.at
Saša Prelovšek, Ljubljana, sasa.prelovsek@ijs.si
Mitja Rosina, Ljubljana, mitja.rosina@ijs.si
Jonathan Rosner, Chicago, rosner@hep.uchicago.edu
Helios Sanchis Alepuz, Graz, helios.sanchis-alepuz@uni-graz.at
Jugoslav Stahov, Tuzla, jugoslav.stahov@untz.ba
Finn Stokes, Jülich, f.stokes@fz-juelich.de
Simon Širca, Ljubljana, simon.sirca@fmf.uni-lj.si
Herbert Weigel, Stellenbosch, South Africa, weigel@sun.ac.za*

Electronic edition (in colour)

<http://www-fl.ijs.si/BledPub/>

The presentations can be found at
<http://www-fl.ijs.si/Bled2019/Program.html>

The articles are peer reviewed by the Editorial Board

Contents

| | |
|--|-----|
| Preface | V |
| Predgovor | VII |
| Photocouplings of pentaquark states | |
| <i>Roelof Bijker and Emmanuel Ortiz-Pacheco</i> | 1 |
| Resonances and contour deformations | |
| <i>Gernot Eichmann</i> | 5 |
| Flavor Mixing, Neutrino Oscillations and Neutrino Masses | |
| <i>Harald Fritzsch</i> | 9 |
| Hidden Charm Molecular Pentaquarks: Some Open Questions | |
| <i>Marek Karliner</i> | 15 |
| A unified approach for the structure of light and heavy baryons | |
| <i>Hyun-Chul Kim</i> | 21 |
| Improved pion mean fields | |
| <i>June-Young Kim, Hyun-Chul Kim</i> | 25 |
| Light- and strange-quark mass dependence of the $\rho(770)$ meson properties | |
| <i>R. Molina, J. Ruiz de Elvira</i> | 29 |
| Electromagnetic Form Factors of the Nucleons, the Δ, and the Hyperons | |
| <i>W. Plessas</i> | 43 |
| Heavy-Quark Exotics | |
| <i>Jonathan L. Rosner</i> | 48 |
| Effect of intermediate resonances in the quark-photon vertex | |
| <i>Hèlios Sanchis-Alepuz</i> | 57 |

| | |
|--|-----|
| Partial Wave Analysis of Pion Photoproduction Data with Fixed-t Analyticity Imposed | |
| <i>J. Stahov, H. Osmanović, M. Hadžimehmedović, R. Omerović</i> | 63 |
| Structure and transitions of nucleon excitations from lattice QCD | |
| <i>Finn M. Stokes, Waseem Kamleh, Derek B. Leinweber</i> | 68 |
| Exotic Baryons in Skyrme Type Models | |
| <i>H. Weigel</i> | 75 |
| News from Belle on Hadron Spectroscopy | |
| <i>M. Bračko</i> | 80 |
| The enigmatic $\Delta(1600)$ resonance | |
| <i>B. Golli</i> | 85 |
| A phenomenological lower bound for the Ξ_{cc}^{++} mass | |
| <i>Mitja Rosina</i> | 89 |
| Measurement of G_A and the GDH sum rule at high energies at Jefferson Lab: two proposals | |
| <i>S. Širca</i> | 93 |
| Povzetki v slovenščini | 103 |

Preface

At the beautiful Lake Bled, the tradition of hadronic Mini-Workshops with their lively discussions continues. We are happy to greet our regular participants, as well as to attract new devotees. At every new meeting we witness upgrades of previously discussed topics and seed new ones.

Electroweak form-factors are a perennial repertory on our stage, and we have heard of new proposals to accurately measure the nucleon electromagnetic and axial form factors. The covariant relativistic approach in the constituent quark model that was so successful for the nucleons has been extended Δ , Λ Σ and Ω baryons. Its success is based on including the essential degrees of freedom and respecting the relevant symmetries. Good fits are typically achieved without resorting to five-quark admixtures, and there seems to be no evidence for diquark clustering.

The ideas of the chiral quark-soliton model with mesonic mean fields have also been extended to calculate the spectra and the structure of heavy baryons. Strong mixing effects are expected in the case of light baryons belonging to different $SU(3)$ flavour representations.

Both static and dynamic electromagnetic properties test our models and understanding of new phenomena. Electro- and photo-excitation has always been a favourite topic at Bled, and it was no different this time around: through these processes one explores not only the photoproduction of pions and light baryon resonances, but also exotic hadrons such as pentaquarks. The advances in analytic methods for resonances have clarified some open questions about nucleon resonances, such as the Roper $N(1440)$ and $\Delta(1600)$.

This year's "champions" were the recently discovered double-heavy baryons. They pave the way to potentially rich spectra and to double-heavy exotics. We discussed phenomenological methods for the calculation of double-heavy baryons, tetraquarks and "molecules" such as dimesons $D\bar{D}$, DD^* and pentaquarks. There is evidence that the heavy quarks stabilize such molecules.

Lattice QCD simulations, apart from being a bleeding-edge approach by itself, continue to be a most welcome supplement to quark model calculations. The examples discussed at the Workshop were the Z_b tetraquarks, the ρ meson decay parameters, and the parity expanding technique for extractions of the elastic and transition form factors involving the nucleon ground state and its excitations.

Quark and lepton flavour mixing angles and neutrino masses, are always a "hit" suitable to animate a meeting. It is interesting to see how the assumption of four vanishing matrix elements in the mass matrix can give realistic relations between masses and mixing angles.

Predgovor

Ob prelepem Blejskem jezeru se nadaljuje tradicija hadronskih Mini-delavnic z značilnimi živahnimi diskusijami. Z veseljem pozdravljamo stalne udeležence in pritegujemo nove navdušence. Na vsakem novem srečanju smo priča nadgradnji prejšnjih tem in sejemo semena novih.

Elektrošibki oblikovni faktorji na našem odru sodijo že v dolgoletni repertoar, letos pa smo slišali tudi nove predloge, kako natančneje meriti elektromagnetne in aksialne oblikovne faktorje nukleona. Kovariantni relativistični pristop pri modelu s konstituentnimi kvarki, ki se je tako dobro izkazal za nukleon, so razširili še na barione Δ , Λ , Σ in Ω . Uspeh pristopa sloni na upoštevanju bistvenih prostostnih stopenj in spoštovanju pomembnih simetrij. Dobro ujemanje so značilno dosegli brez petkvarkovskih primesi; zdi se tudi, da ni evidence za dvokvarkovske gruče v omenjenih barionih.

Zamisli kiralnega solitonskega modela s kvarki v povprečnem mezonskem polju so razširili tudi na račune spektrov in zgradbe težkih barionov. Pričakujejo pa se znatni učinki mešanja pri lahkih barionih, ki pripadajo različnim upodobitvam grupe $SU(3)$ za okuse.

Tako statične kot dinamične elektromagnetne lastnosti preverjajo naše modele in razumevanje novih pojavov. Elektronsko in fotonsko vzbujanje sta bila vedno priljubljena tema na Bledu in tudi to pot ni bilo nič drugače: s temi procesi ne raziskujemo zgolj fotoprodukcije pionov in lahkih barionskih resonanc, temveč tudi eksotične hadrone, na primer pentakvarke. Napredek pri analitičnih metodah za resonance pa je pojasnil nekatera odprta vprašanja o nukleonskih resonancah, kot so Roperjeva, $N(1440)$, in $\Delta(1600)$.

Letošnji "junaki" so bili nedavno odkriti dvojno težki barioni. Utirajo pot morda bogatim spektrom in dvojno težkim eksotičnim hadronom. Razpravljali smo o fenomenoloških metodah za računanje dvojno težkih barionov, tetrakvarkov in "molekul", kot so dimezoni $D\bar{D}$, DD^* in pentakvarki. Izkušnje podpirajo zamisel, da težki kvarki stabilizirajo takšne molekule.

Simulacije s kromodinamiko na mreži, ki so avantgarda same po sebi, so dobrodošlo dopolnilo tudi za račune s kvarkovimi modeli. Razpravljali smo o zgleidih, kot so tetrakvark Z_b , razpadni parametri mezona ρ in metoda za razvoj po parnostih za elastične in prehodne oblikovne faktorje osnovnega in vzbujenih stanj nukleona.

Mešalni koti za okuse pri kvarkih in leptonih ter mase nevtrinov so "poživilo" prenekaterega srečanja. Zanimivo je bilo videti, kako predpostavka o štirih ničelnih matričnih elementih v masni matriki vodi do realističnih povezav med masami in mešalnimi koti.

Workshops organized at Bled

▷ *What Comes beyond the Standard Model*

- | | |
|---|---|
| (June 29–July 9, 1998), Vol. 0 (1999) No. 1 | (July 15–25, 2008), Vol. 9 (2008) No. 2 |
| (July 22–31, 1999) | (July 14–24, 2009), Vol. 10 (2009) No. 2 |
| (July 17–31, 2000) | (July 12–22, 2010), Vol. 11 (2010) No. 2 |
| (July 16–28, 2001), Vol. 2 (2001) No. 2 | (July 11–21, 2011), Vol. 12 (2011) No. 2 |
| (July 14–25, 2002), Vol. 3 (2002) No. 4 | (July 9–19, 2012), Vol. 13 (2012) No. 2 |
| (July 18–28, 2003), Vol. 4 (2003) Nos. 2-3 | (July 14–21, 2013), Vol. 14 (2013) No. 2 |
| (July 19–31, 2004), Vol. 5 (2004) No. 2 | (July 20–28, 2014), Vol. 15 (2014) No. 2 |
| (July 19–29, 2005), Vol. 6 (2005) No. 2 | (July 11–20, 2015), Vol. 16 (2015) No. 2 |
| (September 16–26, 2006), Vol. 7 (2006) No. 2 | (July 11–19, 2016), Vol. 17 (2016) No. 2 |
| (July 17–27, 2007), Vol. 8 (2007) No. 2 | (July 10–18, 2017), Vol. 18 (2017) No. 2 |
| | (June 23–30, 2018), Vol. 19 (2018) No. 2 |
| | (July 6–14, 2019), Vol. 20 (2019) No. 2 |

▷ *Hadrons as Solitons* (July 6–17, 1999)

- ▷ *Few-Quark Problems* (July 8–15, 2000), Vol. **1** (2000) No. 1
- ▷ *Statistical Mechanics of Complex Systems* (August 27–September 2, 2000)
- ▷ *Selected Few-Body Problems in Hadronic and Atomic Physics* (July 7–14, 2001), Vol. **2** (2001) No. 1
- ▷ *Studies of Elementary Steps of Radical Reactions in Atmospheric Chemistry* (August 25–28, 2001)
- ▷ *Quarks and Hadrons* (July 6–13, 2002), Vol. **3** (2002) No. 3
- ▷ *Effective Quark-Quark Interaction* (July 7–14, 2003), Vol. **4** (2003) No. 1
- ▷ *Quark Dynamics* (July 12–19, 2004), Vol. **5** (2004) No. 1
- ▷ *Exciting Hadrons* (July 11–18, 2005), Vol. **6** (2005) No. 1
- ▷ *Progress in Quark Models* (July 10–17, 2006), Vol. **7** (2006) No. 1
- ▷ *Hadron Structure and Lattice QCD* (July 9–16, 2007), Vol. **8** (2007) No. 1
- ▷ *Few-Quark States and the Continuum* (September 15–22, 2008), Vol. **9** (2008) No. 1
- ▷ *Problems in Multi-Quark States* (June 29–July 6, 2009), Vol. **10** (2009) No. 1
- ▷ *Dressing Hadrons* (July 4–11, 2010), Vol. **11** (2010) No. 1
- ▷ *Understanding hadronic spectra* (July 3–10, 2011), Vol. **12** (2011) No. 1
- ▷ *Hadronic Resonances* (July 1–8, 2012), Vol. **13** (2012) No. 1
- ▷ *Looking into Hadrons* (July 7–14, 2013), Vol. **14** (2013) No. 1
- ▷ *Quark Masses and Hadron Spectra* (July 6–13, 2014), Vol. **15** (2014) No. 1
- ▷ *Exploring Hadron Resonances* (July 5–11, 2015), Vol. **16** (2015) No. 1
- ▷ *Quarks, Hadrons, Matter* (July 3–10, 2016), Vol. **17** (2016) No. 1
- ▷ *Advances in Hadronic Resonances* (July 2–9, 2017), Vol. **18** (2017) No. 1
- ▷ *Double-charm baryons and dimesons* (June 17–23, 2018), Vol. **19** (2018) No. 1
- ▷ *Electroweak Processes of Hadrons* (July 15–19, 2019), Vol. **20** (2019) No. 1





Photocouplings of pentaquark states^{*}

Roelof Bijker and Emmanuel Ortiz-Pacheco

Instituto de Ciencias Nucleares, Universidad Nacional Autónoma de México, A.P. 70-543,
04510 Ciudad de México, México

Abstract. In this contribution, we discuss the electromagnetic couplings of pentaquark states with hidden charm. This work is motivated by recent experiments at CERN by the LHCb Collaboraton and current experiments at JLab to confirm the existence of hidden-charm pentaquarks in photoproduction experiments.

1 Introduction

The observation of possible hidden-charm pentaquark states by the LHCb Collaboration [1,2] has led to an enormous amount of theoretical studies on the nature of these states and on different possible interpretations of the observed signals, *e.g.* kinematical effects, molecular states, compact pentaquarks, meson-baryon states coupled to a five-quark compact core [3]-[8] and baryo-quarkonium states [9]. In addition, new experiments were suggested at JLab to confirm the existence of hidden-charm pentaquarks in photoproduction experiments [10]-[15].

In the present contribution we discuss the electromagnetic couplings of $uudc\bar{c}$ hidden-charm pentaquark states which are relevant for the photoproduction experiments at JLab.

2 Pentaquark states

Pentaquark states depend both on the orbital degrees of freedom and the internal degrees of freedom of color, spin and flavor

$$\psi = \psi^o \psi^c \phi^f \chi^s . \quad (1)$$

The construction of the classification scheme of $uudc\bar{c}$ pentaquark states was carried out explicitly in Ref. [16] using the following two conditions: (i) the pentaquark wave function should be a color singlet and (ii) the wave function of the four-quark subsystem should be antisymmetric. The permutation symmetry of four-quark states can be characterized by the S_4 Young tableaux [4], [31], [22], [211] and [1111] or, equivalently, by the irreducible representations of the tetrahedral group \mathcal{T}_d (which is isomorphic to S_4) as A_1 , F_2 , E , F_1 and A_2 , respectively.

^{*} Talk presented by Roelof Bijker

The first condition that the pentaquark wave function has to be a color-singlet, implies that the color wave function of the four-quark configuration has to be a [211] triplet with F_1 symmetry under \mathcal{T}_d . As a consequence, the second condition that the total q^4 wave function has to be antisymmetric (A_2), means that the orbital-spin-flavor part is a [31] triplet with F_2 symmetry

$$\psi = \left[\psi_{F_1}^c \times \psi_{F_2}^{\text{osf}} \right]_{A_2}, \quad (2)$$

where the subindices refer to the symmetry properties of the four-quark subsystem under permutation. In this contribution we discuss ground-state pentaquark states, *i.e.* without orbital excitations, which means that the orbital part of the pentaquark wave functions is symmetric (A_1). Therefore, the spin-flavor part is a [31] state with F_2 symmetry

$$\psi = \psi_{A_1}^o \left[\psi_{F_1}^c \times \psi_{F_2}^{\text{sf}} \right]_{A_2}. \quad (3)$$

In Ref. [16] it was shown that there are in total seven $uudc\bar{c}$ ground-state pentaquark configurations with angular momentum and parity $J^P = 3/2^-$ (which is quoted in the literature as the most likely value of the angular momentum and parity of the P_c pentaquark [1]), three of which belong to a flavor decuplet and the remaining four to a flavor octet (see Fig. 1 and first column of Table 1).

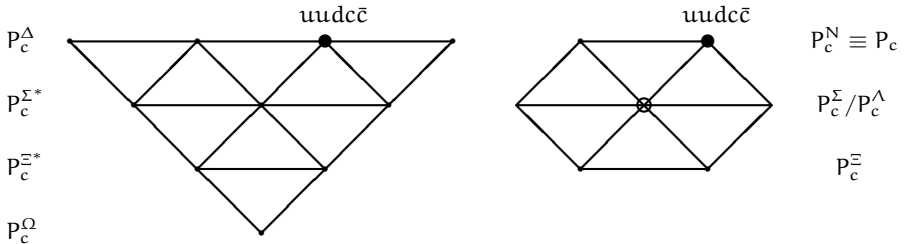


Fig. 1. Pentaquark decuplet and octet

3 Electromagnetic couplings

For experiments that aim to study pentaquarks through near threshold J/ψ photoproduction at JLab, the size of the electromagnetic couplings of the pentaquarks is important. Here we discuss the electromagnetic couplings for the ground state pentaquarks with spin and parity $J^P = 3/2^-$. For the process of interest, $P_c \rightarrow N + \gamma$, the relevant contribution is the annihilation of a pair of $c\bar{c}$ quarks (see Fig. 2). In the present calculation we use the nonrelativistic form of the interaction. The radiative decay widths can be calculated as

$$\Gamma(P_c \rightarrow N + \gamma) = \frac{\rho}{(2\pi)^2} \frac{2}{2J+1} \sum_{\nu>0} |A_\nu(k)|^2, \quad (4)$$

where ρ is the phase space factor, and A_ν denotes the helicity amplitude

$$A_\nu(\mathbf{k}) = \langle N, 1/2^+, \nu - 1; \gamma | \mathcal{H}_{\text{em}}^{\text{nr}} | P_c, 3/2^-, \nu \rangle = \sqrt{\frac{4\pi\alpha}{k_0}} \beta_\nu F(\mathbf{k}). \quad (5)$$

Here α is the fine-structure constant, and k_0 and $k = |\mathbf{k}|$ represent the energy and the momentum of the photon. The coefficient β_ν is the contribution from the color-spin-flavor part for the annihilation of a $c\bar{c}$ color-singlet pair with spin $S = S_z = 1$. The color-spin-flavor part is common to all quark models. In Table 1 we show the results for the contribution from the color-spin-flavor part to the helicity amplitudes for different configurations of $uudc\bar{c}$ pentaquarks [16]. Out of a total of seven $uudd\bar{c}$ ground-state pentaquark configurations only three have nonvanishing photocouplings, all corresponding to octet pentaquarks. The strongest coupling is to the octet pentaquark configuration with ϕ_{F_1} , followed by ϕ_E and ϕ_{F_2} .

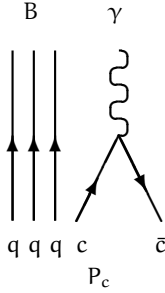


Fig. 2. Electromagnetic decay of pentaquark P_c into a baryon B and a photon, $P_c \rightarrow B + \gamma$.

Since the photon momentum for the photocouplings $P_c \rightarrow N + \gamma$ is large (of the order of $k \sim 2.1$ GeV), one expects a large suppression due to the form factor $F(k)$ which denotes the contribution from the orbital part of the pentaquark wave function. Although its specific form depends on the type of quark model used: harmonic oscillator, hypercentral, or other, for this value of the photon momentum the effect is large resulting in a very small photocoupling. The first measurement of the J/ψ exclusive photoproduction cross section by the GlueX Collaboration saw no evidence for the LHCb pentaquark candidates P_c [17].

4 Summary and conclusions

In conclusion, in this contribution we discussed the electromagnetic couplings of ground-state $uudc\bar{c}$ pentaquark states with angular momentum and parity $J^P = 3/2^-$. It was shown that only three pentaquark configurations, all belonging to a flavor octet, have a nonvanishing photocoupling. Since the photon momentum is large, we expect that these couplings are strongly suppressed by the form factor, $F(k)$, representing the contribution from the orbital part of the pentaquark wave function. This seems to be confirmed in recent photoproduction

Table 1. Contribution from the color-spin-flavor part to the helicity amplitudes for the electromagnetic decays of $uudc\bar{c}$ decuplet (top) and octet (bottom) pentaquark states into $N + \gamma$ [16]. Here e_c is the electric charge of the charm quark $e_c = 2/3$.

| State | Name | $\beta_{1/2}$ | $\beta_{3/2}$ |
|--|--------------|---------------------------|---------------------------|
| $[\phi_{A_1} \times \chi_{F_2}]_{F_2}$ | P_c^Δ | 0 | 0 |
| $[\phi_{F_2} \times \chi_{A_1}]_{F_2}$ | P_c^Δ | 0 | 0 |
| $[\phi_{F_2} \times \chi_{F_2}]_{F_2}$ | P_c^Δ | 0 | 0 |
| $[\phi_{F_2} \times \chi_{A_1}]_{F_2}$ | P_c^N | 0 | 0 |
| $[\phi_{F_2} \times \chi_{F_2}]_{F_2}$ | P_c^N | $\frac{1}{6\sqrt{2}}e_c$ | $\frac{1}{2\sqrt{6}}e_c$ |
| $[\phi_E \times \chi_{F_2}]_{F_2}$ | P_c^N | $-\frac{1}{6}e_c$ | $-\frac{1}{2\sqrt{3}}e_c$ |
| $[\phi_{F_1} \times \chi_{F_2}]_{F_2}$ | P_c^N | $-\frac{1}{2\sqrt{6}}e_c$ | $-\frac{1}{2\sqrt{2}}e_c$ |

experiments by the GlueX Collaboration in which no evidence was found for the P_c pentaquarks. It is important to emphasize that this null result does not rule out an interpretation of the LHCb signals in terms of pentaquarks.

Acknowledgements

This work was supported in part by grant IN109017 from DGAPA-UNAM, Mexico and grants 251817 and 340629 from CONACyT, Mexico.

References

1. Aaij R *et al.* (LHCb Collaboration) 2015 *Phys. Rev. Lett.* **115** 072001
2. Aaij R *et al.* (LHCb Collaboration) 2019 *Phys. Rev. Lett.* in press [arXiv:1904.03947]
3. Chen H X, Chen W, Liu X and Zhu S L 2016 *Phys. Rep.* **639** 1
4. Esposito A, Pilloni A and Polosa A D 2016 *Phys. Rep.* **668** 1
5. Ali A, Lange J S and Stone S 2018 *Prog. Part. Nucl. Phys.* **97** 123
6. Olsen S L, Skwarnicki T and Zieminska D 2018 *Rev. Mod. Phys.* **90** 015003
7. Karliner M, Rosner J L and Skwarnicki T 2018 *Ann. Rev. Nucl. Part. Sci.* **68** 17
8. Guo F-K, Hanhart C, Meißner U-G, Wang Q, Zhao Q and Zou B-S 2018 *Rev. Mod. Phys.* **90** 015004
9. Ferretti J, Santopinto E, Naeem Anwar M and Bedolla M A 2019 *Phys. Lett. B* **789** 562
10. Kubarovsky V and Voloshin M B 2015 *Phys. Rev. D* **92** 031502(R)
11. Wang Q, Liu X H and Zhao Q 2015 *Phys. Rev. D* **92** 034022
12. Karliner M and Rosner J L 2016 *Phys. Lett. B* **752** 329
13. Hiller Blin A N, Fernández-Ramírez C, Jackura A, Mathieu V, Mokeev V I, Pilloni A and Szczepaniak A P 2016 *Phys. Rev. D* **94** 034002
14. Fernández-Ramírez C, Hiller Blin A N and Pilloni A 2017 *J Phys Conf Ser* **876** 012007
15. Meziani Z E *et al.* 2016 *arXiv:1609.00676*
16. Ortiz-Pacheco E, Bijker R and Fernández-Ramírez C 2019 *J. Phys. G: Nucl. Part. Phys.* **46** 065104 [arXiv:1808.10512]
17. Ali A *et al.* (GlueX Collaboration) 2019 *Phys Rev Lett* **123** 072001



Resonances and contour deformations

Gernot Eichmann

CFTP, Instituto Superior Técnico, Universidade de Lisboa, 1049-001 Lisboa, Portugal

Abstract. We exemplify the extraction of resonance properties from Lorentz-invariant integral equations. To this end we solve the Bethe-Salpeter and scattering equations for a scalar model and determine the resonance pole locations and phase shifts. It turns out that the scalar model does not produce resonance poles in the complex plane but instead virtual states on the real axis of the second Riemann sheet.

Understanding the properties of resonances is a central task in nonperturbative QCD studies. Most of the ‘bound states’ in QCD are actually resonances which decay and thus correspond to poles in the complex momentum plane of scattering amplitudes. In the following we focus on the extraction of resonances from Lorentz-invariant integral equations, which is motivated by calculations of hadron spectra and matrix elements in the functional approach of Dyson-Schwinger equations (DSEs) and Bethe-Salpeter equations (BSEs), see e.g. [1–3] and references therein. These calculations typically use a Euclidean metric, and even though a ‘naive’ Euclidean integration path allows one to calculate non-perturbative propagators, vertices and Bethe-Salpeter amplitudes in the complex momentum plane, one is typically limited by the nearest singularities appearing in the integrands. As a consequence, the calculations are restricted to low-lying meson and baryon excitations, states below thresholds, and form factors within a certain Q^2 range. As discussed below, in principle these obstacles can be overcome by employing contour deformations [4–12]. Another motivation for our work is to build a bridge toward similar calculations using a Minkowski metric, see e.g. [13–17].

We exemplify the situation for a scalar theory consisting of two scalar fields with masses m and μ and a three-point interaction. This leaves two parameters, namely a dimensionless coupling constant $c = g^2/(4\pi m)^2$ and the mass ratio $\beta = \mu/m$. The relevant equations are shown in Fig. 1: The first is the homogeneous BSE, which determines the mass spectrum and BS amplitude in a given J^{PC} channel; the second is the inhomogeneous BSE which determines the corresponding vertex function; and the third is the scattering equation which determines the scattering amplitude. For simplicity we work with tree-level propagators and restrict the kernel to a scalar ladder exchange with mass μ , which is the massive Wick-Cutkosky model [18–20]. For details on the setup and solution techniques we refer to Ref. [12]; in particular, we use a Euclidean metric and do not employ further approximations such as three-dimensional reductions but instead solve the full Lorentz-invariant integral equations in four dimensions.

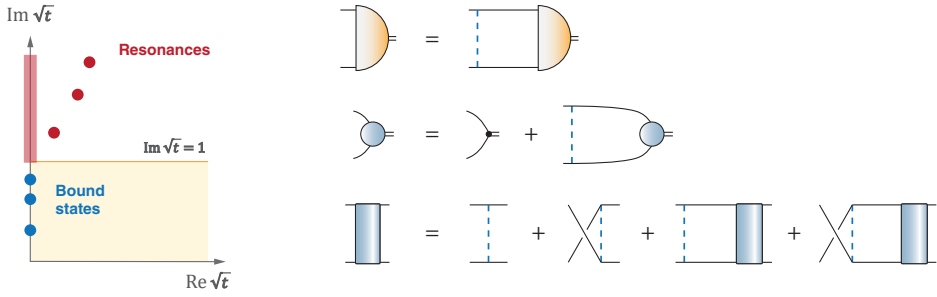


Fig. 1. *Left:* singularity structure in the complex \sqrt{t} plane. *Right:* homogenous BSE, inhomogeneous BSE and scattering equation.

The left panel in Fig. 1 shows the typical singularity structure in the complex plane of the variable \sqrt{t} , where $t = P^2/(4m^2)$ is the total momentum squared in Euclidean conventions (i.e., positive t means spacelike and negative t timelike). Below the threshold $\text{Im}\sqrt{t} = 1$ there can be bound states on the imaginary \sqrt{t} axis, whose locations depend on the parameters c and β . The two-particle cut starts at the threshold and extends to infinity, and above the threshold one would expect resonances on the second Riemann sheet, with complex masses M_i corresponding to $\text{Im}\sqrt{t} = \text{Re}M_i/(2m)$.

Let us investigate the trajectory of the ground-state pole depending on the coupling c . A stronger coupling entails stronger binding, so that by increasing c the pole will slide down on the imaginary axis. Below a certain coupling strength the pole (presumably) moves above the threshold and becomes a resonance, whereas above a certain strength it becomes tachyonic and continues its trajectory on the real \sqrt{t} axis. In our context, the latter case is mainly a truncation artifact: since the internal propagators remain at tree level, they do not depend on c which can be tuned freely; hence there is always a critical strength above which the state becomes tachyonic. This is most clearly seen from the eigenvalues of the homogeneous BSE, cf. Fig. 10 in Ref. [12]. As a consequence, the ground state is bound only within a certain window of the parameter c . If one increases the coupling further, eventually the first excited state becomes bound and follows a similar trajectory, followed by the second excited state and so on. These properties readily follow from solving the homogeneous BSE for real values of $t > -1$. The question is therefore: What is the nature of a state *before* it becomes bound, i.e., for small couplings?

To answer it, one has to overcome several technical difficulties. Solving the BSE for complex values of \sqrt{t} is only straightforward as long as $\text{Im}\sqrt{t} < 1$, which is the colored region in Fig. 1. To access the first sheet *above* the threshold, however, one must employ contour deformations: After integrating over the inner integration variable, the poles in the integrand from the constituent and exchange propagators become cuts and one has to deform the integration path in the outer integration variable to avoid those cuts. A contour deformation in the Euclidean metric is equivalent to picking up the correct poles in a Minkowski treatment, which is colloquially referred to as ‘going to Minkowski space’. With contour

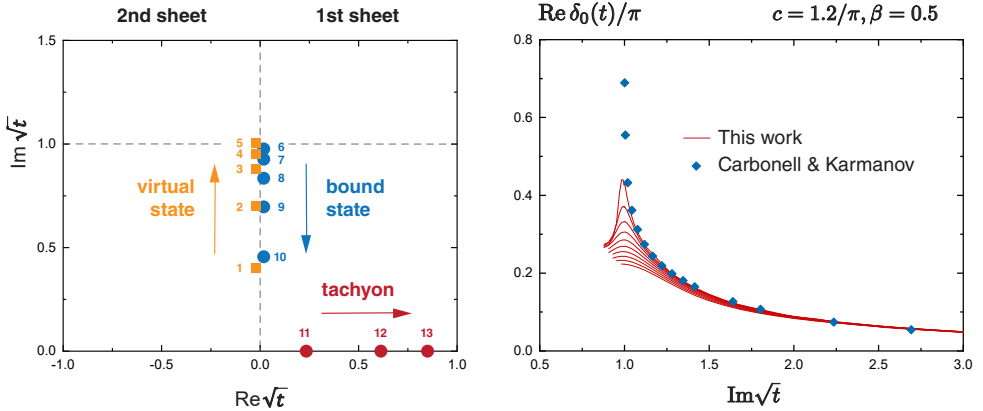


Fig. 2. *Left:* Ground-state pole trajectory for $\beta = 4$ as a function of the coupling [12]. *Right:* Phase shift of the leading partial wave compared to Ref. [16].

deformations, the homogeneous BSE can be solved in the entire first sheet of the complex \sqrt{t} plane [12].

The homogeneous BSE contains the full resonance information. However, extracting the resonance locations requires access to the second sheet, which is not directly possible from numerical solutions of the (in-)homogeneous BSEs and relies on analytic continuation methods such as the Schlessinger-point or Resonances-via-Padé method [21–23]. The strategy is then to solve the BSE on the first sheet (below and above the threshold) and determine the singularity structure on the second sheet by analytic continuation. Examples and results for the scalar model can be found in Ref. [12].

Another option, which does not require analytic continuation and provides direct access to the second sheet, is to solve the scattering equation for the four-point function at the bottom of Fig. 1. From the scattering equation one derives the two-body unitarity relation, which yields a self-consistent relation between the amplitudes on the first and second sheet. In other words, when solving the scattering equation the information on the second sheet, including the singularity structure of the amplitude, comes for free. In turn, one has to deal with more complicated contour deformations and first solve the half-offshell scattering equation, from where the onshell scattering amplitude, where all four external legs are on their mass shells, is extracted afterwards [12].

The left panel in Fig. 2 shows the resulting ground-state pole trajectory in the complex \sqrt{t} plane determined from the scattering equation. It turns out that the model does not produce resonances but instead virtual states on the imaginary \sqrt{t} axis (or negative t axis) of the second sheet. If one increases the coupling c starting at $c = 0$, the pole moves up to the threshold until it turns over to the first sheet, where the state becomes bound. When increasing the coupling further, the pole slides down on the first sheet until it eventually becomes tachyonic. The same pattern is repeated for excited states.

The contour-deformation technique also allows one to extract phase shifts, which are related to the partial-wave amplitudes at $\text{Re}\sqrt{t} = 0$ and $\text{Im}\sqrt{t} > 1$

in a partial-wave expansion of the onshell scattering amplitude. The right panel in Fig. 2 shows the resulting phase shift for the leading partial wave. We cannot extract the phase shifts directly *on* the imaginary axis because here the deformed contour lies along a cut; instead we calculate it along lines in the complex \sqrt{t} plane with $\text{Re}\sqrt{t}$ fixed and approaching the imaginary axis. The results are compared to those in Ref. [16], where the authors employed a Minkowski-space approach to determine the phase shift for the same parameter set in the scalar model. Although moving closer to the axis requires increasingly better numerics, there is satisfactory agreement between the two approaches.

In summary, contour deformations provide a practical toolkit for treating resonances with integral equations. The formalism can be taken over without changes to systems with spin, such as $N\pi$ or NN scattering. Moreover, contour deformations are generally applicable for circumventing singularities in integrals and integral equations — e.g. in QCD, where the singularities of the quark propagator and other Green functions usually prohibit access to highly excited states, timelike form factors or form factors at large Q^2 .

Acknowledgments: I would like to thank my collaborators Pedro Duarte, Teresa Peña and Alfred Stadler, and I am grateful to the organizers of the Bled 2019 Workshop for an enjoyable stay. This work was funded by the FCT Investigator Grant IF/00898/2015.

References

1. I. C. Cloet and C. D. Roberts, *Prog. Part. Nucl. Phys.* **77** (2014) 1–69
2. G. Eichmann, H. Sanchis-Alepuz, R. Williams, R. Alkofer, and C. S. Fischer, *Prog. Part. Nucl. Phys.* **91** (2016) 1–100
3. H. Sanchis-Alepuz and R. Williams, *Comput. Phys. Commun.* **232** (2018) 1–21
4. P. Maris, *Phys. Rev.* **D52** (1995) 6087–6097
5. S. Strauss, C. S. Fischer, and C. Kellermann, *Phys. Rev. Lett.* **109** (2012) 252001
6. A. Windisch, R. Alkofer, G. Haase, and M. Liebmann, *Comput. Phys. Commun.* **184** (2013) 109–116
7. A. Windisch, M. Q. Huber, and R. Alkofer, *Phys. Rev.* **D87** (2013) no. 6, 065005
8. J. M. Pawłowski, N. Strodthoff, and N. Wink, *Phys. Rev.* **D98** (2018) no. 7, 074008
9. R. Williams, *Phys. Lett.* **B798** (2019) 276–280
10. A. S. Miramontes and H. Sanchis-Alepuz, 1906.06227 [hep-ph]
11. E. Weil, G. Eichmann, C. S. Fischer, and R. Williams, *Phys. Rev.* **D96** (2017) no. 1, 014021
12. G. Eichmann, P. Duarte, M. T. Peña, and A. Stadler, 1907.05402 [hep-ph]
13. K. Kusaka and A. G. Williams, *Phys. Rev.* **D51** (1995) 7026–7039
14. V. Sauli and J. Adam, Jr., *Phys. Rev.* **D67** (2003) 085007
15. T. Frederico, G. Salmè, and M. Viviani, *Phys. Rev.* **D89** (2014) 016010
16. J. Carbonell and V. A. Karmanov, *Phys. Rev.* **D90** (2014) no. 5, 056002
17. S. Leitão, Y. Li, P. Maris, M. T. Peña, A. Stadler, J. P. Vary, and E. P. Biernat, *Eur. Phys. J.* **C77** (2017) no. 10, 696
18. G. C. Wick, *Phys. Rev.* **96** (1954) 1124–1134
19. R. E. Cutkosky, *Phys. Rev.* **96** (1954) 1135–1141
20. N. Nakanishi, *Prog. Theor. Phys. Suppl.* **43** (1969) 1–81
21. L. Schlessinger, *Phys. Rev.* **167** (1968) 1411
22. I. Haritan and N. Moiseyev, *J. Chem. Phys.* **147** (2017) 014101
23. R.-A. Tripolt, I. Haritan, J. Wambach, and N. Moiseyev, *Phys. Lett.* **B774** (2017) 411–416



Flavor Mixing, Neutrino Oscillations and Neutrino Masses

Harald Fritzsch

Department für Physik, Universität München, Theresienstraße 37, D-80333 München, Germany

Abstract. We discuss mass matrices with four texture zeros for the quarks and leptons. The three flavor mixing angles for the quarks are functions of the quark masses and can be calculated. The results agree with the experimental data. The texture zero mass matrices for the leptons and the see-saw mechanism are used to calculate the matrix elements of the lepton mixing matrix as functions of the lepton masses. The neutrino masses are calculated: $m_1 \approx 1.4$ meV, $m_2 \approx 9$ meV, $m_3 \approx 51$ meV. The neutrinoless double beta decay is discussed. The effective Majorana neutrino mass, describing the double beta decay, can be calculated - it is about 5 meV. The present experimental limit is 140 meV.

The flavor mixing of the quarks is described by the CKM matrix:

$$V_{\text{CKM}} = \begin{pmatrix} V_{ud} & V_{us} & V_{ub} \\ V_{cd} & V_{cs} & V_{cb} \\ V_{td} & V_{ts} & V_{tb} \end{pmatrix}. \quad (1)$$

The absolute values of the nine matrix elements have been measured in many experiments:

$$|U_{\text{CKM}}| \Rightarrow \begin{pmatrix} 0.974 & 0.224 & 0.004 \\ 0.218 & 0.997 & 0.042 \\ 0.008 & 0.040 & 1.019 \end{pmatrix}. \quad (2)$$

There are several ways to describe the CKM-matrix in terms of three angles and one phase parameter. I prefer the parametrization, which Z. Xing and I introduced years ago (ref. [1]), given by the angles θ_u , θ_d , θ and a phase parameter ϕ , which describes CP violation:

$$V_{\text{CKM}} = \begin{pmatrix} c_u & s_u & 0 \\ -s_u & c_u & 0 \\ 0 & 0 & 1 \end{pmatrix} \times \begin{pmatrix} e^{-i\phi} & 0 & 0 \\ 0 & c & s \\ 0 & -s & c \end{pmatrix} \times \begin{pmatrix} c_d & -s_d & 0 \\ s_d & c_d & 0 \\ 0 & 0 & 1 \end{pmatrix}. \quad (3)$$

Here we used the short notation: $c_{u,d} \sim \cos \theta_{u,d}$, $s_{u,d} \sim \sin \theta_{u,d}$, $c \sim \cos \theta$ and $s \sim \sin \theta$.

Relations between the quark masses and the mixing angles can be derived, if the quark mass matrices have "texture zeros", as shown by S. Weinberg and me

in 1977 (ref. [2]). For six quarks the mass matrices have four "texture zeros":

$$M = \begin{pmatrix} 0 & A & 0 \\ A^* & 0 & B \\ 0 & B^* & C \end{pmatrix}. \quad (4)$$

We can now calculate the angles θ_u and θ_d as functions of the mass eigenvalues:

$$\theta_d \simeq \sqrt{m_d/m_s}, \quad \theta_u \simeq \sqrt{m_u/m_c}. \quad (5)$$

Using the observed masses for the quarks, we find for these angles:

$$\theta_d \simeq (13.0 \pm 0.4)^\circ, \quad \theta_u \simeq (5.0 \pm 0.7)^\circ. \quad (6)$$

The experimental values agree with the theoretical results:

$$\theta_d \simeq (11.7 \pm 2.6)^\circ, \quad \theta_u \simeq (5.4 \pm 1.1)^\circ. \quad (7)$$

There is a relation between the four heavy quark masses and V_{cb} :

$$V_{cb} \cong \sqrt{m_s/m_b} - \sqrt{m_c/m_t}. \quad (8)$$

We use the following values for the quark masses:

$$m_s \simeq 0.08 \text{ GeV}, \quad m_b \simeq 4.7 \text{ GeV}, \quad m_c \simeq 1.3 \text{ GeV}, \quad m_t \simeq 172 \text{ GeV}. \quad (9)$$

In this case we find $V_{cb} \cong 0.043$. This value agrees with the experimental result: $0.039 < V_{cb} < 0.043$.

In the Standard Theory of particle physics the neutrinos do not have a mass. But a mass term can be introduced analogous to the mass term for the electrons. Nevertheless the masses of the neutrinos must be very small, much smaller than the mass of the electron. According to the limit from cosmology the sum of the neutrino masses must be less than 0.23 eV.

If the neutrinos have a small mass and if they are superpositions of mass eigenstates, there would be also a flavor mixing of the leptons. An electron neutrino, emitted from a nucleus, can turn into a muon neutrino after travelling a certain distance. Afterwards it would again become an electron neutrino, etc. These neutrino oscillations were first discussed by P. Minkowski and me in 1975 (see ref. [3]).

The flavor mixing of the leptons is described by a unitary 3x3-matrix, which is similar to the CKM-matrix for the quarks:

$$U = \begin{pmatrix} U_{e1} & U_{e2} & U_{e3} \\ U_{\mu1} & U_{\mu2} & U_{\mu3} \\ U_{\tau1} & U_{\tau2} & U_{\tau3} \end{pmatrix}. \quad (10)$$

This matrix can be described by three angles and a phase parameter. Here we use the standard parametrization, given by the three angles θ_{12} , θ_{13} and θ_{23} . The phase parameter describes the CP-violation.

In the nuclear fusion on the sun many electron neutrinos are produced. In 1963 John Bahcall calculated the flux of the solar neutrinos. He concluded that this flux could be measured by experiments. Raymond Davis prepared such an experiment. It was placed in the Homestake Gold Mine in Lead, South Dakota and took data from 1970 until 1994. One observed only about 1/3 of the flux, calculated by Bahcall. Thus there were problems with the solar neutrinos, or the calculation of the flux by Bahcall was wrong. Today we know that the reduction of the solar neutrino flux is due to neutrino oscillations.

In the Japanese Alps, near the small village "Kamioka", a big detector was built in 1982. It is located about 1000 m underground. This detector "Kamiokande" was built in order to find the hypothetical decay of a proton. Thus far no proton decay has been observed, but the detector can also be used to study neutrinos, in particular the atmospheric neutrinos, produced by the decay of pions in the upper atmosphere.

In 1996 a new detector "Superkamiokande" started to investigate these neutrinos. This detector consists of a water tank, containing 50 000 liters of purified water, surrounded by about 11 000 photo multipliers. With this detector one could measure the flux of the neutrinos. The flux of neutrinos, coming from the atmosphere above Kamioka, was as high as expected, but the flux of the neutrinos, coming from the other side of the earth, was only about 50% of the expected rate.

Afterwards a neutrino beam, sent from the KEK laboratory near Tsukuba towards Kamioka, was investigated. Again the flux of muon neutrinos was less than expected. Oscillations between the muon neutrinos and the tau neutrinos could explain the observed reduction of the flux. These oscillations are described by the angle θ_{23} . According to the experiments this angle is very large:

$$40,3^\circ \leq \theta_{23} \leq 52,4^\circ. \quad (11)$$

In Canada a neutrino detector was built near Sudbury (Ontario), the Sudbury Neutrino Observatory (SNO). With this detector one could observe the solar neutrinos. An solar neutrino hits a deuteron, which splits up into two protons and an electron - this process can be observed. Furthermore it was possible to observe the neutral current interaction of the neutrinos. If a solar neutrino collides with a deuteron, it splits up into a proton and a neutron. Also this reaction can be observed.

The neutral current interaction is not affected by oscillations, since all neutrinos have the same neutral current interaction. However oscillations can be observed for the charged current interaction. An electron neutrino, which becomes a muon neutrino, will not produce an electron after colliding with a nucleus. By comparing the interaction rates for the neutral and for the charged current interactions one has observed the oscillations of the solar neutrinos. For the corresponding mixing angle θ_{12} one finds:

$$31,6^\circ \leq \theta_{12} \leq 36,3^\circ. \quad (12)$$

Nuclear reactors emit electron antineutrinos. These neutrinos have been investigated at a few nuclear reactors, e.g, at the CHOOZ reactor in Belgium and

afterwards at the Daia Bay reactors in China. Here neutrino oscillations have been observed, and one could measure the mixing angle θ_{13} :

$$8,2^\circ \leq \theta_{13} \leq 9,0^\circ. \quad (13)$$

Also the two small mass differences between the three neutrinos have been measured. The mass difference between the first and the second neutrino is about 0.0086 eV, and the mass difference between the second and the third neutrino is about 0.05 eV.

Using the measured mixing angles, we can calculate the mixing matrix for the leptons. The mixing matrix of the quarks is close to the unit matrix, since the mixing angles are small. However this is not the case for the leptons, since two of the mixing angles are large. Thus the mixing matrix of the leptons is quite different from the mixing matrix of the quarks.

Thus far it is not clear, how large the CP-violation is for the leptons. A violation of this symmetry implies, that the oscillation of two neutrinos is different from the oscillation of the corresponding antineutrinos. For example, the oscillation between electron neutrinos and muon neutrinos would be different from the oscillation between electron antineutrinos and muon antineutrinos. The results from the experiment T2K in Japan indicate that there might be a large CP-violation.

In 2027 two new experiments will start to measure CP-violation. At Fermilab the new experiment DUNE ("Deep Underground Neutrino Experiment") is prepared. In Japan the new experiment "Hyper-Kamiokande" will start in 2027. Thus in about 10 years we shall know, whether there is a large CP-violation for leptons.

The neutrino masses are very small, and the question arises, if the neutrino masses are different from the Dirac masses of the charged leptons. Since the neutrinos are neutral, the neutrino masses might be Majorana masses. The smallness of the neutrino masses can be understood by the "seesaw"-mechanism. The mass matrix of the neutrinos is a matrix with one "texture zero" in the (1,1)-position. The two off-diagonal terms are given by the Dirac mass term D - a large Majorana mass term is in the (2,2)-position:

$$M_\nu = \begin{pmatrix} 0 & D \\ D & M \end{pmatrix}. \quad (14)$$

After diagonalization one obtains a large Majorana mass M and a small neutrino mass:

$$m_\nu \simeq D^2/M. \quad (15)$$

Now we assume that the Dirac mass matrices of the leptons also have four texture zeros:

$$M_D = \begin{pmatrix} 0 & A & 0 \\ A^* & 0 & C \\ 0 & C^* & D \end{pmatrix}. \quad (16)$$

In the seesaw formula we replace the Dirac mass by the texture zero mass matrix M_D and the Majorana mass by a Majorana mass matrix M_D :

$$M_\nu = M_D^\top M_R^{-1} M_D. \quad (17)$$

Since the Majorana masses are much larger than the masses of the leptons and quarks, we assume, that the Majorana mass matrix is proportional to the unit matrix. In this case the mixing angles are functions of the ratios of the charged lepton masses and of the neutrino masses.

But the mass ratios of the charged leptons are very small and cannot give large mixing angles. These angles must be related to large ratios of the neutrino masses (ref. [4,5,6,7]). In first approximation we can neglect the mass ratios of the charged leptons and can calculate the matrix elements of the mixing matrix, in the particular those matrix elements, mentioned below:

$$\begin{aligned} |U_{e2}| &\cong \left(\frac{m_1}{m_2}\right)^{1/4}, \\ |U_{\mu 3}| &\cong \left(\frac{m_2}{m_3}\right)^{1/4}, \\ |U_{e3}| &\cong \left(\frac{m_2}{m_3}\right)^{1/2} \left(\frac{m_1}{m_3}\right)^{1/2}. \end{aligned} \quad (18)$$

We use these relations and the experimental results for the mixing angles to determine the three neutrino masses:

$$\begin{aligned} m_1 &\simeq 1.4 \text{ meV}, \\ m_2 &\simeq 9 \text{ meV}, \\ m_3 &\simeq 51 \text{ meV}. \end{aligned} \quad (19)$$

One expects that the Dirac term D is similar to the corresponding charged lepton mass. For example, let us consider the tau lepton and its neutrino. If D is given by the tau lepton mass and the corresponding neutrino mass is 51 meV, we obtain for the heavy Majorana mass M :

$$M \simeq 6.3 \times 10^{10} \text{ GeV}. \quad (20)$$

The only way to test the nature of the neutrino masses is to study the neutrinoless double beta decay, which violates lepton number conservation. Two neutrons inside an atomic nucleus decay by emitting two electrons and two neutrinos. The two Majorana neutrinos annihilate - only two electrons are emitted. The annihilation rate is a function of the Majorana mass of the neutrino.

If neutrinos mix, all three neutrino masses will contribute to the decay rate. Their contributions are given by the masses of the neutrinos and by the mixing angles. Using the neutrino masses and the observed mixing angles, one finds for the effective neutrino mass, relevant for the neutrinoless double beta decay:

$$\tilde{m} \simeq 5 \text{ meV}. \quad (21)$$

In various experiments one has searched for the neutrinoless double beta decay, for example for the decay of tellurium. Thus far the decay has not been observed. Here is the present limit for this effective mass, given by the Cuore and the Gerda experiments in the Gran Sasso Laboratory:

$$\tilde{m} < 140 \text{ meV}. \quad (22)$$

This limit is about thirty times larger than the expected value.

In 2025 a new detector will be ready: "LEGEND" ("Large Enriched Germanium Experiment for Neutrinoless Double-Beta Decay"). This detector will be able to establish a new limit for the effective neutrino mass, about 1 meV. Since I expect about 5 meV for this mass, I predict that the neutrinoless double beta decay will be discovered with this detector.

Conclusions: Using 4 texture zeros for the mass matrices of the quarks and leptons, we derived relations between the flavor mixing angles and the mass ratios of the leptons and quarks. For the quarks the results agree with the experimental values. Using the observed mixing angles of the leptons, we calculated the three neutrino masses. The effective neutrino mass, describing the neutrinoless double beta decay, is much smaller than the present limit of the experiments. The neutrinoless double beta decay will be observed after 2025 with the new detector "LEGEND".

References

1. H. Fritzsch and Z. Z. Xing, Phys. Lett. B 413, (1997) 396,
H. Fritzsch and Z. Z. Xing, Phys. Rev. D 57, 594 (1998).
2. H. Fritzsch, Phys. Lett. 70B (1977) 436,
S. Weinberg, Trans. New York Acad. Sci. 38, 185 (1977),
H. Fritzsch, Phys. Lett. 73B (1978) 317.
3. H. Fritzsch and P. Minkowski, Phys. Lett. B 62 (1976) 76 .
4. M. Fukugita, M. Tanimoto, T. Yanagida, Prog.Theor.Phys. 89 (1993) 263.
5. Z. Xing, Phys.Lett. B550 (2002) 178.
6. M. Fukugita, M. Tanimoto, T. Yanagida, Phys.Lett. B562 (2003) 273.
7. M. Fukugita, Y. Shimizu, M. Tanimoto, T. Yanagida, Phys.Lett. B716 (2012) 294.



Hidden Charm Molecular Pentaquarks: Some Open Questions

Marek Karliner

School of Physics and Astronomy, Tel Aviv University, Tel Aviv 69978, Israel

Abstract. LHCb has recently reported three narrow states in $\Lambda_b^0 \rightarrow J/\psi p K^-$ decays, $P_c(4312)$, $P_c(4440)$ and $P_c(4457)$, decaying into $J/\psi p$, i.e., having minimal quark content $c\bar{c}uud$. Two states are slightly below $\Sigma_c \bar{D}^*$ threshold and one state is slightly below the $\Sigma_c \bar{D}$ threshold. This is highly suggestive of hadronic molecules and immediately triggers some intriguing follow-up questions.

The relevant issues which seem interesting to me include

- Four additional P_c states with Σ_c^* instead of Σ_c : $\Sigma_c^* \bar{D}$ and $\Sigma_c^* \bar{D}^*$?
- Decay of P_c -s into $\Lambda_c \bar{D}$?
- So far no signal of P_c -s in $\gamma p \rightarrow J/\psi p$ photoproduction
- If $P_c(4312)$ is a $\Sigma_c \bar{D}$ molecule, why don't we see a $D \bar{D}$ molecule?
- Why are P_c binding energies \gg other hidden-charm hadronic molecules?
- $P_c(4440)$ and $P_c(4457)$: likely $\Sigma_c \bar{D}^*$, $S = \frac{1}{2}, \frac{3}{2}$
17 MeV spin splitting \gg deuteron ($S=1$) vs. $p n$ $S=0$
- What can we learn about the P_c -s from the lattice?

In the following I discuss several of these questions in some detail.

Four additional $\Sigma_c^* \bar{D}(\bar{D}^*)$ molecules?

Three narrow P_c states have recently been reported by LHCb [1]. The state $P_c(4312)$ is just a few MeV below $\Sigma_c \bar{D}$ threshold, and is a natural candidate for a $\Sigma_c \bar{D}$ molecule. Similarly, the states $P_c(4440)$ and $P_c(4457)$ are natural candidates for $\Sigma_c \bar{D}^*$ molecules, one with spin $\frac{1}{2}$ and the other with spin $\frac{3}{2}$ (we don't know which is which yet). In the $m_c \rightarrow \infty$ limit the Σ_c and Σ_c^* baryons are degenerate. So are the \bar{D} and \bar{D}^* mesons. Therefore in the heavy quark limit one expects Σ_c^* to form molecules by binding with \bar{D} and \bar{D}^* . In this limit the only difference is that Σ_c^* has spin $\frac{3}{2}$, so there is one $\Sigma_c^* \bar{D}$ molecule with spin $\frac{3}{2}$ and there are three $\Sigma_c^* \bar{D}^*$ molecules, with $S = \frac{1}{2}, \frac{3}{2}, \frac{5}{2}$.

In the real world, however, Σ_c^* is about 36 MeV heavier than Σ_c and has a significantly shorter lifetime, $\Gamma(\Sigma_c^*) \approx 15$ MeV $\sim \Gamma(P_c)$, vs. $\Gamma(\Sigma_c) \approx 2$ MeV. As a

general rule it only makes sense to talk about a bound state if the lifetime of the constituents is significantly longer than the lifetime of a bound state. A $\Sigma_c \bar{D}^{(*)}$ molecule is therefore a borderline case. This issue should be investigated carefully from the theoretical point of view, and of course it will be extremely interesting to see whether such states are observed experimentally.

Additional decay mode $P_c \rightarrow \Lambda_c \bar{D}(\bar{D}^*)$?

The $(c\bar{c}uud)$ quark content of the P_c states at 4312, 4440, 4457 MeV is the same as that of $\Lambda_c \bar{D}$ and $\Lambda_c \bar{D}^*$. Both are well below the P_c masses, $m(\Lambda_c) + m(\bar{D}^0) = 4150$ MeV, $m(\Lambda_c) + m(\bar{D}^{0*}) = 4293$ MeV. Spin & parity conservation allow the decays

$$(\Sigma_c \bar{D}^*, S=\frac{3}{2}) \rightarrow \Lambda_c \bar{D}^*,$$

$$(\Sigma_c \bar{D}^*, S=\frac{1}{2}) \rightarrow \Lambda_c \bar{D}, \Lambda_c \bar{D}^*,$$

$$(\Sigma_c \bar{D}, S=\frac{1}{2}) \rightarrow \Lambda_c \bar{D}, \Lambda_c \bar{D}^*.$$

Unlike in the decay to $J/\psi p$, the $\Sigma_c \bar{D}^{(*)}$ molecules can decay to $\Lambda_c \bar{D}^{(*)}$ without having to bring the charmed and anticharmed quarks close to each other. Therefore it is likely that $|\langle P_c | \Lambda_c \bar{D}(\bar{D}^*) \rangle|^2 \gg |\langle P_c | J/\psi p \rangle|^2$, so we expect $\Gamma(P_c \rightarrow \Lambda_c \bar{D}^{(*)}) \gg \Gamma(P_c \rightarrow J/\psi p)$. This immediately brings up the question why $\Lambda_c \bar{D}(\bar{D}^*)$ decays have not been seen? This question is discussed below.

Why has $P_c \rightarrow \Lambda_c \bar{D}^0$ not been seen?

Most likely this an experimental issue in LHCb: a product of several small BR-s, large number of charged tracks and background rejection.

Compare $P_c \rightarrow J/\psi p$ and $P_c \rightarrow \Lambda_c \bar{D}^0$. J/ψ is identified by its dimuon decay, $\text{BR}(J/\psi \rightarrow \mu^+ \mu^-) = 6\%$, so finally $P_c \rightarrow \mu^+ \mu^- p$, i.e. 3 charged tracks. On the other hand, in $P_c \rightarrow \Lambda_c \bar{D}^0$ $\text{BR}(\Lambda_c \rightarrow K^- p \pi^+) = 6.28\%$, $\text{BR}(\bar{D}^0 \rightarrow K^+ \pi^-) = 4\%$, so $\text{BR}(\dots) \times \text{BR}(\dots) = 0.25\%$, with 5 charged tracks. Each additional charged track comes with an efficiency penalty, so detection efficiency \times BR for the all charged final state in $P_c \rightarrow \Lambda_c \bar{D}^0$ is much smaller.

Why $P_c \rightarrow \Lambda_c \bar{D}^{*0}$ hasn't been seen?

On top of $\Lambda_c \bar{D}^0$ issues, \bar{D}^{*0} needs to be identified through its characteristic decays $\bar{D}^{*0} \rightarrow \bar{D}^0 \pi^0$ or $\bar{D}^{*0} \rightarrow \bar{D}^0 \gamma$. These decays necessitate identification of soft π^0 or γ , both of which have rather low efficiency in LHCb. The upshot is $P_c \rightarrow \Lambda_c \bar{D}^0(\bar{D}^{*0})$ should eventually be seen, but with much more data.

The hierarchy of partial widths, $\text{BR}(P_c \rightarrow \Lambda_c \bar{D}(\bar{D}^*)) \gg \text{BR}(P_c \rightarrow J/\psi p)$ suggests a relatively small coupling in $\gamma p \rightarrow P_c \rightarrow J/\psi p$, relevant for the photoproduction experiments.

Why no signal of P_c -s in $\gamma p \rightarrow J/\psi p$ photoproduction?

For obvious reasons it is essential to confirm the LHCb findings and to observe the P_c resonances in another experiment. At the moment no other experiment has a comparable number of Λ_b -s and a suitable detector in order to repeat the

LHCb analysis in the same channel. Instead, several groups proposed to look for $P_c(4450)$ as an s -channel resonance in photoproduction, $\gamma p \rightarrow J/\psi p$ [4–6]. In fixed target mode the required energy of the photon is about 10 GeV. Several fixed-target experiments are currently under way at JLab. The first results have recently been published by GlueX Collaboration [7]. They do not see the relevant resonances in the γp channel and are able to set model-dependent upper limits on their branching fractions $\mathcal{B}(P_c^+ \rightarrow J/\psi p)$ and cross sections $\sigma(\gamma p \rightarrow P_c^+) \times \mathcal{B}(P_c^+ \rightarrow J/\psi p)$. The most likely explanation, within the molecular model, is that the $P_c \rightarrow J/\psi p$ partial width is rather small, much smaller than $P_c \rightarrow \Lambda_c \bar{D}^{(*)}$, as discussed above. But eventually, with sufficient integrated luminosity, the $\gamma p \rightarrow P_c \rightarrow J/\psi p$ process should be seen.

In principle it is also possible to look for a bottom analogue of $P_c(4450)$, a $\Sigma_b B^*$ molecule around 7.778 GeV in the reaction $\gamma p \rightarrow \Upsilon p$. But since the required lab photon energy is 65.7 GeV, it is far from clear that such an experiment is feasible.

$P_c \rightarrow \eta_c p$?

This channel is expected in addition to $P_c \rightarrow J/\psi p$ and $P_c \rightarrow \Lambda_c \bar{D}^{(*)}$. Since η_c has $J^P = 0^-$, only P_c states with $S = \frac{1}{2}$ can decay through this channel. Detection is difficult.

The quark spin wave function for $\Sigma_c^{+\downarrow} \bar{D}^{*0\uparrow\uparrow}$, $S = \frac{1}{2}$: $(c^\uparrow u^\downarrow d^\downarrow)(\bar{c}^\uparrow u^\uparrow)$ implies decay to $J/\psi(c^\uparrow \bar{c}^\uparrow)$ is preferred, while for $\Sigma_c \bar{D}$ no preference is expected for $J/\psi(c^\uparrow \bar{c}^\uparrow)$ over $\eta_c(c^\uparrow \bar{c}^\downarrow)$.

If $P_c(4312)$ is a $\Sigma_c \bar{D}$ molecule, why no $D\bar{D}$ molecule?

Hadronic molecules consist of two color-singlet hadrons, which are analogous to proton and neutron in a deuteron. Binding is provided by exchange of light mesons. The lightest meson is the pion, so one expects that one-pion exchange plays a significant role in generating the necessary attraction. This immediately explains why we observe $\bar{D}D^*$ [$X(3872)$ and $Z_c(3900)$] and \bar{D}^*D^* [$Z_c(4020)$], as well as $\bar{B}B^*$ [$Z_b(10610)$] and \bar{B}^*B^* [$Z_b(10650)$] hadronic molecules, but not $\bar{D}D$, nor $\bar{B}B$.

The reason for absence of $\bar{D}D$ and $\bar{B}B$ is that parity and angular momentum conservation forbid a three-pseudoscalar vertex like $D-D-\pi$. So $\bar{D}D$ cannot bind by exchanging one pion. The same logic suggests one-pion exchange can bind a $\Sigma_c \bar{D}^*$ molecule, but not a $\Sigma_c \bar{D}$ molecule [2]. But $P_c(4312)$ very much looks like a $\Sigma_c \bar{D}$ molecule. So what mechanism binds $\Sigma_c \bar{D}$, but does not bind $D\bar{D}$?

What binds $\Sigma_c \bar{D}$ but not $D\bar{D}$?

If one-pion exchange is impossible, the next obvious thing to look at is two-pion exchange, illustrated in Fig. 1. In $D\bar{D}$ system, shown in Fig. 1(a), the intermediate state consists of $D^*\bar{D}^*$, which is 284 MeV heavier than $D\bar{D}$. This is a very large energy denominator, and consequently two-pion exchange does not contribute to $D\bar{D}$ binding. The situation is dramatically different in $\Sigma_c \bar{D}$ system, shown in

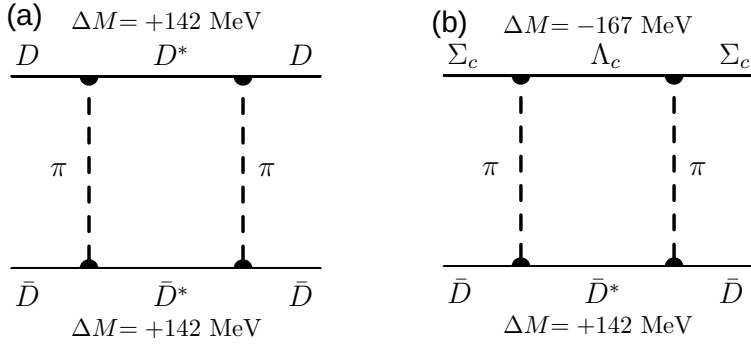


Fig. 1. Two-pion exchange diagrams for (a) $D\bar{D}$ (b) $\Sigma_c\bar{D}$. The intermediate states are denoted, together with ΔM , the mass difference from the original hadron.

Fig. 1(b). There the intermediate system consists of $\Lambda_c\bar{D}^*$. The crucial difference from $D\bar{D}$ is that Λ_c is 167 MeV *lighter* than Σ_c . As a result, the intermediate $\Lambda_c\bar{D}^*$ state is only 25 MeV below $\Sigma_c\bar{D}$, instead of 284 MeV above in the $D\bar{D}$ case, and therefore in this case two-pion exchange does contribute to binding.

In addition to this crucial difference, there are two additional factors which work in favor of $\Sigma_c\bar{D}$ vs. $D\bar{D}$: (a) Σ_c has $I = 1$ vs. D with $I = \frac{1}{2}$, implying that Σ_c has a stronger coupling to light hadrons; (b) larger reduced mass: $M_{\text{reduced}}(\Sigma_c\bar{D}) = 1060 \text{ MeV} > M_{\text{reduced}}(D\bar{D}) = 932 \text{ MeV}$, making the repulsive kinetic energy 12% smaller.

It is not clear if this is the whole story, but the above do provide a suggestive binding mechanism. The alternative, advocated by Voloshin, is that “ $D\bar{D}$ *does exist, but hard to see*” [3].

If a $X(3872)$ -like $D\bar{D}$ exists, could it have evaded experiments?

In my opinion this is very unlikely. Such a $X(3872)$ -like $D^0\bar{D}^0$ molecule $X(3729)$ would lie close to the threshold at 3729 MeV, have $J^{PC} = 0^{++}$, and be a mixture of $I = 0$ and $I = 1$.

Its production mechanisms would be analogous to $X(3872)$ and χ_{c0} ,

$$B \rightarrow KX(3729), \quad \text{cf. } B \rightarrow KX(3872);$$

$$e^+e^- \rightarrow \gamma X(3729), \quad \text{cf. } e^+e^- \rightarrow \gamma\chi_{c0}.$$

Expected decay modes are

$$X(3729) \rightarrow J/\psi\rho, \quad J/\psi\gamma, \quad \psi'\gamma.$$

These are right in LHCb, BESIII, BaBar and Belle courts, but no such state has been reported.

Why P_c binding energies \gg other hidden-charm molecules?

$X(3872)$ lies $\ll 1 \text{ MeV}$ from $\bar{D}D^*$ threshold, $Z_c(3900)$ and $Z_c(4020)$ are *above* the \bar{D}^0D^{*+} and $\bar{D}^{*0}D^{*+}$ thresholds, For comparison, the deuteron is 2.2 MeV below p n. So why are P_c -s $5 \div 22 \text{ MeV}$ below $\Sigma_c\bar{D}(\bar{D}^*)$?

Alternatively, why is their size so much smaller? Estimating the size from $r \approx 1/\sqrt{2\mu_{\text{red}}|\Delta E|}$, where μ_{red} is the reduced mass and ΔE is the binding energy, we have for the deuteron size $r_d \approx 3$ fm. Similarly, from $\Delta E(X(3872)) < 1$ indicates that $r_{X(3872)} > 4.5$ fm.

These are to be compared with

$P_c(4312)$: $r \approx 1.6$ fm,

$P_c(4440)$: $r \approx 0.9$ fm,

$P_c(4457)$: $r \approx 1.9$ fm.

17 MeV spin splitting between $P_c(4457)$ and $P_c(4440)$

In the molecular model these two states are naturally interpreted as spin $\frac{1}{2}$ and spin $\frac{3}{2}$ $\Sigma_c \bar{D}^*$ molecules. There is one hadronic molecule where the spin splitting is known. This is the deuteron, which has spin 1. We know there is a spin-0 pn state just above threshold. So the spin splitting for the deuteron is ~ 2.2 MeV $\ll 17$ MeV that we see here. This is probably related to the deeper binding and smaller size discussed above. Spin-spin interaction is usually short range, so having a smaller molecule enhances the splitting.

An obvious difference between the P_c and the meson-meson hadronic molecules with hidden charm is the fact that Σ_c has $I=1$ and is heavier than the charmed mesons. Both of these enhance the net attraction. Hopefully detailed calculations in specific models can elucidate this question and show if these are sufficient to generate the observed larger binding and spin splitting.

Acknowledgements

The original results referred to in this talk were obtained in collaboration with Jon Rosner. I wish to thank the organizers of the 2019 Bled Mini-Workshop for creating a stimulating environment for discussions of current problems in hadronic physics.

The references appearing below are not meant assign credit where it belongs, but rather to help the reader in locating the specific additional background that might needed. Extensive sets of references can be found in recent reviews, e.g., [8] and [9].

References

1. R. Aaij *et al.* [LHCb Collaboration], Phys. Rev. Lett. **122**, 222001 (2019) [arXiv:1904.03947 [hep-ex]].
2. M. Karliner and J. L. Rosner, Phys. Rev. Lett. **115**, 122001 (2015) [arXiv:1506.06386 [hep-ph]].
3. M. Voloshin, private communication.
4. Q. Wang, X. H. Liu and Q. Zhao, Phys. Rev. D **92**, 034022 (2015) [arXiv:1508.00339 [hep-ph]].

5. V. Kubarovsky and M. B. Voloshin, Phys. Rev. D **92**, 031502 (2015) [arXiv:1508.00888 [hep-ph]].
6. M. Karliner and J. L. Rosner, Phys. Lett. B **752**, 329 (2016) [arXiv:1508.01496 [hep-ph]].
7. A. Ali *et al.* [GlueX Collaboration], Phys. Rev. Lett. **123**, no. 7, 072001 (2019) doi:10.1103/PhysRevLett.123.072001 [arXiv:1905.10811 [nucl-ex]].
8. S. L. Olsen, T. Skwarnicki and D. Zieminska, Rev. Mod. Phys. **90**, 015003 (2018) [arXiv:1708.04012 [hep-ph]].
9. M. Karliner, J.L. Rosner and T. Skwarnicki, Ann. Rev. Nucl. Part. Sci. **68**, 17 (2018) [arXiv:1711.10626 [hep-ph]].



A unified approach for the structure of light and heavy baryons

Hyun-Chul Kim

Department of Physics, Inha University, Incheon 22212, Republic of Korea,
School of Physics, Korea Institute for Advanced Study (KIAS), Seoul 02455,
Republic of Korea

Abstract. In the present talk, we summarize a series of recent works on the structure of light and heavy baryons, based on the chiral quark-soliton model. The present summary can be considered as a brief guide to the model. For details, we refer to the references given.

1. The chiral quark-soliton model (χ QSM), which was constructed as a pion mean-field theory for the structure of the nucleon many years ago [1], has been successfully applied to the description of not only low-lying $SU(3)$ hyperons but also singly heavy baryons (See the following reviews [2–4]). The χ QSM was mainly motivated by Witten’s seminal works [5,6], in which a baryon can be considered as a system consisting of N_c valence quarks bound by meson mean fields. Here, N_c denotes the number of colors. This is justified in the large N_c limit. In this limit, the nucleon mass is proportional to N_c whereas its width is of order $\mathcal{O}(1)$. Mesons are weakly interacting and the meson-loop fluctuations are suppressed by $1/N_c$.

The starting point of the χ QSM is the effective chiral action given as

$$S_{\text{eff}}[\pi^a] = -N_c \text{Tr} \ln(i\not{\partial} + iM\mathbf{U}^{\gamma_5} + i\hat{m}), \quad (1)$$

where the chiral field \mathbf{U}^{γ_5} is defined as

$$\mathbf{U}^{\gamma_5} := \exp(i\pi^a \lambda^a \gamma_5) = \mathbf{U}(x)P_R + \mathbf{U}(x)^\dagger P_L. \quad (2)$$

P_R and P_L denote the projection operators defined by $P_R = (1 + \gamma_5)/2$ and $P_L = (1 - \gamma_5)/2$. \hat{m} designates the current quark mass matrix: $\hat{m} := \text{diag}(m_u, m_d, m_s) = m_0 \mathbf{1} + m_3 \lambda^3 + m_8 \lambda^8$. When isospin symmetry is imposed, m_3 is set equal to zero $m_3 = (m_u - m_d)/2$. The Tr represents the functional trace over the space-time and all internal spaces. The effective chiral action in Eq. (2) can be derived from the low-energy QCD partition function through the instanton vacuum [7,?]. While the original one contains the momentum-dependent dynamical quark mass $M(p)$, which arises from the Fourier transform of the fermionic zero modes, we turn off the momentum dependence, so the dynamical quark mass M becomes constant as in Eq. (2). However, we have to pay the price for taking the constant M : the

regularization of the quark loop. The value of the cut-off mass for the regularization is fixed by reproducing the experimental data of the pion decay constant. The up or down quark mass is determined by the experimental value of the pion mass. Thus, the only remaining free parameter in this model is the value of the dynamical quark mass. However, its value will be determined to be around 420 MeV by computing the charge radius of the proton.

The presence of N_c *valence* quarks in this large N_c limit, which consist of the lowest-lying baryons, produce the pion mean fields by which they are influenced *self-consistently*. This picture is very similar to a Hartree approximation in many-body theories. Explicitly, we start from a trial solution of the classical equation of motion and derive the eigenenergies and eigenvectors of the one-body Dirac equation. Using these results, we obtain a new profile of the chiral soliton or the mean-field solution. We repeat this procedure till the classical soliton energy is reached to a converged value. We identify this energy as a classical mass of the soliton. The next step is the collective quantization of the classical soliton. Since the soliton does not have rotational and translational symmetries, we restore this symmetries by using the zero-mode quantization. Then the nucleon and lowest-lying hyperons arise as rotational collective states.

2. We can apply exactly the same procedure to singly heavy baryon systems. A singly heavy baryon contains a pair of light quarks and a heavy quark. Since the mass of the heavy quark is much heavier than that of a light quark, one can consider the infinitely heavy quark mass limit, i.e. $m_Q \rightarrow \infty$. In this limit, the spin of the heavy quark is conserved, since the infinitely heavy mass does not allow the spin of the quark to be flipped. It leads to the conservation of the total spin of light quarks: $J_L \equiv J - J_Q$, where J_L , J_Q , and J stand for the spin of the light-quark pair, that of the heavy quark, and the total spin of the heavy baryon. This is coined as the heavy-quark spin symmetry that allows J_L to be a good quantum number. Furthermore, the physics is kept intact under the placement of heavy quark flavors. This is known as the heavy-quark flavor symmetry [9–12]. Then the heavy quark becomes static, so that it can be considered as a static color source. It indicates that the heavy quark inside a singly heavy baryon can be stripped off from the baryon and the dynamics of the heavy baryon is mainly governed by the light quarks.

The flavor structure of the heavy baryon also comes from the light-quark constituents. Since a singly heavy baryon contains two light quarks, there are two $SU_f(3)$ irreducible representations, i.e. $3 \otimes 3 = \bar{3} \oplus 6$. The spatial part of the heavy-baryon ground state is symmetric due to the zero orbital angular momentum, so that the color part is totally antisymmetric to satisfy the generalized Pauli principle. Moreover, since the flavor anti-triplet ($\bar{3}$) is antisymmetric, the spin state of $\bar{3}$ should be antisymmetric. Thus, a baryon belonging to the anti-triplet should have $J_L = 0$. By the same token, the flavor-symmetric sextet (6) should be symmetric in spin space, i.e. $J_L = 1$. This leads to the fact that the baryon antitriplet has spin $J = 1/2$, while the baryon sextet carries spin $J = 1/2$ or $J = 3/2$, with the spin of the light-quark pair being coupled with the heavy quark spin $J_Q = 1/2$. So, we can classify 15 different lowest-lying heavy baryons as shown in Fig. 1 in the case of charmed baryons. The bottom baryons are also classified as shown

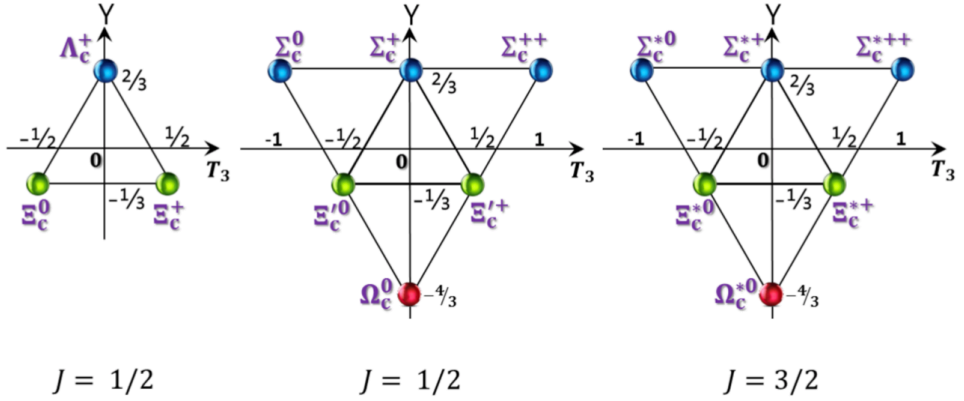


Fig. 1. The anti-triplet ($\bar{3}$) and sextet (6) representations of the lowest-lying heavy baryons. The left panel draws the weight diagram for the anti-triplet with the total spin $\frac{1}{2}$. The centered panel corresponds to that for the sextet with the total spin $1/2$ and the right panel depicts that for the sextet with the total spin $3/2$.

in Fig. 1. The only difference of the bottom baryons is the charge of the bottom quark from that of the charm quark.

The pion mean-field approach was developed in Ref. [13] to describe the masses of singly heavy baryons, being motivated by Ref. [14]. In fact, it is straightforward to extend the original mean-field approach to the singly heavy baryons in which we have $N_c - 1$ light valence quarks with the single heavy quark stripped off (Fig. 2). The presence of the $N_c - 1$ valence quarks will also create the pion mean fields in which they are bound by the pion mean fields self-consistently.

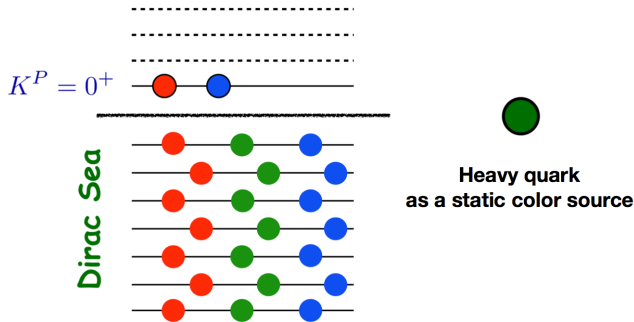


Fig. 2. Schematic picture of a heavy baryon. The $N_c - 1$ valence quarks are filled in the lowest-lying valence level $K^P = 0^+$ with the heavy quark stripped off. K^P denotes the grand spin which we will explain later and P is the corresponding parity of the level. The presence of the valence quarks will interact with the sea quarks filled in the Dirac sea each other. This interaction will bring about the pion mean field.

The constraint right hyper charge is taken to be $Y' = (N_c - 1)/3$ and allows the lowest-lying representations: the baryon anti-triplet ($\bar{3}$), the baryon sextet (6),

the baryon anti-decaplet ($\overline{15}$). The model reproduced successfully the mass splitting of the baryon anti-triplet and sextet in both the charm and bottom sectors [13,15]. In addition, the mass of the Ω_b^* baryon, which has not yet found, was predicted [16,16]. The magnetic moments baryons [18] and electromagnetic form factors [19] of the singly heavy baryons were also studied within the same framework. The χ QSM was also used to interpret the five Ω_c baryons newly found by the LHCb Collaboration [16,17]. Within the present framework, two of the Ω_c s with the smaller widths are classified as the members of the baryon $\overline{15}$, whereas all other Ω_c 's belong to the excited baryon sextet. The widths were quantitatively well reproduced without any free parameter.

Acknowledgements

I want to express my gratitude to the organizers of the wonderful Bled Mini-Workshop. I am very grateful to J.-Y. Kim, M. V. Polyakov, M. Praszalowicz, and Gh.-S. Yang for fruitful collaborations and discussions. The present work is supported by Basic Science Research Program through the National Research Foundation of Korea funded by the Ministry of Education, Science and Technology (2018R1A2B2001752).

References

1. D. Diakonov, V. Y. Petrov and P. V. Pobylitsa, Nucl. Phys. B **306**, 809 (1988).
2. C. V. Christov, A. Blotz, H.-Ch. Kim, P. Pobylitsa, T. Watabe, T. Meissner, E. Ruiz Arriola and K. Goeke, Prog. Part. Nucl. Phys. **37**, 91 (1996).
3. D. Diakonov, hep-ph/9802298.
4. H.-Ch. Kim, J. Korean Phys. Soc. **73**, no. 2, 165 (2018) [arXiv:1804.04393 [hep-ph]].
5. E. Witten, Nucl. Phys. B **160**, 57 (1979).
6. E. Witten, Nucl. Phys. B **223**, 422 (1983) and Nucl. Phys. B **223**, 433 (1983).
7. D. Diakonov and V. Y. Petrov, Nucl. Phys. B **245**, 259 (1984).
8. D. Diakonov and V. Y. Petrov, Nucl. Phys. B **272**, 457 (1986).
9. N. Isgur and M. B. Wise, Phys. Lett. B **232**, 113 (1989).
10. N. Isgur and M. B. Wise, Phys. Rev. Lett. **66**, 1130 (1991).
11. H. Georgi, Phys. Lett. B **240**, 447 (1990).
12. A. V. Manohar and M. B. Wise, Camb. Monogr. Part. Phys. Nucl. Phys. Cosmol. **10**, 1 (2000).
13. Gh.-S. Yang, H.-Ch. Kim, M. V. Polyakov and M. Praszalowicz, Phys. Rev. D **94**, 071502 (2016)
14. D. Diakonov, arXiv:1003.2157 [hep-ph].
15. J. Y. Kim, H.-Ch. Kim and G. S. Yang, arXiv:1801.09405 [hep-ph].
16. H.-Ch. Kim, M. V. Polyakov and M. Praszalowicz, Phys. Rev. D **96**, no. 1, 014009 (2017) Addendum: [Phys. Rev. D **96**, no. 3, 039902 (2017)] [arXiv:1704.04082 [hep-ph]].
17. H.-Ch. Kim, M. V. Polyakov, M. Praszalowicz and G. S. Yang, Phys. Rev. D **96**, no. 9, 094021 (2017) Erratum: [Phys. Rev. D **97**, no. 3, 039901 (2018)] [arXiv:1709.04927 [hep-ph]].
18. G. S. Yang and H. C. Kim, Phys. Lett. B **781**, 601 (2018) doi:10.1016/j.physletb.2018.04.042 [arXiv:1802.05416 [hep-ph]].
19. J. Y. Kim and H.-Ch. Kim, arXiv:1803.04069 [hep-ph].



Improved pion mean fields*

June-Young Kim^a, Hyun-Chul Kim^{a,b}

^a Department of Physics, Inha University, Incheon 22212, Republic of Korea

^b School of Physics, Korea Institute for Advanced Study (KIAS), Seoul 02455, Republic of Korea

Abstract. In this presentation, we report recent results on improved pion mean fields within the chiral quark-soliton model. We investigate effects of the reduction of the number of the valence quarks from N_c to $N_c - 1$ and $N_c - 2$ on the pion mean fields, and their physical implications are discussed.

1 Introduction

The light baryon has been studied within a pion mean-field approach in the limit of large N_c or the chiral quark-soliton model (χ QSM) [1] over decades. The model has succeeded in describing the structure of the lowest-lying light baryons [2,3]. In a similar manner, the χ QSM idea has been recently applied to the singly heavy baryon sector to investigate how the pion mean fields explain various properties of heavy baryons. The main idea is that heavy baryons consist of $N_c - 1$ light valence quark bound by the pion mean fields. While the sea-quark polarization is kept to be intact and the heavy quark is treated as a mere static color source in the limit of infinitely heavy quark mass, e.g. $m_Q \rightarrow \infty$, the contribution of the $N_c - 1$ light valence quarks are modified. By doing that, we were able to describe the properties of the singly heavy baryons [4,5]. However, the pion mean fields should explicitly be obtained by solving the classical equation of motion in the presence of the $N_c - 1$ valence quarks instead of N_c quarks.

In this talk, we will present a recent work on how the pion mean fields can be modified by changing the number of the light valence quarks from N_c to $N_c - N_Q$, where N_Q denotes the number of the heavy quarks. We find that indeed the pion mean fields undergo the changes by reducing the number of the light valence quarks.

2 Result and discussion

The detailed formalism for solving the classical equation of motion within the present framework is presented in [6].

Fig. 1 depicts soliton mass as a function of the dynamical quark mass for the pion mean fields with the N_c valence quarks. In the presence of the N_c valence

* Talk presented by June-Young Kim

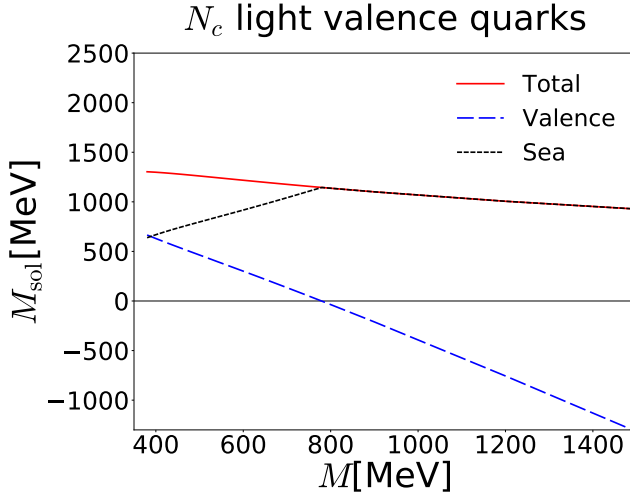


Fig. 1. Soliton mass as a function of the dynamical quark mass for the pion mean fields in the presence of the N_c valence quarks. The long-dashed line draws the valence-quark contribution, whereas the short-dashed one depicts the sea-quark contribution. The solid line represents the soliton mass.

quarks, the solutions of the classical equation of motion exist when the dynamical quark mass M is larger than the critical mass $M_{\text{cr}} \approx 350$ MeV. Note that the dynamical quark mass M acts as a coupling between the pion and the quark. For that reason, the vacuum polarization becomes stronger as M increases. On the other hand, the strength of the interaction is not strong enough to get the N_c valence quarks being bound over the values of M below M_{cr} . In the meanwhile, even though sea- and valence-quark contributions vary noticeably with M , the classical mass is not much changed. When the value M reaches around 800 MeV, valence energy crosses into the negative energy. It indicates that, from that point, the soliton energy does solely come from the sea-quark contribution.

Fig. 2 depicts soliton mass as a function of the dynamical quark mass for $N_c - 1$ mean fields. The $N_c - 1$ mean fields, singly heavy baryon, consist of $N_c - 1$ valence quarks and a heavy quark. It means that the number of the valence quarks is reduced by one. That is to say, the pion mean fields are weakened as much as the absence of the valence quark, which affects the vacuum polarization. As a result, the critical point of the dynamical quark mass is found to be $M_{\text{cr}} \approx 400$ MeV. By the same token, the vacuum is weakly polarized all over the region. The dependence of the dynamical quark mass of valence- and sea-quark energies is similar to the case of the N_c mean fields.

Fig. 3 presents the values of the soliton mass for the pion mean fields in the presence of the $N_c - 2$ valence quarks, as a function of M . Note that in this case the soliton consists of only a single valence quark. we do not find any stabilized soliton till M is reached to $M_{\text{cr}} \approx 600$ MeV. It indicates that the present framework is not suitable to study doubly heavy baryons.

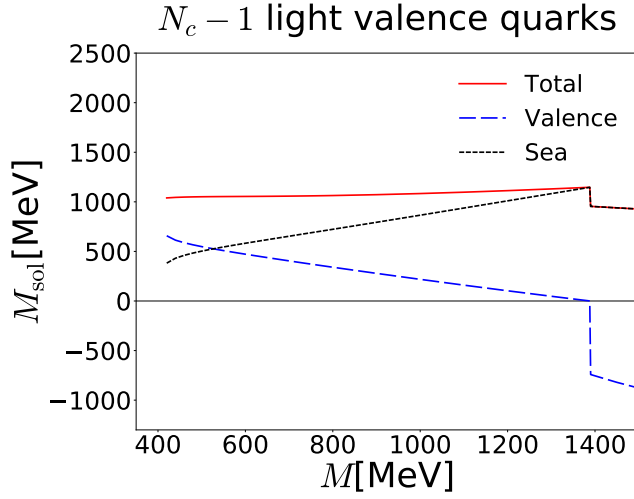


Fig. 2. Soliton mass as a function of the dynamical quark mass for the pion mean fields in the presence of the $N_c - 1$ valence quarks. The long-dashed line draws the valence-quark contribution, whereas the short-dashed one depicts the sea-quark contribution. The solid line represents the soliton mass.

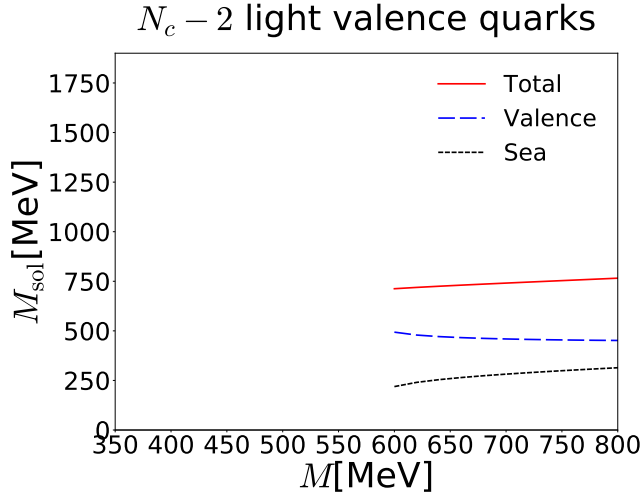


Fig. 3. Soliton mass as a function of the dynamical quark mass for the pion mean fields in the presence of the $N_c - 2$ valence quarks. The long-dashed line draws the valence-quark contribution, whereas the short-dashed one depicts the sea-quark contribution. The solid line represents the soliton mass.

3 Summary and conclusion

In this talk, we present the recent results on the improved pion mean fields. We present the classical soliton masses by solving the classical equation of motion, varying the number of the valence quarks. Then, we find the weaker vacuum polarization as the number of the valence quarks is reduced. When it comes to doubly heavy baryon($N_c - 2$), its solutions do not exist within the proper range of the dynamical quark mass. Such a result is comprehensible, because the number of light valence quarks $N_c - 2$ means a singly light quark. In other words, the pion mean fields with the single valence quark are not strong enough to bind a doubly heavy baryon within the present framework. The numerical analysis in detail was made in Ref. [6].

Acknowledgments

The authors want to express their gratitude to the organizers for the invitation to the Bled Mini-Workshop. They are grateful to M. V. Polyakov, M. Praszalowicz, and Gh.-S. Yang for fruitful discussions and criticism. The present work is supported by Basic Science Research Program through the National Research Foundation of Korea funded by the Ministry of Education, Science and Technology (2018R1A5A1025563).

References

1. D. Diakonov, V. Y. Petrov and P. V. Pobylitsa, Nucl. Phys. B **306**, 809 (1988).
2. A. Blotz, D. Diakonov, K. Goeke, N. W. Park, V. Petrov and P. V. Pobylitsa, Nucl. Phys. A **555**, 765 (1993).
3. C. V. Christov, A. Blotz, H.-Ch. Kim, P. Pobylitsa, T. Watabe, T. Meissner, E. Ruiz Arriola and K. Goeke, Prog. Part. Nucl. Phys. **37**, 91 (1996).
4. Gh.-S. Yang, H.-Ch. Kim, M. V. Polyakov, and M. Praszalowicz, Phys. Rev. D **94**, 071502 (2016).
5. J. Y. Kim, H.-Ch. Kim and G. S. Yang, Phys. Rev. D **98**, no. 5, 054004 (2018).
6. J. Y. Kim and H. C. Kim, arXiv:1909.00123 [hep-ph].



Light- and strange-quark mass dependence of the $\rho(770)$ meson properties^{*}

R. Molina^a, J. Ruiz de Elvira^b

^a Departamento de Física Teórica II, Plaza Ciencias, 1, 28040 Madrid, Spain and Institute of Physics of the University of São Paulo, Rua do Matão, 1371 -Butantã, São Paulo -SP, 05508-090

^b Albert Einstein Center for Fundamental Physics, Institute for Theoretical Physics, University of Bern, Sidlerstrasse 5, 3012 Bern, Switzerland

Abstract. From an analysis of recent ($I = J = 1$)- $\pi\pi$ -phase-shift and pseudoscalar-meson decay-constant lattice data on two distinct chiral trajectories, where either the sum of the up, down and strange quark masses, or the mass of the strange quark is kept fixed, we extract the light and strange quark mass dependence of the rho meson parameters, and make predictions of those on chiral trajectories which involve lighter masses than the physical strange quark mass. We find that the mass of the rho meson can get as light as 700 MeV for strange quark mass zero at physical pion masses. While the ratio of the couplings to the $\pi\pi$ and $K\bar{K}$ channels is equal to $\sqrt{2}$ at the SU(3) symmetric chiral trajectory.

1 Introduction

In the past, most of the LatticeQCD simulations have been done on chiral trajectories $m_s = m_s^0$. Therefore, previous analysis of lattice data cannot track the behavior of pseudoscalar decay constants and rho meson parameters on trajectories involving variations of the strange quark mass. Recently, the CLS Collaboration has generated ensembles on chiral trajectories like $\text{Tr}M = c$ (with $c = m_u + m_d + m_s$) in large volumes [1,2]. Thus, the hadron properties in these trajectories will manifest as a consequence of both, variations in the light and strange quark masses. In this talk, I present the results of a global analysis of lattice data over the $\text{Tr}M = c$ and $m_s = m_s^0$ trajectories, which include the pseudoscalar decay constant data from Refs. [1,3–6] and phase shift data of Ref. [7–9,2].

2 Theoretical Framework

To perform the lattice data analysis, we employ the inverse amplitude method [10] based on one-loop Chiral Perturbation Theory (NLO ChPT) [11,12] taking the expressions of Ref. [13] similarly as in Ref. [14] for the scattering amplitudes t_2

^{*} Talk presented by R. Molina

¹ “0” means the physical value.

and t_4 ($\mathcal{O}(p^2)$ and $\mathcal{O}(p^4)$) of the $\pi\pi - K\bar{K}$ coupled-channel system. The scattering amplitude, t , read as

$$t = t_2[t_2 - t_4]^{-1}t_2. \quad (1)$$

The elements t_{ij} related to the channels i, j of the 2×2 t -matrix are related to S -matrix elements, $S_{ij} = \delta_{ij} + 2i\sqrt{\sigma_i\sigma_j}t_{ij}$, where $\sigma_i = \theta(\sqrt{s} - 2m_i)\sqrt{1 - 4m_i^2/s}$, and the S -matrix is parameterized as $S_{ii} = \eta e^{2i\delta_i}$, $i = 1, 2$; and $S_{21} = S_{12} = i(1 - \eta^2)^{1/2}e^{i(\delta_1 + \delta_2)}$. The relations for the pseudoscalar meson masses and decay constants of NLO ChPT [11,12] are used. The chiral trajectories followed by the NLO masses, $M_K^2 (M_\pi^2)$ are determined from their LO relations. The ones considered here are

$$M_{0K}^2 = \begin{cases} -\frac{1}{2}M_{0\pi}^2 + c B_0; & \text{Tr}M = c \\ +\frac{1}{2}M_{0\pi}^2 + k B_0; & m_s = k \\ M_{0\pi}^2; & m_s = m_{ud} \\ (r + m_s) B_0; M_{0\pi}^2 = 2rB_0 & m_{ud} = r, \end{cases} \quad (2)$$

and $m_\pi = m_\pi^0$. In the above relations, $B_0 = \frac{\Sigma_0}{f_0^2}$, with $\Sigma_0 = -\langle 0|\bar{q}q|0\rangle_0$, $m_{ud} = (m_u + m_d)/2$, and f_0 stands for the pion decay constant in the chiral limit. The free parameters are the NLO LECs, $L_{12}^r = 2L_1^r - L_2^r$ and L_i^r , $i = 3, 8$, and $\{c, k\} \times B_0$, which are adjusted to the chiral trajectories. In the fits, μ is fixed to 770 MeV, and f_0 is set to 80 MeV. Pseudoscalar meson decay constant data and ρ -phase-shift data are fitted simultaneously. The function minimized is the χ^2 , defined as,

$$\chi^2 = (\mathbf{W}_1 - \mathbf{W}_0)^T \mathbf{C}^{-1} (\mathbf{W}_1 - \mathbf{W}_0) + \sum_{ij} (h_{ij} - h_{ij}^l)^2 / e_{ij}^{l2} + \lambda \sum_{ij} \int |(\mathbf{S} \mathbf{S}^\dagger)_{ij} - \delta_{ij}|^2 dE \quad (3)$$

where \mathbf{W}_0 is the vector of eigenenergies measured on the lattice, \mathbf{C} the covariance matrix of these energies, and \mathbf{W}_1 the corresponding energies of the fit function. Instead of fitting directly the eigenenergies from lattice, these are reconstructed by means of a Taylor expansion, and phase shift data are fitted as done first in Refs. [15,16]. This avoids the discretization of loops. In the above equation, $i = 1, 3$ and $j = 1, n$, with n the number of data. $h_1 = m_\pi/f_\pi$, $h_2 = m_K/f_K$ and $h_3 = m_K/f_\pi$. The superscript l indicates values of these ratios from lattice simulations. The last term in Eq. (3) is added to guarantee that the LECs obtained satisfy unitarity at some degree depending on the λ value. We checked that for $\lambda \simeq 40$, the values of the LECs are stable, the minimum value of $\chi^2(\lambda)$ lies in a flat range of λ , and the S -matrix obtained is unitary at a higher degree. The bootstrap method is used to evaluate the errors assuming that the lattice energies are multivariate normally distributed with the same original covariance matrix, and the resampled-phase-shift data are obtained as a function of the energy expanded at linear order. Additionally, we assume that the lattice spacing in Ref. [1], where two sets of lattice

spacings are determined in different ways, is normally distributed with the mean the average between the two different determinations and the typical deviation half the difference between them. Results are shown with error bands that mean 68 and 95 % confidence intervals (CI) evaluated from the corresponding quantiles of phase shifts and decay constant ratios.

3 Results

In Figs. 1, 2, and 3, the chiral trajectories studied together with the decay constant ratios are plotted. The lattice data fitted correspond to the extrapolation to the continuum limit with finite volume effects corrected. For $m_s = m_s^0$, these are, UKQCD[3] (purple diamonds), MILC[4,5] (brown dashed curves with light-brown error bands² and Laiho[6] (orange dashed curves and error bands). For other trajectories $m_s = k$, there are no much data as commented previously, except for the ratio m_π/f_π extracted by MILC[4] (brown dotted line). The TrM= c data from the CLS Collaboration are given for different strengths of a parameter of the lattice simulation, $\beta = 3.4$ (green square), 3.55 (blue triangle), and 3.7 (yellow pentagon). The error in the x-axes correspond to the half the difference between the two different lattice spacing determinations. The other trajectories plotted are $m_s = \{0, 0.02, 0.045, 0.1, 0.2, 0.4, 0.6\} m_s^0$, and $m_u = \{1, 1.5\} m_u^0$, $m_\pi = m_\pi^0$, which start near $m_s \simeq 0$, cross the symmetric line, and end up at the $m_s = m_s^0$ curve. As seen, all ratios and chiral trajectories are reproduced well inside the 95 % CI till $m_\pi \simeq 400$ MeV, where the ChPT predictions start to deviate. Phase shifts are very well described being also inside the 95 % CI, as shown in Figs. 4–6. The extrapolation to the physical point in comparison with experimental data is plotted in Fig. 6 (bottom). The agreement with the experimental data is impressive. The physical point we get for the masses and decay constant ratios is given in Table 1. The values of the LECs are given in Table 2. For L_4^r, L_5^r, L_6^r and L_8^r , we obtain values in line with the Flag average [17]. However, notice that our values are much more precise since our result comes from an analysis of data over several chiral trajectories.

Table 1. Values of the ratios of pseudoscalar masses and decay constants extrapolated at the physical point as a result of fit which can be interpreted in terms of probability. The central value represents the median (or 0.5 quantile), the first upper and down indices gives the 68% CI, while the sum of the absolute values of the two upper(down) indices provide the upper(down) limits of the 95% CI.

| m_K^0/m_π^0 | m_π^0/f_π^0 | m_K^0/f_π^0 | m_K^0/f_K^0 |
|------------------------------------|--------------------------------------|------------------------------------|------------------------------------|
| $3.55^{+0.02(0.04)}_{-0.02(0.05)}$ | $1.51^{+0.013(0.03)}_{-0.012(0.03)}$ | $5.33^{+0.05(0.11)}_{-0.05(0.13)}$ | $4.45^{+0.04(0.09)}_{-0.03(0.10)}$ |

² The error band for the MILC data is extrapolated from the error at the physical point.

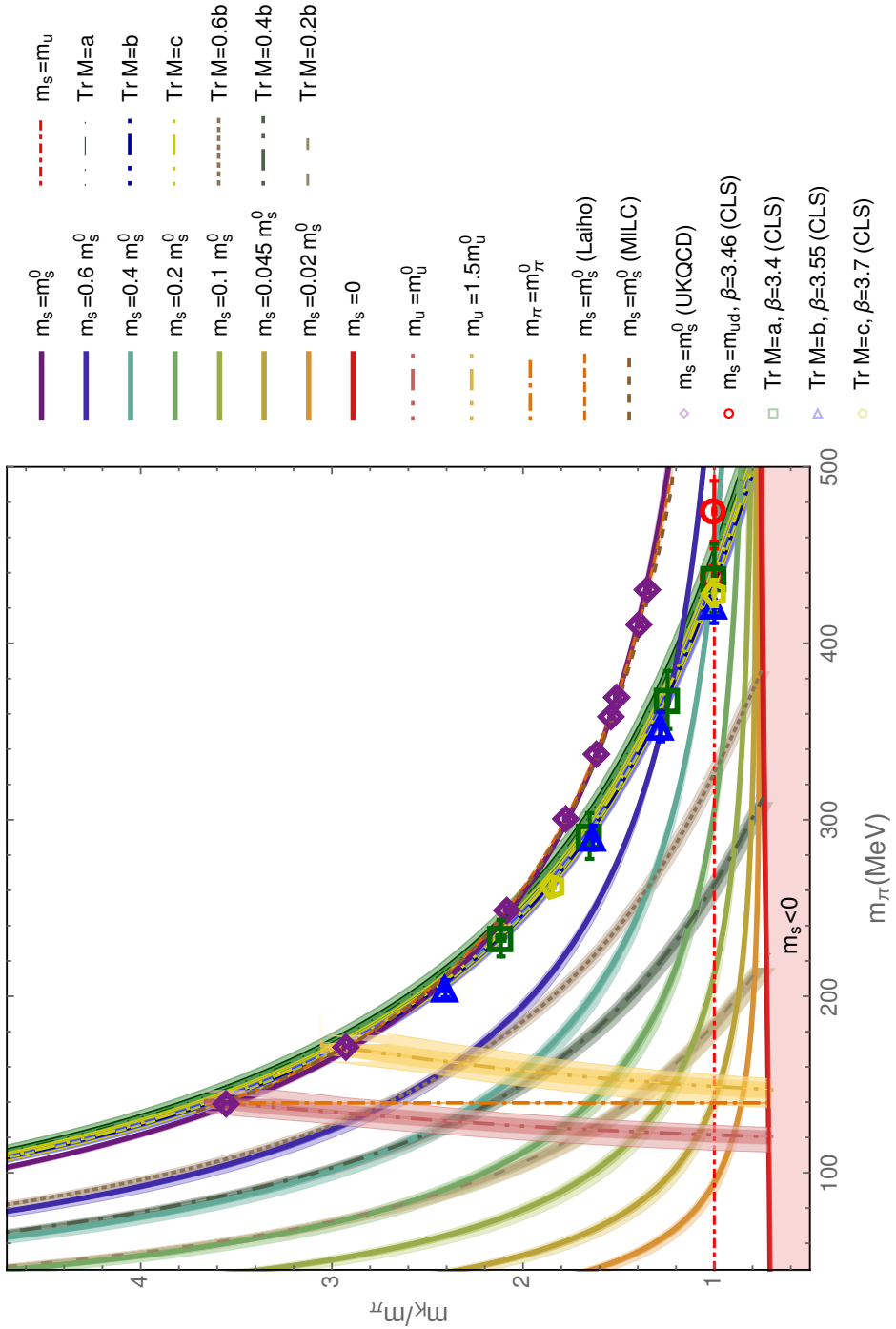


Fig. 1. Chiral trajectories in comparison with lattice data. Chiral trajectories in comparison with lattice data.

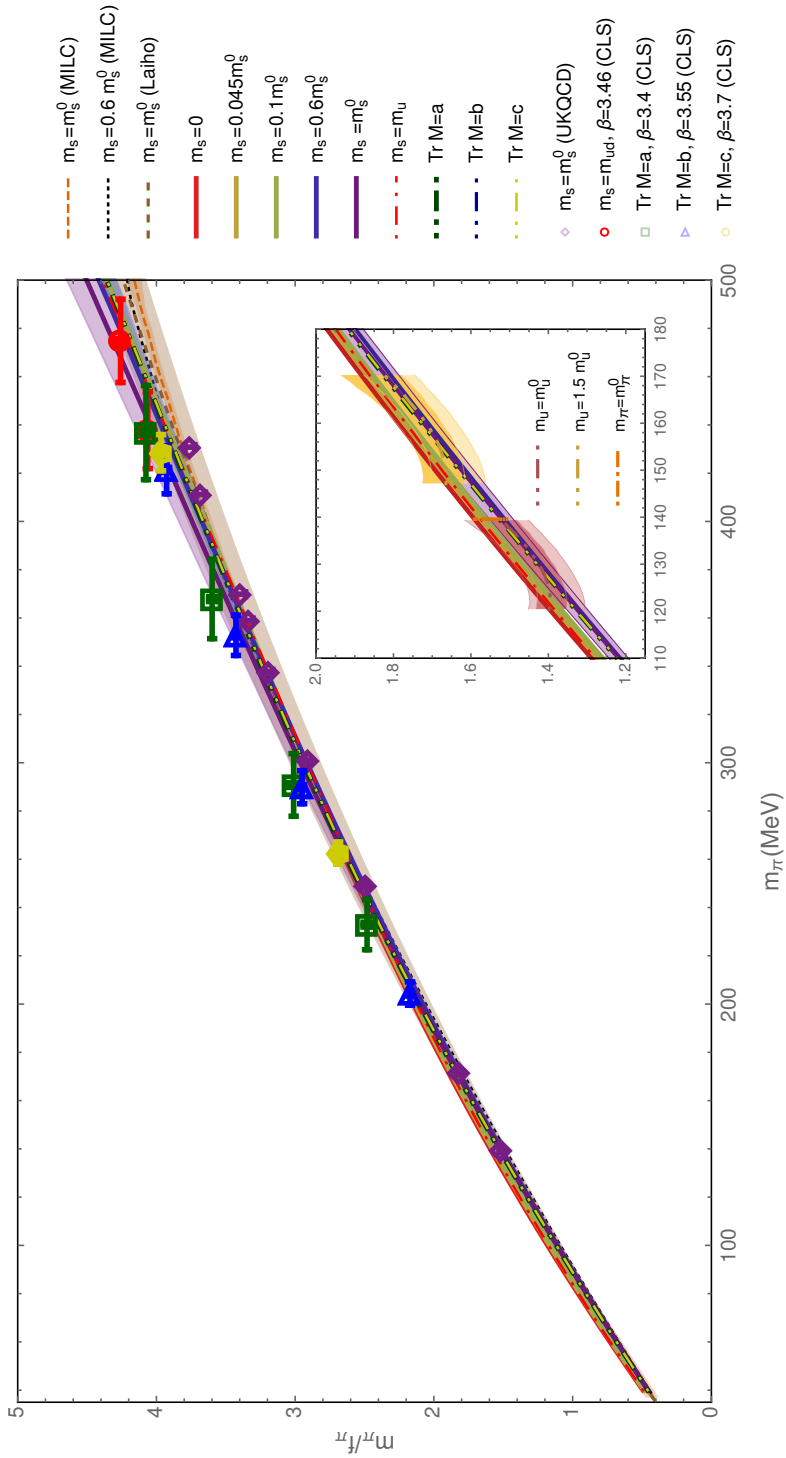


Fig. 2. The ratio m_ρ/f_ρ in comparison with lattice data.

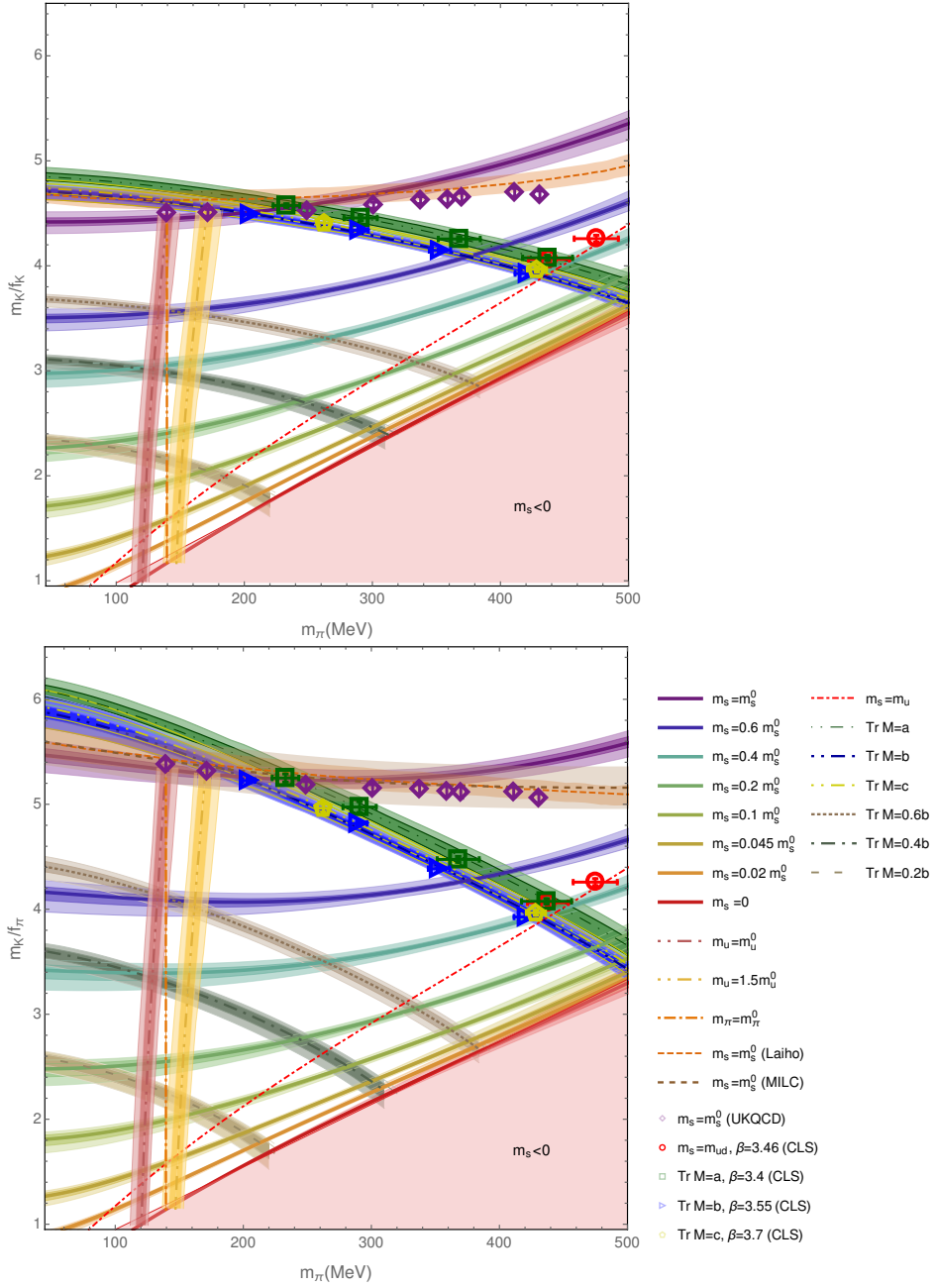


Fig. 3. Decay constant ratios, $m_K/f_{\pi K}$ (top panel) and m_K/f_K (bottom panel) in comparison with lattice data.

Table 2. Values of the parameters obtained in the fit which can be interpreted in terms of probability. The central value represents the median (or 0.5 quantile), the first upper and down indices gives the 68% CI, while the sum of the absolute values of the two upper(down) indices provide the upper(down) limits of the 95% CI.

| $L_i^r \times 10^3, c_{B_0} \times 10^{-3} (\text{MeV}^2), k_{B_0} \times 10^{-3} (\text{MeV}^2)$ | | | |
|---|-------------------------------------|-------------------------------------|------------------------------------|
| L_{12}^r | L_3^r | L_4^r | L_5^r |
| $0.36^{+0.02(0.06)}_{-0.02(0.02)}$ | $-3.44^{+0.04(0.07)}_{-0.04(0.06)}$ | $-0.08^{+0.03(0.05)}_{-0.04(0.03)}$ | $0.98^{+0.07(0.06)}_{-0.05(0.04)}$ |
| L_6^r | L_7^r | L_8^r | |
| $0.24^{+0.08(0.16)}_{-0.06(0.05)}$ | $0.008^{+0.09(0.12)}_{-0.14(0.15)}$ | $0.098^{+0.10(0.11)}_{-0.11(0.16)}$ | |
| $c_{\beta=3.4} B_0$ | $c_{\beta=3.55} B_0$ | $c_{\beta=3.7} B_0$ | k_{B_0} |
| $268^{+14(8)}_{-18(20)}$ | $254^{+11(7)}_{-18(18)}$ | $257^{+12(7)}_{-17(19)}$ | $224^{+14(10)}_{-18(20)}$ |

In Figs. 7 and 8, the behavior of the rho meson mass obtained as $E(\delta = 90^\circ)$ over the $m_s = k$ and $\text{Tr}M = c$ trajectories is depicted. Indeed, this dependence with the pion mass over the $m_s = m_s^0$ and $\text{Tr}M = \text{Tr}M^0$ trajectories is indistinguishable till around 400 MeV. For higher pion masses, the resonance becomes a bound state in the m_s^0 trajectory³, while the ρ gets in between the two thresholds starting to decay in $K\bar{K}$ in the $\text{Tr}M = \text{Tr}M^0$ trajectory. For other trajectories $m_s = k$ and around the physical point, almost no change in the ρ meson mass is observed. However, when m_s starts to decrease below $0.5 m_s$, m_ρ decreases faster till around 690 – 700 MeV when it reaches the $m_s = 0$ line. This value is close to the extrapolation to the physical point obtained from two-flavor lattice data analyses [15,18]. This is more clear in the $m_{u,\pi} = r$ trajectories, where the mass of the u quark (or pion) is kept fixed. The mass of the ρ meson decreases faster as m_s decreases and the ρ meson starts to decay into $K\bar{K}$. While other $\text{Tr}M = c$ trajectories present less dependence with the pion mass being flatter.

Couplings are shown in Fig. 9. In these kind of trajectories, when the ρ approaches the $K\bar{K}$ threshold, its coupling increases, while the coupling to $\pi\pi$ looks quite constant overall. At the symmetric line, the ratio of couplings $g_{\pi\pi}/g_{K\bar{K}}$ is exactly $\sqrt{2}$, what coincides with the ratio of SU(3) Clebsch-Gordan-Coefficients (CGC).

4 Conclusions

We performed a global analysis of most recent data on $m_s = m_s^0$, $\text{Tr}M = c$ trajectories, including both, phase shifts and decay constant data. The bootstrap method employed here (resampling both energies and lattice spacing) provides a satisfactory solution at 95 % confidence level. The IAM method has also proven itself

³ When this happens, the $\pi\pi$ threshold is plotted.

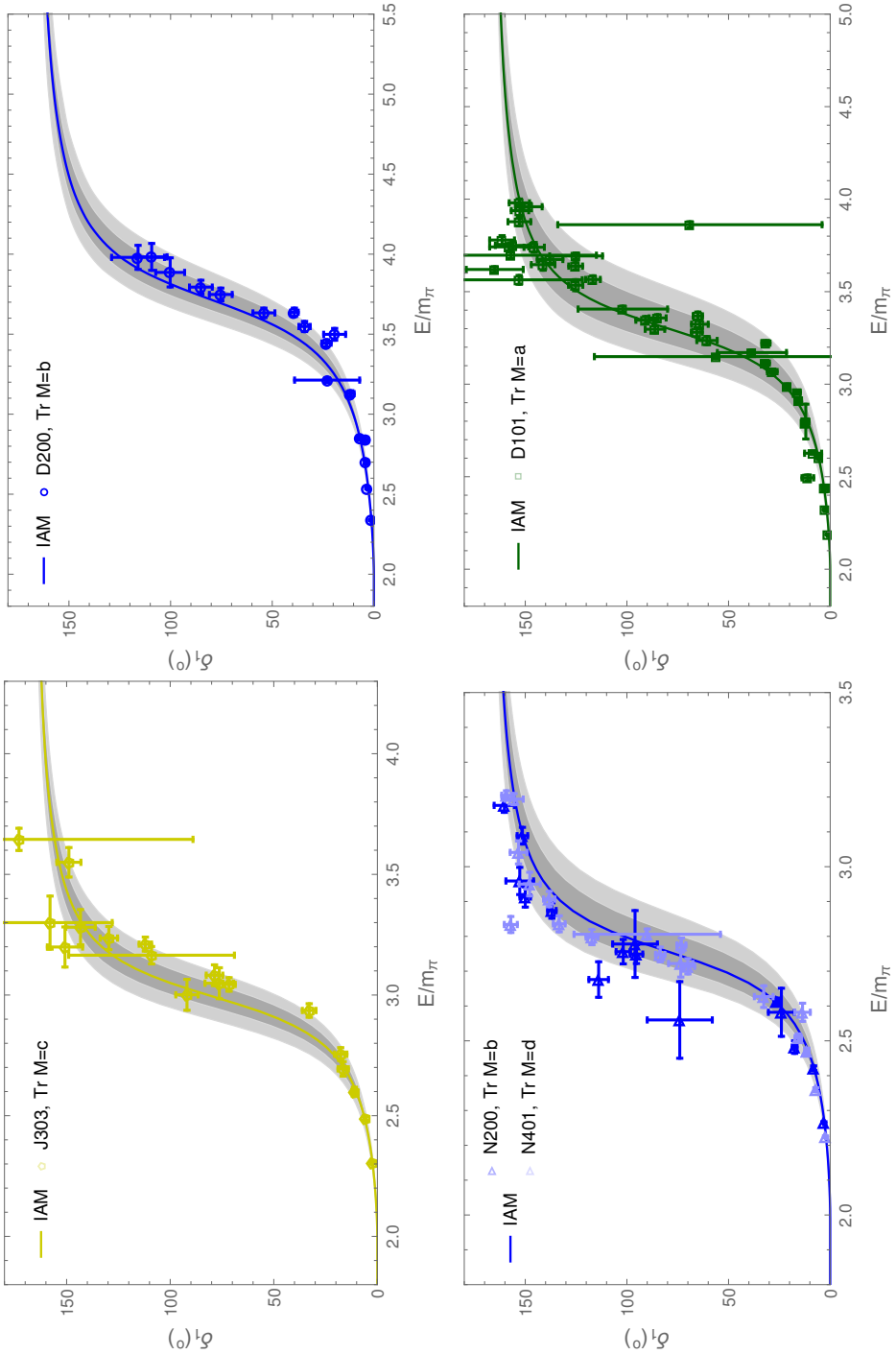


Fig. 4. Result of the fit in comparison with the $\text{Tr} M = c$ data of the CLS ensembles, D200, D101, J303, and N200, N401, for pion masses $m_\pi \simeq 200, 230, 260$ and 290 MeV, respectively.

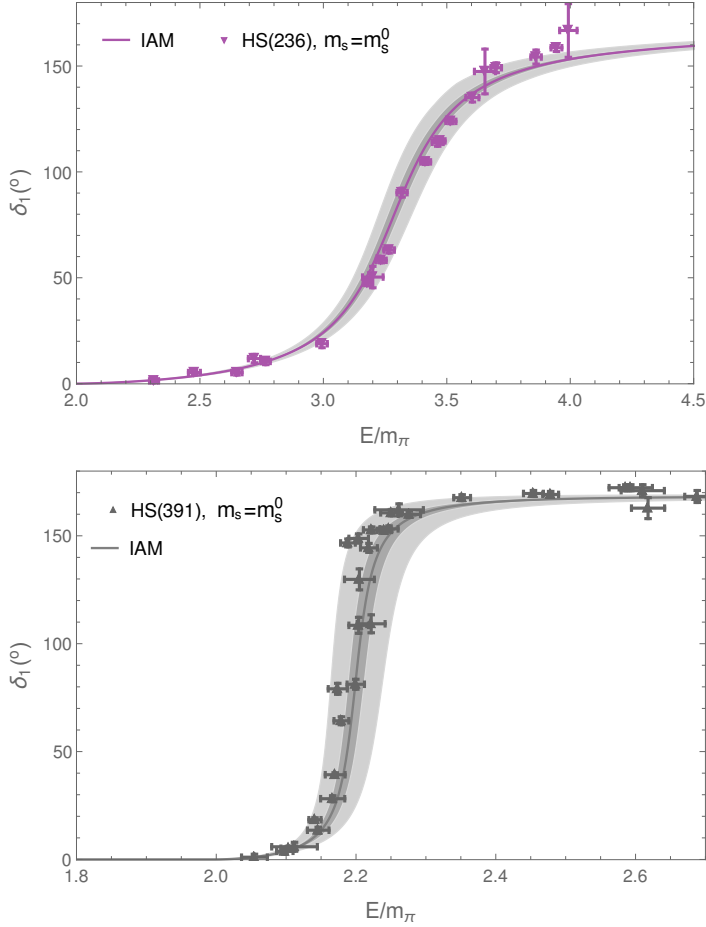


Fig. 5. Result for the ρ phase shifts in the $m_s = m_s^0$ trajectory, in comparison with the HS (HadSpec) data at $m_\pi = 236$ and 391 MeV.

to explain the behavior of the ρ meson with variations of the quark masses. The values of LECs obtained can describe both, the m_s and $m_{u,d}$ dependence in the $I = 1, J = 1$ two-(pseudoscalar) meson scattering, being thus, more precise than previous determinations based on the $m_s = m_s^0$ trajectory. Beyond that, we observed interesting effects which involve the $K\bar{K}$ channel. First, as m_π increases and the ρ meson pole gets closer to the $K\bar{K}$ threshold, $g_{K\bar{K}}$ becomes larger, the ρ becomes bound in the $m_s = m_s^0$ trajectories, and starts to decay in $K\bar{K}$ in the $\text{Tr}M = c$ ones. Second, as m_s decreases, the mass of the ρ starts decreasing faster as it gets closer to the $m_s = 0$ line. While, in the symmetric trajectory, we find $g_{\pi\pi}/g_{K\bar{K}} = \sqrt{2}$, corresponding to the $SU(3)$ CGC. Our analysis shows that all operators which could be relevant in the energy region should be considered in the lattice simulation because of the dynamics of the interaction with the quark mass. We hope that the results obtained here motivate the lattice community for-

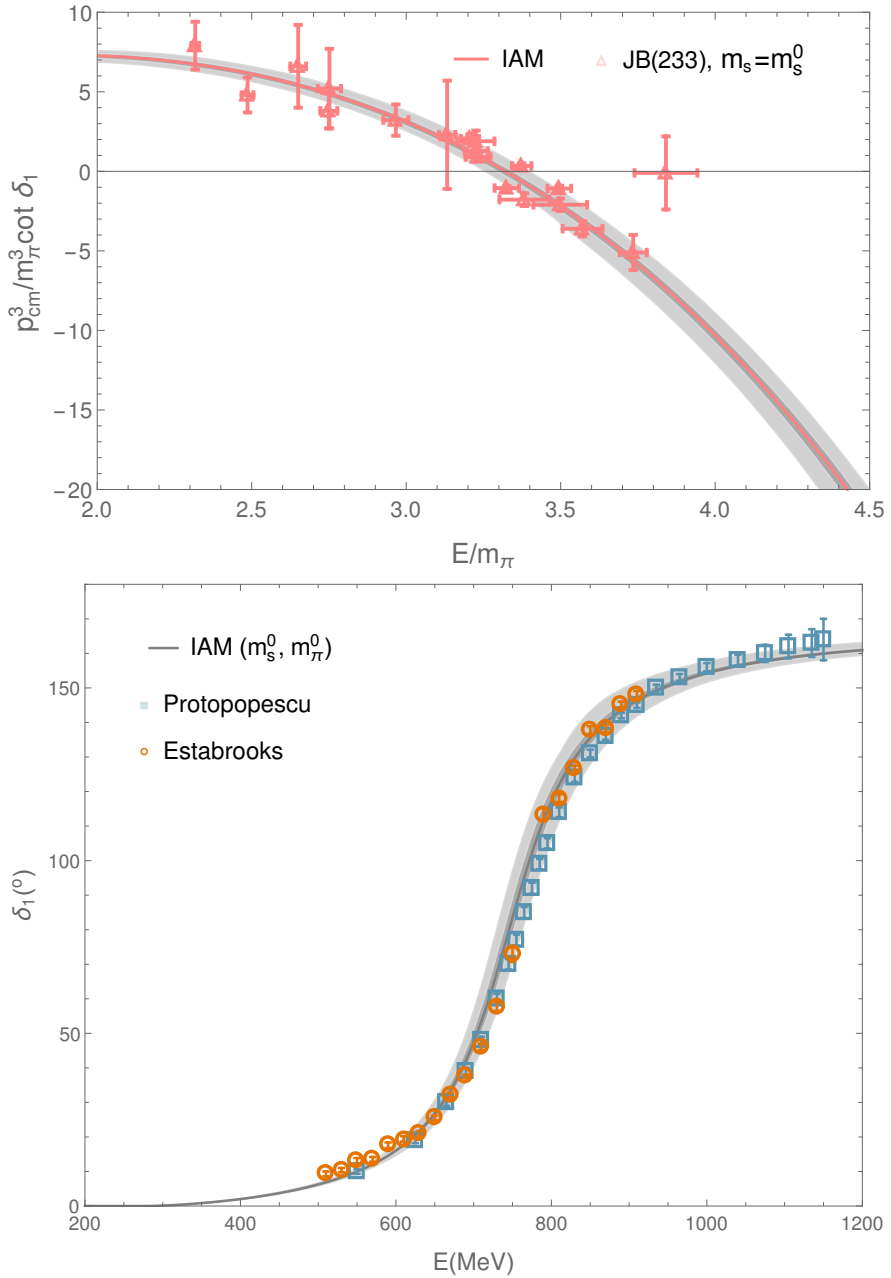


Fig. 6. Result of the fit in comparison with the data of Ref. [9] (JB) for $m_\pi = 233$ (top panel), and extrapolation to the physical point in comparison with the experimental data (bottom panel).

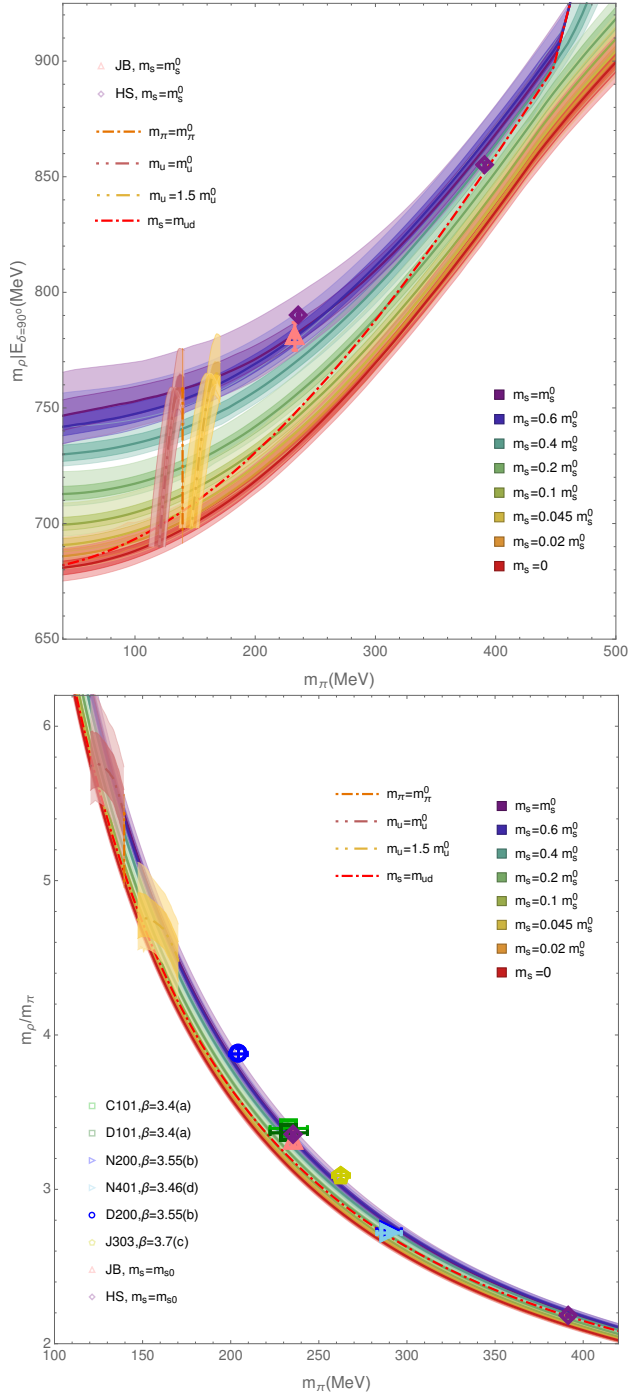


Fig. 7. ρ -meson mass (top) and this in pion mass units (bottom) as a function of the pion mass for $m_s = k$, $m_u = r$, $m_\pi = m_\pi^0$, and $m_s = m_u$ trajectories.

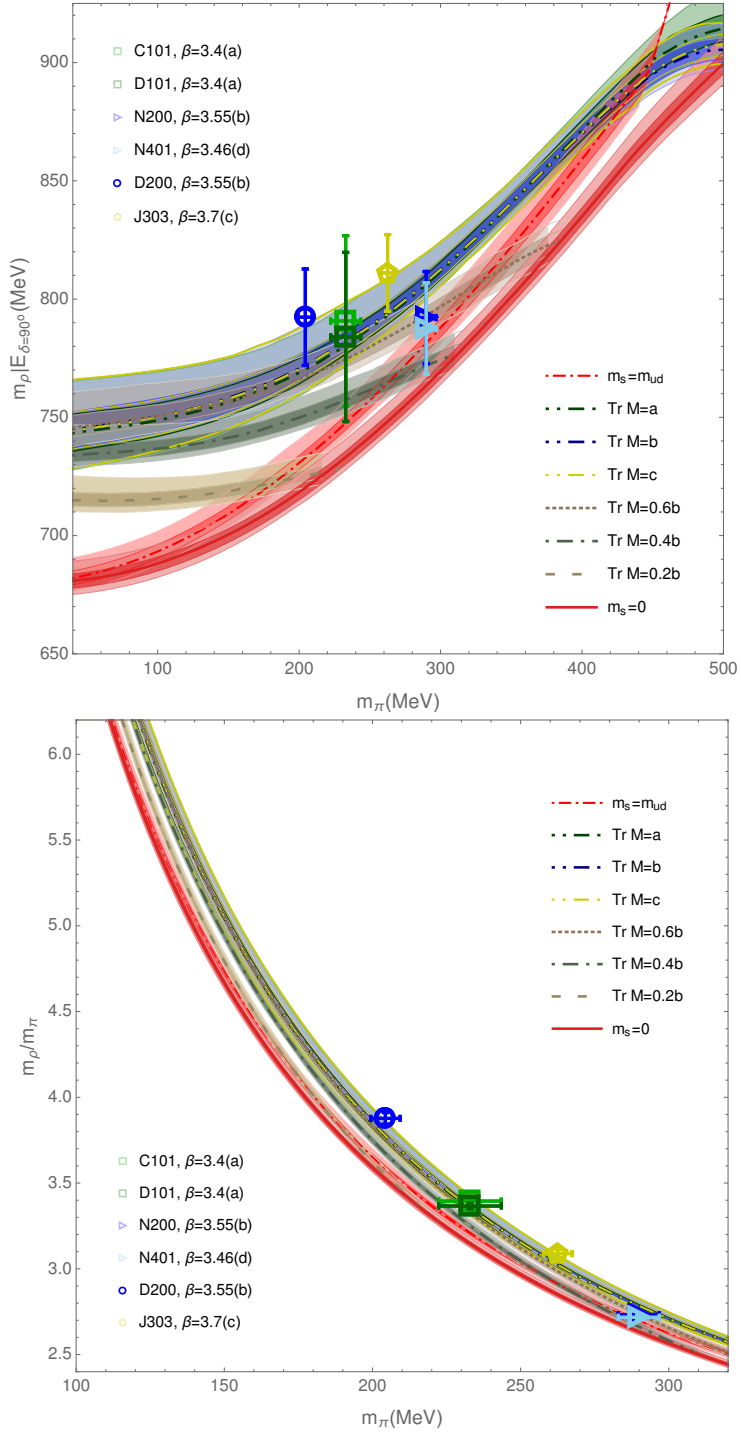


Fig. 8. Same as Fig. 7, but for the $\text{Tr} M = c$ trajectories in comparison with that for the $m_s = 0$ and $m_s = m_u$ trajectories, and lattice data.

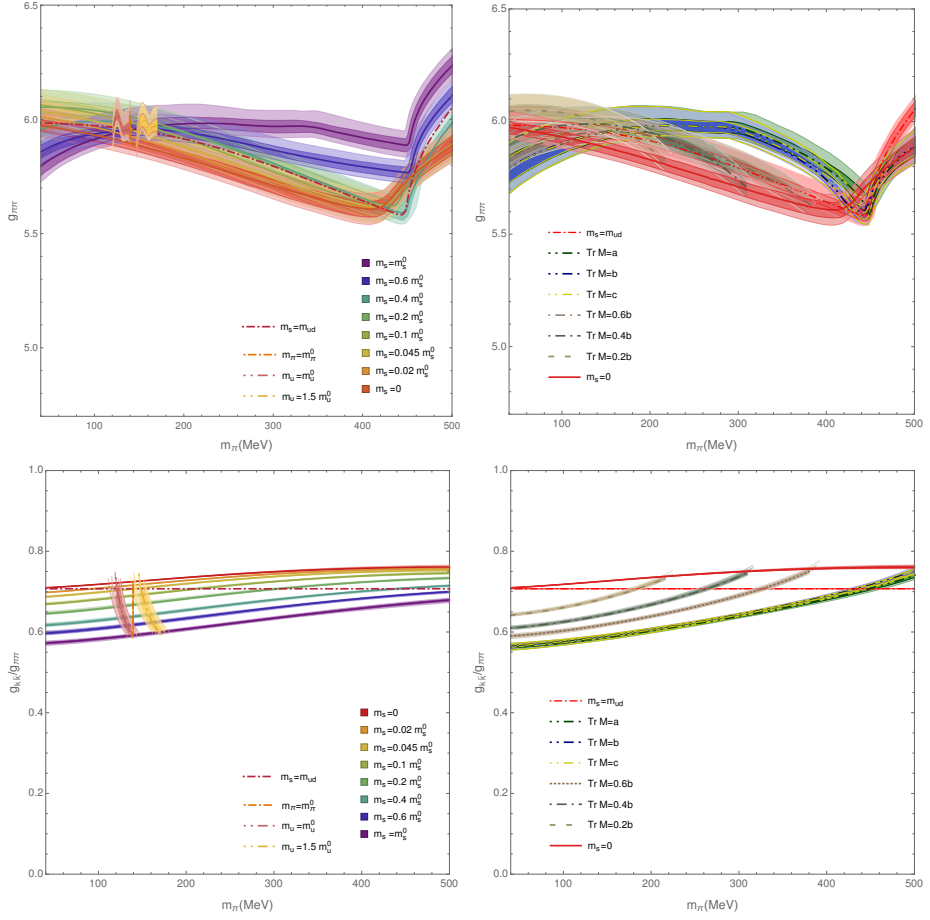


Fig. 9. Top: couplings of the rho meson to the $\pi\pi$ channel in different chiral trajectories; Bottom: the ratio $g_{K\bar{K}}/g_{\pi\pi}$ in different chiral trajectories.

ward to investigate more on these chiral trajectories, which indeed provide useful information to push forward the field.

5 Acknowledgements

This work is partly supported by the Talento Program of the Community of Madrid and the Complutense University of Madrid, under the project with Ref. 2018-T1/TIC-11167. R.M. acknowledges financial support from the Fundaço de amparo  pesquisa do estado de So Paulo (FAPESP), processo No. 2017/02534-3. R. M. also acknowledges discussions with C. Bernard, S. Schaefer, M. Bruno, and to the MILC Collaboration, and J. Bulava for providing the data.

References

1. M. Bruno, T. Korzec and S. Schaefer, *Phys. Rev. D* **95** (2017) no.7, 074504
2. C. Andersen, J. Bulava, B. Hörz and C. Morningstar, *Nucl. Phys. B* **939** (2019) 145
3. T. Blum *et al.* [RBC and UKQCD Collaborations], *Phys. Rev. D* **93** (2016) no.7, 074505
4. A. Bazavov *et al.* [MILC Collaboration], *PoS LATTICE* **2010** (2010) 074
5. A. Bazavov *et al.* [MILC Collaboration], *Rev. Mod. Phys.* **82** (2010) 1349
6. C. Aubin, J. Laiho and R. S. Van de Water, *PoS LATTICE* **2008** (2008) 105
7. J. J. Dudek *et al.* [Hadron Spectrum Collaboration], *Phys. Rev. D* **87** (2013) no.3, 034505
Erratum: [*Phys. Rev. D* **90** (2014) no.9, 099902]
8. D. J. Wilson, R. A. Briceño, J. J. Dudek, R. G. Edwards and C. E. Thomas, *Phys. Rev. D* **92** (2015) no.9, 094502
9. J. Bulava, B. Fahy, B. Hörz, K. J. Juge, C. Morningstar and C. H. Wong, *Nucl. Phys. B* **910** (2016) 842
10. T. N. Truong, *Phys. Rev. Lett.* **61** (1988) 2526.
11. J. Gasser and H. Leutwyler, *Annals Phys.* **158** (1984) 142.
12. J. Gasser and H. Leutwyler, *Nucl. Phys. B* **250** (1985) 465.
13. A. Gomez Nicola and J. R. Pelaez, *Phys. Rev. D* **65** (2002) 054009
14. J. Nebreda and J. R. Pelaez, *Phys. Rev. D* **81** (2010) 054035
15. B. Hu, R. Molina, M. Döring and A. Alexandru, *Phys. Rev. Lett.* **117**, no. 12, 122001 (2016)
16. B. Hu, R. Molina, M. Döring, M. Mai and A. Alexandru, *Phys. Rev. D* **96** (2017) no.3, 034520
17. S. Aoki *et al.* [Flavour Lattice Averaging Group], arXiv:1902.08191 [hep-lat].
18. D. Guo, A. Alexandru, R. Molina and M. Döring, *Phys. Rev. D* **94** (2016) no.3, 034501



Electromagnetic Form Factors of the Nucleons, the Δ , and the Hyperons

W. Plessas

Theoretical Physics, Institute of Physics, University of Graz, A-8010 Graz, Austria

Abstract. We discuss the electromagnetic structures of baryons on the basis of a unified relativistic constituent quark model. After recalling the covariant nucleon elastic form factors including their flavor decompositions we continue on the same route towards the Δ , Λ , Σ , and Ω form factors. Specific features of elastic electromagnetic form factors of baryons belonging to either octet or decuplet flavor multiplets are exemplified.

In order to be meaningful and comprehensively applicable, any effective tool for the description of low-energy hadronic physics has not only to reproduce the hadron spectroscopy but must also correctly provide for the hadron structures as seen in reactions with external probes. Nowadays we have a wealth of experimental data especially from electron scattering, which put stringent tests on electromagnetic form factors. This is particularly true for the nucleons, as one has gained specific insights into the flavor compositions of both the proton and neutron elastic form factors [1–4].

For now almost two decades the Graz group has studied the electroweak structures of baryons along a relativistic constituent quark model (RCQM) that had already provided for a reasonable description of the baryon spectra with u , d , and s flavors based on the dynamics of Goldstone-boson exchange (GBE) [5,6]. As we discussed at the 2018 Bled Mini-Workshop the same model has subsequently been extended to reach a unified description of the spectroscopy of all known baryons [7,8].

The investigations of the baryon electromagnetic structures started, of course, with the nucleons, whose form factors are most comprehensively and most accurately measured in experiments. Already in 2000 and the following years it was found that the covariant predictions for the elastic proton and neutron form factors as well as their electric radii and magnetic moments were obtained (without any introduction of additional parameters beyond the already established GBE RCQM) in surprisingly good agreement with phenomenological data [9–11]. We remark that a similarly good performance had then be obtained also with regard to the axial and induced pseudoscalar form factors, G_A and G_P , of the nucleons as well as the axial charge g_A [10,12]. All the predictions for covariant electroweak form factors have been calculated in the framework of point-form relativistic dynamics and thus all symmetry requirements of the Poincaré group could be fulfilled.

Once the flavor components in the nucleon electromagnetic form factors had been revealed by the analysis of the world data from elastic electron scattering on both the proton and neutron (under the assumption of charge symmetry), the GBE RCQM was also subject to these compelling tests. The model passed them quite satisfactorily [13]. As a result, all aspects of the elastic electromagnetic nucleon structures up to momentum transfers of $Q^2 \sim 4 \text{ GeV}^2$ have been well explained. Of course, such subtle, and still lasting, problems like the differences of proton electric radii from distinct measurements (see, e.g., the values reported by the Particle Data Group [14] and the corresponding references therein) could not be resolved in the framework of a RCQM.

Here, we like to add the remark that the probing of the nucleon structure not only in electromagnetic and weak processes but also by strong and gravitational interactions has likewise led to satisfactory results. The covariant predictions of the πNN vertex form factor $G_{\pi\text{NN}}$, including the πNN coupling constant $f_{\pi\text{NN}}$, as well as the gravitational form factor $A(Q^2)$ all turn out as quite reasonable [15,16]. For a more detailed discussion of these aspects see the review in ref. [17].

The lessons that had been learned from the investigations addressed above were in the first instance:

- It is most important to have nucleon/baryon wave functions including all, even small, symmetry components supported by spatial, angular momentum, spin, flavor, and color degrees of freedom.
- A fully relativistic framework must be employed such that frame independence is met.
- Current conservation must be guaranteed for.

In this spirit we have subsequently extended the investigations of the electromagnetic and axial structures to all of the baryons with u , d , and s flavors [18–21]. Except for baryon magnetic moments and electric radii, already studied in ref. [11], there are hardly any further experimental data available. However, one can compare with a series of results from lattice quantum chromodynamics (QCD). In particular, such results exist by various groups for the electromagnetic form factors of the Δ , Λ , Σ , Ξ , and the Ω , see, e.g., refs. [22,15,24,25]. Of course, such comparisons must be taken with care, since the same lattice-QCD calculations may not be entirely reliable, as they are facing already problems in the nucleon sector, especially with the description of the neutron electric form factor in comparison with experimental data, and they still exhibit considerable uncertainties. Additional doubts may be put on previous lattice-QCD calculations of electromagnetic form factors due to opposite-parity contaminations in the lattice data [11]; see also the contribution by Finn M. Stokes in the present proceedings.

Some of our results for electromagnetic form factors of singlet, octet, and decuplet baryons have already been published in refs. [13,17,21,27], and we refrain from repeating them here. In refs. [13,27] we have also presented flavor decompositions of the Λ , Σ , and Δ electromagnetic form factors. All of the predictions by the GBE RCQM appear to be quite reasonable, and no striking failures are found for the electromagnetic structures of the nucleon, Δ , and hyperon ground states.

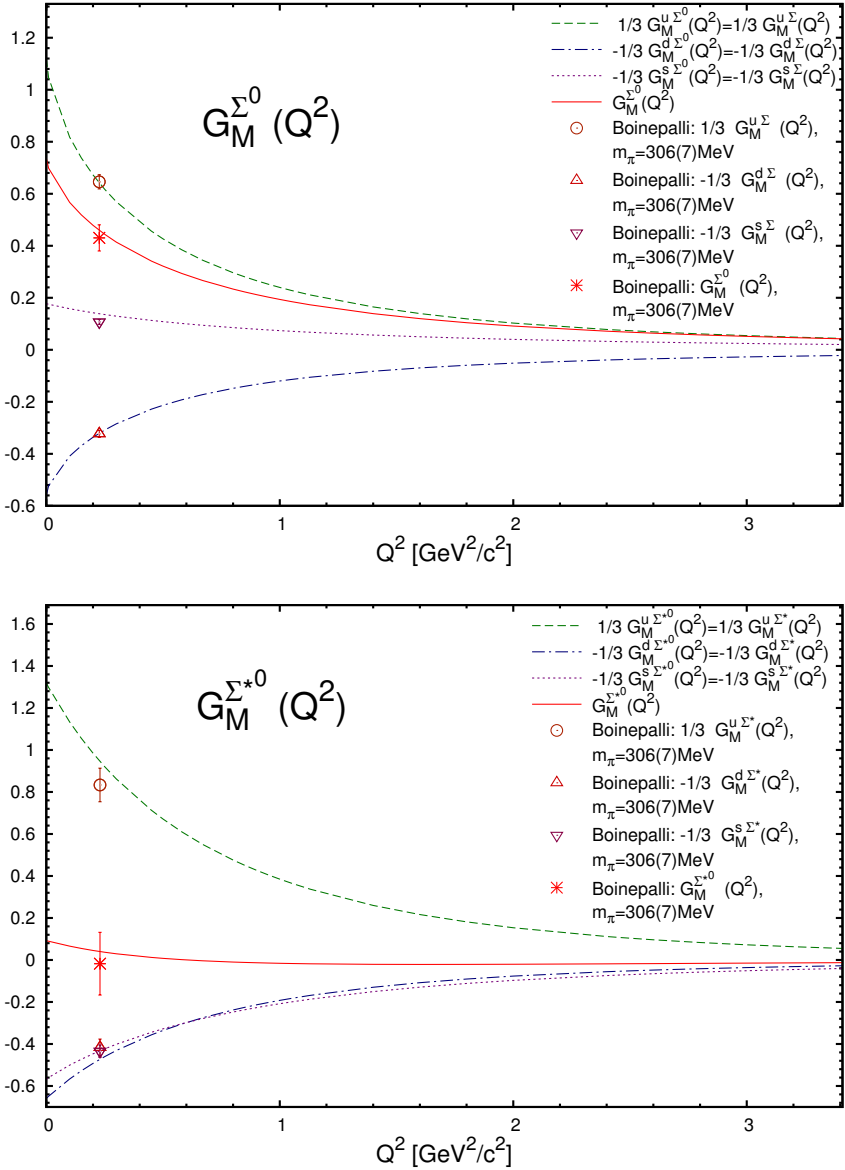


Fig. 1. Comparison of the elastic magnetic form factors of the octet $\Sigma^0(u, d, s)$ and the decuplet $\Sigma^{*0}(u, d, s)$ together with their individual $u, d,$ and s flavor contents as predicted by the GBE RCQM [5] under the assumption of charge symmetry. The data points at $Q^2=0.227$ GeV² are due to the lattice-QCD calculations by Boinepalli et al. [15,24].

In order to stress the necessity for refined baryon wave functions for applications beyond spectroscopy, we show here only a comparison of the distinct features of the flavor compositions of form factors of hyperons with the same flavor contents but belonging to different flavor multiplets, i.e. either to the octet

or decuplet. Take, for instance, the octet $\Sigma^0(u, d, s)$ vs. the decuplet $\Sigma^{*0}(u, d, s)$ ground states. While the flavor part of the latter is completely symmetric, the one of the former is mixed-symmetric, like the one of the neutron, say, sitting in the same octet. This has decisive consequences especially for magnetic form factors with regard to both the total results as well as the different flavor contributions. The situation is illustrated in Fig. 1. While the contributions by the u and d flavors are similar in both cases, the s contributions are completely different. They come even with different signs, what is simply a consequence of the distinct flavor symmetries in the pertinent wave functions.

Quite similar behaviours as shown in Fig. 1 are found for the octet $\Xi(d, s, s)$ and the decuplet $\Xi^*(d, s, s)$, which have again the same flavor contents. These findings simply stress the necessity of having baryon wave functions with accurate flavor components in interplay with the other (spatial, angular momentum, spin, and color) ingredients.

From the results of our investigations one may conclude that $\{QQQ\}$ valence-quark degrees of freedom are essentially sufficient to reproduce the electromagnetic structures of baryons (elastic form factors) at low momentum transfers. Higher Fock components play no or at most a minor role. Explicit π (and maybe other mesonic) contributions will finally have to be included in order to reach a more accurate and a more consistent description, especially in concordance with excited resonance states, e.g., for $N \rightarrow \Delta$ electromagnetic transitions.

First attempts to simultaneously cover the nucleons (as ground states) and their first few excitations (as true resonant states) are under way along coupled-channels (CC) RCQMs. So far only the bare \tilde{N} and $\tilde{\Delta}$ states coupled to $\pi\tilde{N}$ and $\pi\tilde{\Delta}$ channels have been considered [28,29]. One has seen that coupling of bare $\{Q\tilde{Q}Q\}$ states to these channels produces pionic effects in the N mass of about 10-15 %. For the form factors, however, the corresponding effects are tentatively found to be smaller [30–32]. It will be a challenging task for future investigations to treat the baryon ground states together with their resonances in CC frameworks both with regard to spectroscopy as well as all kind of form factors and reactions.

Acknowledgements

The author is very grateful to Bojan Golli, Mitja Rosina, and Simon Sirca for their continuous efforts of organizing every year the Bled Mini-Workshops. These meetings, largely characterized by an informal atmosphere, serve as a valuable institution of exchanging ideas and of mutual learning among an ever growing community of participating colleagues engaged in hadronic physics. In 2019 we have enjoyed the 21st edition thereof, and our best wishes are due for many more such Mini-Workshops to happen in the future. Corresponding efforts should be supported in every respect.

Results of the GBE RCQM regarding electromagnetic baryon form factors cited and addressed in this contribution have mainly been obtained in collaboration with Robert Wagenbrunn, Ki-Seok Choi, and Martin Rohmoser.

References

1. G. D. Cates, C. W. de Jager, S. Riordan and B. Wojtsekhowski, *Phys. Rev. Lett.* **106**, 252003 (2011)
2. I. A. Qattan and J. Arrington, *Phys. Rev. C* **86**, 065210 (2012)
3. M. Diehl and P. Kroll, *Eur. Phys. J. C* **73**, 2397 (2013)
4. I. A. Qattan, J. Arrington and A. Alsaad, *Phys. Rev. C* **91**, 065203 (2015)
5. L. Y. Glozman, W. Plessas, K. Varga, and R. F. Wagenbrunn, *Phys. Rev. D* **58**, 094030 (1998)
6. L. Y. Glozman, Z. Papp, W. Plessas, K. Varga, and R. F. Wagenbrunn, *Phys. Rev. C* **57**, 3406 (1998).
7. J. P. Day, K.-S. Choi, and W. Plessas, *Few-Body Syst.* **54**, 329 (2013)
8. W. Plessas, in: Proceedings of the Mini-Workshop *Double-Charm Baryons and Dimesons*, Bled, Slovenia, ed. by B. Golli, M. Rosina, and S. Sirca. Bled Workshops in Physics **19**, 18 (2018)
9. R. F. Wagenbrunn, S. Boffi, W. Klink, W. Plessas, and M. Radici, *Phys. Lett. B* **511**, 33 (2001)
10. S. Boffi, L. Y. Glozman, W. Klink, W. Plessas, M. Radici, and R. F. Wagenbrunn, *Eur. Phys. J. A* **14**, 17 (2002)
11. K. Berger, R. F. Wagenbrunn, and W. Plessas, *Phys. Rev. D* **70**, 094027 (2004)
12. L. Y. Glozman, M. Radici, R. F. Wagenbrunn, S. Boffi, W. Klink, and W. Plessas, *Phys. Lett. B* **516**, 183 (2001)
13. M. Rohrmoser, K. S. Choi, and W. Plessas, *Acta Phys. Polon. Supp.* **6**, 371 (2013)
14. M. Tanabashi *et al.* [Particle Data Group], *Phys. Rev. D* **98**, 030001 (2018)
15. T. Melde, L. Canton, and W. Plessas, *Phys. Rev. Lett.* **102**, 132002 (2009)
16. J. P. Day, PhD Thesis, University of Graz (2013)
17. W. Plessas, *Int. J. Mod. Phys. A* **30**, 1530013 (2015)
18. K.-S. Choi, W. Plessas, and R. F. Wagenbrunn, *Phys. Rev. C* **81**, 028201 (2010)
19. K.-S. Choi, W. Plessas, and R. F. Wagenbrunn, *Phys. Rev. D* **82**, 014007 (2010); *ibid.* 039901 (2010)
20. K.-S. Choi, W. Plessas, and R. F. Wagenbrunn, *Few-Body Syst.* **50**, 203 (2011)
21. K.-S. Choi and W. Plessas, *Few-Body Syst.* **54**, 1055 (2013)
22. C. Alexandrou, *Prog. Part. Nucl. Phys.* **67**, 101 (2012)
23. S. Boinepalli, D. B. Leinweber, A. G. Williams, J. M. Zanotti and J. B. Zhang, *Phys. Rev. D* **74**, 093005 (2006)
24. S. Boinepalli, D. B. Leinweber, P. J. Moran, A. G. Williams, J. M. Zanotti and J. B. Zhang, *Phys. Rev. D* **80**, 054505 (2009)
25. H. W. Lin and K. Orginos, *Phys. Rev. D* **79**, 074507 (2009)
26. F. M. Stokes, W. Kamleh and D. B. Leinweber, *Phys. Rev. D* **99**, 074506 (2019)
27. M. Rohrmoser, K. S. Choi, and W. Plessas, *Few-Body Syst.* **58**, 83 (2017)
28. R. A. Schmidt, L. Canton, W. Schweiger and W. Plessas, *J. Phys. Conf. Ser.* **738**, 012045 (2016)
29. R. A. Schmidt, L. Canton, W. Plessas and W. Schweiger, *Few-Body Syst.* **58**, 34 (2017)
30. B. Pasquini and S. Boffi, *Phys. Rev. D* **76**, 074011 (2007)
31. J. H. Jung, W. Schweiger and E. P. Biernat, *Few-Body Syst.* **60**, 13 (2019)
32. W. Plessas and R. A. Schmidt, *Few-Body Syst.* in print



Heavy-Quark Exotics

Jonathan L. Rosner

Enrico Fermi Institute, University of Chicago, 5640 Ellis Avenue, Chicago, IL 60637

Abstract. The heavy quarks c and b stabilize exotic meson ($qq\bar{q}\bar{q}$) and baryon ($qqqq\bar{q}$) states. We discuss work with M. Karliner on molecules containing $c\bar{c}$ and $b\bar{b}$; the first doubly charmed baryon; isospin splittings; Ξ_{cc}^+ = ccd and Ω_{cc} = ccs masses; lifetimes; tetraquarks stable under strong and electromagnetic decay; excited Ω_c states; and P-wave excitation energies.

In 1964 M. Gell-Mann [1] and G. Zweig [2] proposed that the known mesons were $q\bar{q}$ and baryons qqq , with quarks known at the time u (“up”), d (“down”), and s (“strange”) having charges $(2/3, -1/3, -1/3)$. Mesons and baryons would then have integral charges. Mesons such as $qq\bar{q}\bar{q}$ and baryons such as $qqqq\bar{q}$ would also have integral charges. Why weren’t they seen? They *have* now been seen, as “molecules” of heavy-quark hadrons or as deeply bound states involving heavy quarks (charm and bottom).

An early prediction of exotics was based on duality between s -channel and t -channel processes [3]. In antiproton-proton scattering, $q\bar{q}$ is dual to $qq\bar{q}\bar{q}$, predicting “exotic” $qq\bar{q}\bar{q}$ mesons. Where would they occur? One picture of resonance formation is based on $q\bar{q}$ annihilation [4]. If p^* is the momentum of each colliding particle in their center of mass, the first (meson-meson, meson-baryon) resonance forms for $p^* < (350, 250)$ MeV. Optical reasoning then leads one to expect the first baryon-antibaryon resonance to form for $p^* < 200$ MeV. The first “baryonium” candidate was actually the pion [5], envisioned as a nucleon-antinucleon bound state.

A QCD string picture can distinguish a standard $q\bar{q}$ meson, a standard baryon, and an exotic meson from one another. If decays occur via quark pair production (breaking of a QCD string), a $qq\bar{q}\bar{q}$ meson will either decay to baryon-antibaryon or to an ordinary meson plus an exotic one. It was proposed [3] to search for exotic mesons in the backward direction of a meson-baryon collision. Such exotics may fall apart into meson pairs and may be too broad to show up as distinct resonant peaks. No resonances made of u, d, s have been seen which would correspond to $qq\bar{q}\bar{q}$ but not $q\bar{q}$ (e.g., $u\bar{u}d\bar{s}$ decaying to $K^+\pi^+$). Similarly, pentaquark states ($4q\bar{q}$) made only of u, d, s have not been confirmed. R. Jaffe made an extensive study of $qq\bar{q}\bar{q}$ states within the bag model of QCD [6]. Light diquark-antidiquark states could be familiar ones with masses of a GeV or less.

The situation changed with heavy quarks c (charm) and b , which act to stabilize exotic configurations. The charmed quark was introduced in 1964 to preserve

lepton-quark symmetry [7]. The suppression of higher-order weak corrections led Glashow, Iliopoulos, and Maiani [8] to estimate $m_c \simeq 2 \text{ GeV}/c^2$, while Gaillard and Lee (1973) [9] studied the charmed quark's role in gauge theories. Evidence for the charmed quark c appeared in the $c\bar{c}$ bound state J/ψ [10,11]. An abundant charmonium ($c\bar{c}$) spectrum is still evolving.

Particles with one charmed quark also display a rich spectrum. The large value of m_c allows nonrelativistic quantum mechanics to provide some insights. Evidence for a third quark-lepton family began with observation of the τ lepton [12]. The quark-lepton analogy then implied the existence of a quark doublet (t [top], b [bottom]), first predicted by Kobayashi and Maskawa [13] to explain CP violation. Evidence for the b quark came from observation in 1977 at Fermilab of the first members of the Υ family of spin-1 $b\bar{b}$ particles produced in proton-proton interactions, decaying to $\mu^+\mu^-$ [14]. Today there is a rich spectroscopy both of $b\bar{b}$ states and of “ B ” mesons containing a single b quark. Decays of particles with b quarks are an active field. The top quark, discovered in 1995 at the Fermilab Tevatron [15], has a mass $m_t \simeq 173 \text{ GeV}$ so large that it decays too rapidly to have interesting spectroscopy.

The first genuine exotic, $X(3872)$, was seen decaying to $J/\psi\pi^+\pi^-$ by the Belle Collaboration in 2003 [16], and confirmed by CDF [17], D0 [18], and BaBar [19]. Its identification as a $D^0\bar{D}^{*0} + \text{c.c.}$ molecule comes from its proximity to $D^0\bar{D}^{*0}$ threshold: $M(X) = (3871.69 \pm 0.17) \text{ MeV} \simeq M(D^0) + M(\bar{D}^{*0}) = (3871.68 \pm 0.07) \text{ MeV}$. Its decay $X \rightarrow \gamma J/\psi$ is seen, implying $C(X) = +$ and some admixture of $c\bar{c}$ in its wave function. The angular distribution of its decay products implies $J^{PC} = 1^{++}$ as expected for an S-wave state of $D^0\bar{D}^{*0} + \text{c.c.}$ [20]. C invariance implies the $\pi^+\pi^-$ pair in its decay has negative C, as in a ρ meson. The large value of $M(D^{(*)+}) - M(D^{(*)0})$ implies little $D^{(*)\pm}$ in its wave function. The comparable rates for $\Gamma(X \rightarrow \omega J/\psi)$ and $\Gamma(X \rightarrow J/\psi\rho)$ are what one would expect for a state with a $c\bar{c}u\bar{u}$ admixture. In addition to the $X(3872)$ (a mixture of $2^3P_1 c\bar{c}$ and $J^{PC} = 1^{++} c\bar{c}u\bar{u}$) one expects an orthogonal mixture, typically above 3900 MeV in potential models.

The Belle Collaboration saw unexpected structures $Z_b(10610, 10650)$ in $M[\pi^\pm\Upsilon(1S, 2S, 3S)]$ when studying $\Upsilon(10865) \rightarrow \Upsilon(1S, 2S, 3S)\pi^+\pi^-$ [21] (Fig. 1). All spectra showed peaks at $M(\Upsilon(nS)\pi) = 10.61$ and 10.65 GeV , within a few MeV of $M(B) + M(\bar{B}^*)$ and $M(B^*) + M(\bar{B}^*)$. These look like S-wave molecules of $B\bar{B}^*$ (+c.c.) and $B^*\bar{B}^*$.

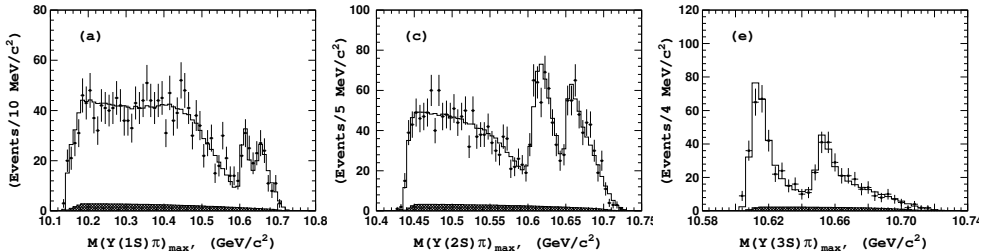


Fig. 1. Mass spectra $M(\Upsilon(1S, 2S, 3S)\pi^+)$ in $\Upsilon(10865) \rightarrow \Upsilon(1S, 2S, 3S)\pi^+\pi^-$ [21].

Evidence for $c\bar{c}uud$ configurations has been provided by LHCb [22], who observed bumps in the J/ψ p invariant mass in the decay $\Lambda_b \rightarrow K^- J/\psi p$ at 4380 and 4450 MeV. (See Fig. 2 for a production mechanism.)

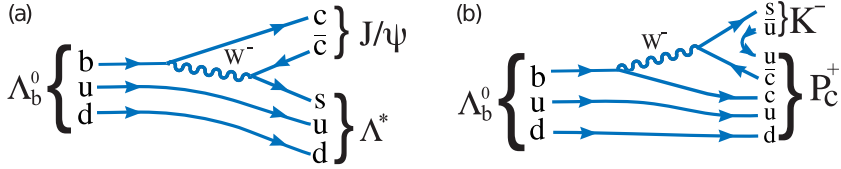


Fig. 2. Production mechanisms in Λ_b decays. Left: Λ^* excitation; right: P_c excitation.

The $K^- J/\psi p$ Dalitz plot (Fig. 3) is populated by many $I = 0$ $K^- p$ states. In an updated result [23], LHCb sees *three* narrow J/ψ resonances at 4311.9, 4440.3, 4457.3 MeV, with widths 9.8, 20.6, 6.4 MeV. The masses are near $\Sigma_c \bar{D}$ and $\Sigma_c \bar{D}^*$ thresholds; if these are molecules, their binding mechanism is unclear. One-pion exchange can't couple to $D\bar{D}$; $\pi^+ \pi^-$ exchange may favor $\Sigma_c \bar{D}$ over $D\bar{D}$: the lowest intermediate state is $\Lambda_c \bar{D}^*$ vs. $D^* \bar{D}^*$. The asymmetric behavior along $M(J/\psi p)$ bands indicates interference with opposite-parity amplitude(s).

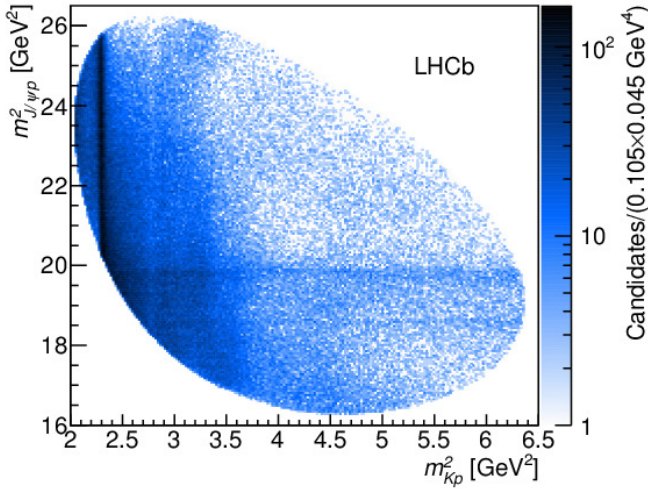


Fig. 3. $K^- J/\psi p$ Dalitz plot in $\Lambda_b \rightarrow K^- J/\psi p$ [23]

So far we have discussed $Q\bar{Q}q\bar{q}'$ or $Q\bar{Q}qqq'$ states, where $Q = \text{heavy}$, $q, q' = \text{light}$. Can we predict masses of (simpler) $QQ'q$ systems? The SELEX Collaboration at Fermilab [24] claimed states $\Xi_{cc}^{++}(3520) = ccu$ and $\Xi_{cc}^+(3460) = ccd$ which were not confirmed by others. Using constituent-quark masses, hyperfine splittings, and estimates of QQ' binding M. Karliner and I [25] predicted the masses in Table 1. In 2017 the LHCb Collaboration found a Ξ_{cc}^{++} candidate with mass 3621.40 ± 0.78 MeV [26], in accord with our estimate. Other estimates (> 30) had

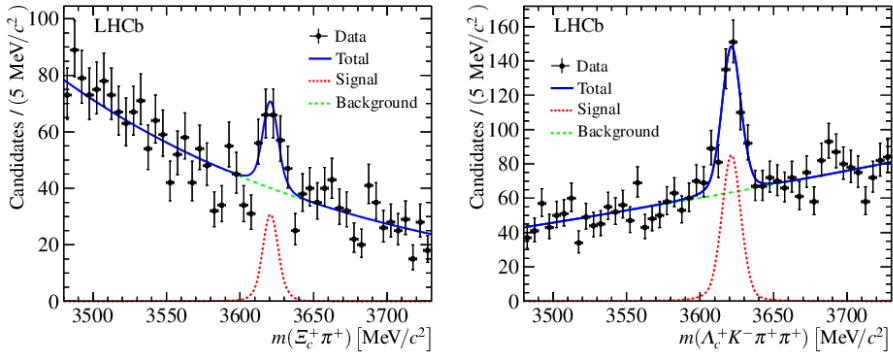
Table 1. Masses of ground-state doubly heavy baryons predicted in Ref. [25]

| State | Quark content | $M(J = 1/2)$ | $M(J = 3/2)$ |
|------------------|---------------|----------------|----------------|
| $\Xi_{cc}^{(*)}$ | ccq | 3627 ± 12 | 3690 ± 12 |
| $\Xi_{bc}^{(*)}$ | b[cq] | 6914 ± 13 | 6969 ± 14 |
| Ξ'_{bc} | b(cq) | 6933 ± 12 | – |
| $\Xi_{bb}^{(*)}$ | bbq | 10162 ± 12 | 10184 ± 12 |

a spread of at least 100 MeV. The spectra displaying the resonance are shown in Fig. 4. No peak is seen in $\Lambda_c K^- \pi^+$.

We predicted $\tau(\Xi_{cc}^{++,+}) = (185,53)$ fs. A $\Lambda_c K^- \pi^+$ peak is disfavored by the LHCb lifetime cut $\tau > 150$ fs. The Ξ_{cc}^{++} lifetime was measured by LHCb to be $256_{-22}^{+24} \pm 14$ fs [27]. The mass in the $\Xi_c^+ \pi^+$ channel was measured to be $3620.6 \pm 1.5 \pm 0.4 \pm 0.3$ MeV [28].

The masses of the doubly heavy baryons were calculated with inputs reproducing the light-quark baryons as shown in Table 2. One describes light-quark


Fig. 4. Spectra with evidence for Ξ_{cc}^{++} .

mesons with quark masses ~ 54 MeV less. $M(\Lambda_{c,b}) - M(\Lambda)$ implies $m_{c,b} = (1710.5, 5043.5)$ MeV. These masses are sufficient to describe nonstrange baryons with one c or b quark, when taking account of deeper cs or bs binding in baryons with one or two strange quarks and one charm or bottom quark (see Table 3). When demanding the same quark masses for mesons and baryons, one adds 161.5 MeV for a baryon string junction. The fit quality remains the same.

A quark pair is more deeply bound when neither is u or d. For example, the binding energy of a $c\bar{s}$ pair is $B(c\bar{s}) = [3M(D_s^*) + M(D_s)]/4 - m_s - m_c = -69.9$ MeV. If one assumes $B(cs)/B(c\bar{s}) = 1/2$ as for single-gluon exchange then $B(cs) = -35$ MeV. A similar calculation gives $B(bs) = -41.8$ MeV. One must rescale hyperfine interactions when neither quark is u or d. We take a cue from $M(D_s^*) - M(D_s) \simeq M(D^*) - M(D)$.

Table 2. Masses of light-quark baryons predicted with $m_u = m_d \equiv m_q = 363$ MeV, $m_s = 538$ MeV, and hyperfine interaction term $a/(m_q)^2 = 50$ MeV

| State (mass in MeV) | Spin | Expression for mass | Predicted mass (MeV) |
|---------------------|------|---------------------------------------|----------------------|
| N(939) | 1/2 | $3m_q - 3a/(m_q)^2$ | 939 |
| Δ (1232) | 3/2 | $3m_q + 3a/(m_q)^2$ | 1239 |
| Λ (1116) | 1/2 | $2m_q + m_s - 3a/(m_q)^2$ | 1114 |
| Σ (1193) | 1/2 | $2m_q + m_s + a/(m_q)^2 - 4a/m_q m_s$ | 1179 |
| Σ (1385) | 3/2 | $2m_q + m_s + a/(m_q)^2 + 2a/m_q m_s$ | 1381 |
| Ξ (1318) | 1/2 | $2m_s + m_q + a/(m_s)^2 - 4a/m_q m_s$ | 1327 |
| Ξ (1530) | 3/2 | $2m_s + m_q + a/(m_s)^2 + 2a/m_q m_s$ | 1529 |
| Ω (1672) | 3/2 | $3m_s + 3a/(m_s)^2$ | 1682 |

Table 3. Predicted masses of baryons containing one charm or bottom quark.

| Charmed baryons | | | Bottom baryons | | |
|-----------------------|------|-------------------|-----------------------|------|-------------------|
| State (M in MeV) | Spin | Predicted M (MeV) | State (M in MeV) | Spin | Predicted M (MeV) |
| Λ_c (2286.5) | 1/2 | Input | Λ_b (5619.5) | 1/2 | Input |
| Σ_c (2453.4) | 1/2 | 2444.0 | Σ_b (5814.3) | 1/2 | 5805.1 |
| Σ_c^* (2518.1) | 3/2 | 2507.7 | Σ_b^* (5833.8) | 3/2 | 5826.7 |
| Ξ_c (2469.3) | 1/2 | 2475.3 | Ξ_b (5792.7) | 1/2 | 5801.5 |
| Ξ_c' (2575.8) | 1/2 | 2565.4 | $\Xi_b'(-)$ | 1/2 | 5921.3 |
| Ξ_c^* (2645.9) | 3/2 | 2628.6 | Ξ_b^* (5949.7) | 3/2 | 5944.1 |
| Ω_c (2695.2) | 1/2 | 2692.1 | Ω_b (6046.4) | 1/2 | 6042.8 |
| Ω_c^* (2765.9) | 3/2 | 2762.8 | $\Omega_b^*(-)$ | 3/2 | 6066.7 |

Charm-anticharm binding gives $B(c\bar{c}) = [3M(J/\psi) + M(\eta_c)]/4 - 2m_c^m = -258$ MeV, so $B(cc) = -129$ MeV. Similar calculations give $B(bb) = -281.4$ MeV and $B(bc) = -167.8 \pm 3.0$ MeV, where the error reflects uncertainty in the B_c^* mass. One now can calculate the doubly heavy ground state baryon masses in Table 1.

A study of isospin splittings in doubly heavy baryons [29] was motivated by the large (60 MeV!) splitting between $\Xi_{cc}^+(3460)$ and $\Xi_{cc}^{++}(3520)$ claimed by SELEX [24]. It was found that $M(\Xi_{cc}^{++}) - M(\Xi_{cc}^+) = 2.17 \pm 0.11$ MeV if separate quark masses are used for light mesons and baryons, or 1.41 ± 0.12 MeV if universal masses are used. Contributions to mass differences are shown in Table 4. For details of these calculations and well-obeyed fits to known isospittings in light-quark and charmed baryons see Ref. [30]. In Table 5 we compare various predictions for $M(\Xi_{cc}^{++}) - M(\Xi_{cc}^+)$.

A spread of values is obtained, but nearly all are at most a few MeV. Some authors still entertain the possibility that the SELEX result is correct, with physics beyond standard model. This could be put to rest if LHCb sees a Ξ_{cc}^+ at or slightly

Table 4. Contributions to isospin splittings (HF=hyperfine interaction) if (separate, universal) quark masses are used.

| Parameter | Quantity | Contribution in MeV to | |
|-----------|-------------|------------------------|------------------------------------|
| | | $M(p) - M(n)$ | $M(\Xi_{cc}^{++}) - M(\Xi_{cc}^+)$ |
| Δ | $m_u - m_d$ | -2.48, -2.67 | -2.48, -2.67 |
| a | Coulomb | 1.02, 0.94 | 4.07, 3.77 |
| b | Strong HF | 0.67, 0.88 | -0.29, -0.33 |
| c | EM HF | -0.51, -0.43 | 0.86, 0.64 |
| | Total | -1.29, -1.29 | 2.17, 1.41 |

Table 5. Comparison of predictions for isospin splittings of Ξ_{cc} states.

| Author(s) | Reference | $M(\Xi_{cc}^{++}) - M(\Xi_{cc}^+)$ (MeV) |
|-------------------|--|---|
| Karliner + Itoh + | PR D 96 , 033004 (2017) PR D 61 , 057502 (2000) | $1.41 \pm 0.12^{+0.76}$ 4.7 |
| Brodsky + | PL B 698 , 251 (2011) | 1.5 ± 2.7 |
| Hwang + | PR D 78 , 073013 (2008) | 2.3 ± 1.7 |
| Borsanyi + | Science 347 , 1452 (2015) | $2.16 \pm 0.11 \pm 0.17$ |
| Lichtenberg | PR D 16 , 231 (1977) | 4.7 |
| Tiwari + | PR D 31 , 642 (1985) | 1.11 |
| Shah + Rai | EPJC 77 , 129 (2017) | -9 |

below 3620 MeV (an observation made more difficult by its expected short lifetime).

The “spectator” process $c \rightarrow sW^*$, where W^* goes to $(e^+\nu_e, \mu^+\nu_\mu, 3 \text{ colors of } u\bar{d})$, dominates Ξ_{cc}^{++} decay. One can emulate kinematic suppression with $\chi_{cc} \equiv [M(\Xi_c)/M(\Xi_{cc})]^2$:

$$\Gamma(\Xi_{cc}^{++}) = \frac{10G_F^2 M(\Xi_{cc}^{++})^5}{192\pi^3} F(\chi_{cc}), \quad F(\chi) \equiv 1 - 8\chi + 8\chi^3 - \chi^4 + 12 \ln(1/\chi),$$

implying $\tau(\Xi_{cc}^{++}) = 188 \text{ fs}$.

An additional “exchange” process $cd \rightarrow su$ contributes to $\Xi_{cc}^+ = ccd$ decay. The “spectator” partial width is $\Gamma_s = \hbar/\tau(\Xi_{cc}^{++}) = \hbar/(256 \text{ fs}) = 2.57 \times 10^{-12} \text{ GeV}$, while the “exchange” partial width is $\Gamma_e = 2[\hbar/\tau(\Xi_c^0) - \hbar/\tau(\Xi_c^+)] = 5.64 \times 10^{-12} \text{ GeV}$. Here we have used $\tau(\Xi_c^0) = 154.5 \pm 1.7 \pm 1.6 \pm 1.0 \text{ fs}$; $\tau(\Xi_c^+) = 458.8 \pm 3.6 \pm 2.9 \pm 3.1 \text{ fs}$ [31]. Adding the two, $\Gamma_s + \Gamma_e = 8.21 \times 10^{-12} \text{ GeV}$ implies $\tau(\Xi_{cc}^+) = 80 \text{ fs}$, our updated prediction.

One can predict the mass of $\Omega_{cc} = ccs$ using the methods just described. The strange quark is about 175 MeV heavier than nonstrange but more deeply bound to the cc diquark than the nonstrange quark. We compare the predictions for ccq and ccs in Table 6.

Table 6. Comparison of predictions for ccq and ccs ground-state baryon masses.

| $\Xi_{cc} = ccq$ | | $\Omega_{cc} = ccs$ | |
|------------------|-----------------|---------------------|-----------------|
| Contribution | Value (MeV) | Contribution | Value (MeV) |
| $2m_c + m_q$ | 3789.0 | $2m_c + m_s$ | 3959.0 |
| cc binding | -129.0 | cc binding | -129.0 |
| $a_{cc}/(m_c)^2$ | 14.2 | $a_{cc}/(m_c)^2$ | 14.2 |
| $-4a/m_q m_c$ | -42.4 | $-4a'/m_s m_c$ | -42.4 |
| Total | 3626.8 ± 12 | Subtotal | 3801.8 ± 12 |

The additional binding of s to cc is -109.4 ± 10.5 MeV, giving $M(\Omega_{cc}) = 3692 \pm 16$ MeV, $M(\Omega_{cc}^*) = 3756 \pm 16$ MeV. With universal quark masses and a 161.5 MeV “string junction” term for baryons one predicts $M(\Omega_{cc}) \sim 40$ MeV higher.

M. Karliner and I investigated $QQ'\bar{u}\bar{d}$ systems [32], where $Q, Q' = c$ or b . We found $cc\bar{u}\bar{d}$ unbound; it could decay to DD^* or $DD\gamma$. The lowest-lying $bc\bar{u}\bar{d}$ state was near $BD\gamma$ threshold and could be bound. We predicted $M(bb\bar{u}\bar{d}) = 10,389 \pm 12$ MeV, 215 MeV below B^-B^{*0} threshold and 170 MeV below $B^-B^0\gamma$ threshold. Regarding bb as a color- 3^* diquark (transforming under QCD as an antiquark), fermi statistics required its spin to be 1. The lightest $\bar{q}\bar{q}'$ state ($q, q' = u, d$) is a color-3 $\bar{u}\bar{d}$ state with isospin zero; fermi statistics require its spin to be zero. The mass prediction then relies on accounting for constituent-quark masses, hyperfine interactions, and binding effects (Table 7).

Table 7. Contributions (in MeV) to mass of lightest $QQ'\bar{q}\bar{q}'$ tetraquark.

| $cc\bar{u}\bar{d}, J^P = 1^+$ | | $bc\bar{u}\bar{d}, J^P = 0^+$ | | $bb\bar{u}\bar{d}, J^P = 1^+$ | |
|-------------------------------|---------------|-------------------------------|---------------|-------------------------------|----------------|
| Contribution | Value | Contribution | Value | Contribution | Value |
| $2m_c^b$ | 3421.0 | $m_b + m_c$ | 6754.0 | $2m_b^b$ | 10087.0 |
| $2m_q^b$ | 726.0 | $2m_q^b$ | 726.0 | $2m_q^b$ | 726.0 |
| cc hyperfine | 14.2 | bc hyperfine | -25.5 | bb hyperfine | 7.8 |
| $-3a/(m_q^b)^2$ | -150.0 | $-3a/(m_q^b)^2$ | -150.0 | $-3a/(m_q^b)^2$ | -150.0 |
| cc binding | -129.0 | bc binding | -170.8 | bb binding | -281.4 |
| Total | 3882 ± 12 | Total | 7134 ± 13 | Total | 10389 ± 12 |

Spin zero is allowed for the $bc\bar{u}\bar{d}$ state, taking advantage of the attractive bc hyperfine interaction. Since $M(cc\bar{u}\bar{d}) > M(D^0) + M(D^+) = 3734$ MeV, it can decay to $D^0D^+\gamma$ (decay to D^0D^+ is forbidden). We cannot tell whether $M(bc\bar{u}\bar{d})$ is less than $M(D^0) + M(B^0) = 7144$ MeV. The estimated lifetime of the $bb\bar{u}\bar{d}$ state is 367 fs.

The LHCb Collaboration has presented evidence for five narrow Ω_c^* states decaying to $\Xi_c^+K^-$ [33]. (Already known were the ground ccs states: $\Omega_c(2695, 1/2^+)$)

and $\Omega_c^*(2766, 3/2^+)$ [4].) Marek Karliner and I [35] identified the narrow states as five P-wave excitations, with an alternative assignment of the two highest-mass states as positive-parity radial excitations of the ground states. In that case two $J^P = 1/2^-$ states would remain to be seen, one around 2904 MeV decaying to $\Omega_c \gamma$ and/or $\Omega_c \pi^0$, and the other around 2978 MeV decaying to $\Xi_c^+ K^-$ in an S-wave.

What does it cost to excite a hadron from S-wave to P-wave [36]? Defining a residual energy $\Delta E_R \equiv \Delta E_{PS} - B_{12}$, where B_{12} is the binding energies of constituents, we found a good fit with $\Delta E_R = (417.37 - 0.2141 \mu_{12})$ MeV, where μ_{12} is the reduced mass.

The prospects for exotic mesons and baryons (beyond $q\bar{q}$ and qqq) are bright. They *do* exist; molecular configurations are at least part of the story. Heavy quarks have a lower kinetic energy and help to stabilize exotic configurations containing them. Techniques for mass estimation (constituent-quark masses, hyperfine interactions, and binding effects) are relatively straightforward and are starting to be tested for $QQ'q$ baryons. One frontier is states $Q_1 Q_2 \bar{Q}_3 \bar{Q}_4$ with all quarks heavy. Are there any $cc\bar{c}$ lighter than $2M(\eta_c)$? Are there any $bb\bar{b}$ lighter than $2M(\eta_b)$? Can the quark-level analogue of nuclear fusion [37] be put to use? Still to be known is what it costs to produce one or more extra heavy quarks via the strong interactions. When do two heavy quarks end up in the same hadron?

My thanks to M. Gronau and M. Karliner for many enjoyable collaborations, and to the Organizers and to the Enrico Fermi Institute for their welcome support.

References

1. M. Gell-Mann, Phys. Lett. B **8**, 214 (1964).
2. G. Zweig, CERN-TH-401; Developments in the Quark Theory of Hadrons, Volume 1, edited by D. Lichtenberg and S. Rosen, p. 22.
3. J. L. Rosner, Phys. Rev. Lett. **21**, 950 (1968).
4. J. L. Rosner, Phys. Rev. D **6**, 2717 (1972).
5. E. Fermi and C. N. Yang, Phys. Rev. **76**, 1739 (1949).
6. R. L. Jaffe, Phys. Rev. D **15**, 267, 281 (1977); Phys. Rev. D **17**, 1444 (1978).
7. J. D. Bjorken and S. L. Glashow, Phys. Lett. **11**, 255 (1964); Z. Maki and Y. Ohnuki, Prog. Theor. Phys. **32**, 144 (1964); Y. Hara, Phys. Rev. **134**, B701 (1964); D. Amati, H. Bacry, J. Nuyts, and J. Prentki, Nuovo Cim. **34**, 1732 (1964); Phys. Lett. **11**, 190 (1964).
8. S. L. Glashow, J. Iliopoulos, and L. Maiani, Phys. Rev. D **2**, 1285 (1970).
9. M. K. Gaillard and B. W. Lee, Phys. Rev. D **10**, 897 (1973).
10. J. J. Aubert *et al.* [E598 Collaboration], Phys. Rev. Lett. **33**, 1404 (1974).
11. J. E. Augustin *et al.* [SLAC-SP-017 Collaboration], Phys. Rev. Lett. **33**, 1406 (1974).
12. M. L. Perl *et al.*, Phys. Rev. Lett. **35**, 1489 (1975).
13. M. Kobayashi and T. Maskawa, Prog. Theor. Phys. **49**, 652 (1973).
14. S. W. Herb *et al.*, Phys. Rev. Lett. **39**, 252 (1977); W. R. Innes *et al.*, Phys. Rev. Lett. **39**, 1240 (1977); Erratum: [Phys. Rev. Lett. **39**, 1640 (1977)].
15. F. Abe *et al.* [CDF Collaboration], Phys. Rev. Lett. **74**, 2626 (1995); S. Abachi *et al.* [D0 Collaboration], Phys. Rev. Lett. **74**, 2632 (1995).
16. S. K. Choi *et al.* [Belle Collaboration], Phys. Rev. Lett. **91**, 262001 (2003).
17. D. Acosta *et al.* [CDF Collaboration], Phys. Rev. Lett. **93**, 072001 (2004).
18. V. M. Abazov *et al.* [D0 Collaboration], Phys. Rev. Lett. **93**, 162002 (2004).
19. B. Aubert *et al.* [BaBar Collaboration], Phys. Rev. D **71**, 071103 (2005).

20. K. Abe *et al.* [Belle Collaboration], contributed to 22nd International Symposium on Lepton-Photon Conference, arXiv:hep-ex/0505038.
21. A. Bondar *et al.* [Belle Collaboration], Phys. Rev. Lett. **108**, 122001 (2012).
22. R. Aaij *et al.* [LHCb Collaboration], Phys. Rev. Lett. **115**, 072001 (2015).
23. R. Aaij *et al.* [LHCb Collaboration], Phys. Rev. Lett. **122**, 222001 (2019).
24. M. Mattson *et al.* [SELEX Collaboration], Phys. Rev. Lett. **89**, 112001 (2002); A. Ocherashvili *et al.* [SELEX Collaboration], Phys. Lett. B **628**, 18 (2005); J. Engelfried [SELEX Collaboration], contribution to the proceedings of HQL06, Munich, 2006, eConf C 0610161, 003 (2006) [hep-ex/0702001].
25. M. Karliner and J. L. Rosner, Phys. Rev. D **90**, 094007 (2014).
26. R. Aaij *et al.* [LHCb Collaboration], Phys. Rev. Lett. **119**, 112001 (2017).
27. R. Aaij *et al.* [LHCb Collaboration], Phys. Rev. Lett. **121**, 052002 (2018).
28. R. Aaij *et al.* [LHCb Collaboration], Phys. Rev. Lett. **121**, 162002 (2018).
29. M. Karliner and J. L. Rosner, Phys. Rev. D **96**, 033004 (2017).
30. M. Karliner and J. L. Rosner, arXiv:1906.07799, submitted to Phys. Rev. D.
31. R. Aaij *et al.* [LHCb Collaboration], Phys. Rev. D **100**, 032001 (2019).
32. M. Karliner and J. L. Rosner, Phys. Rev. Lett. **119**, 202001 (2017). See also E. J. Eichten and C. Quigg, Phys. Rev. Lett. **119**, 202002 (2017).
33. R. Aaij *et al.* [LHCb Collaboration], Phys. Rev. Lett. **118**, 182001 (2017).
34. M. Tanabashi *et al.* [Particle Data Group], Phys. Rev. D **98**, 030001 (2018).
35. M. Karliner and J. L. Rosner, Phys. Rev. D **95**, 114012 (2017).
36. M. Karliner and J. L. Rosner, Phys. Rev. D **98**, 074026 (2018).
37. M. Karliner and J. L. Rosner, Nature **551**, 89 (2017).



Effect of intermediate resonances in the quark-photon vertex

Hèlios Sanchis-Alepuz

University of Graz, A-8010 Graz, Austria

Abstract. We summarise the main results of the paper [1] in which the effects on the quark-photon vertex of intermediate hadronic resonances in the quark-antiquark interaction kernel are studied. This is a first step in the long road of including non-valence contributions to hadron properties in the Bethe-Salpeter approach.

1 Introduction. Non-valence effects

A detailed and quantitatively reliable description of hadron structure at low and medium energy is a decade-old problem that is, curiously, becoming more and more relevant. Its most obvious goal is to characterize hadrons: we wish to be able to calculate their masses, radii, magnetic moments, axial charges, etc. Moreover, we expect to gain understanding of QCD as the theory of the strong interactions: for example, if we are able to interpret measurements of form factors, this gives us a handle on the underlying QCD mechanisms forming hadrons. But also, current experimental facilities searching for beyond Standard model (BSM) physics are mainly hadronic machines; therefore, in order to extract new physics from the measurements one must *convolute* possible effective BSM operators with hadronic states and then calculate the measurable effect. Example of these are the extraction of CKM elements from processes involving heavy mesons or attempts to measure quark electric dipole moments (EDM) from neutron EDMs, etc.

The study of QCD and, in particular, its non-perturbative aspects phenomena can be approached using Dyson-Schwinger (DSE) and Bethe-Salpeter (BSE) equations. DSEs are non-linear integral equations describing the Green's functions (GFs) of the theory and BSEs are linear integral equations for bound states. Even though a full non-perturbative treatment of the quark-photon vertex would require to solve the corresponding DSE, if one is interested in QCD effects only, these can be studied with equations simpler than DSEs, namely inhomogeneous BSEs. The combination of DSEs and (homogeneous and inhomogeneous) BSEs has been extensively and successfully used to study hadron phenomenology [2].

The complexity of non-perturbative calculations entails that nearly always some sort of approximation or simplification is necessary. In the context of DSEs and BSEs, it is necessary to truncate the infinite system of coupled DSEs that describe the theory and the infinite number of interaction terms in a BSE, as described below. Truncations of ever increasing sophistication that perform well

phenomenologically have been developed over the years (see e.g. [3,4,2,5] and references therein). However, the rainbow-ladder (RL) truncation of the BSE interaction kernel is the most sophisticated truncation used so far in the calculation of hadron form factors. Here, the quark-antiquark interaction kernel is simplified to a single-gluon exchange, augmented by an effective interaction, meant to include all other effects. Even though it performs remarkably well on the calculation of hadron form factors for spacelike momentum region, the trend in all cases is that the RL truncation is insufficient to describe the behaviour of form factors at low photon momentum. The reason for that is usually attributed to RL calculations lacking so-called meson-cloud effects on form factors, which stem from the photon coupling to non-valence quarks inside the hadron (sea quarks).

Meson-cloud effects are a manifestation of the presence of non-valence degrees of freedom inside a hadron, which which an external field can and does interact. In the BSE approach these can only appear in the BSE interaction kernel. An example of how this could happen is shown in Fig. 1.

In addition to providing meson-cloud effects, non-valence terms have other crucial implications, such as enabling virtual transitions that account for the non-vanishing decay width of some states or providing a source for the strangeness content of nucleons. We want to focus here on the former, since this suffices as we will see to generate the qualitatively correct analytic structure for a resonant solution of the BSE.

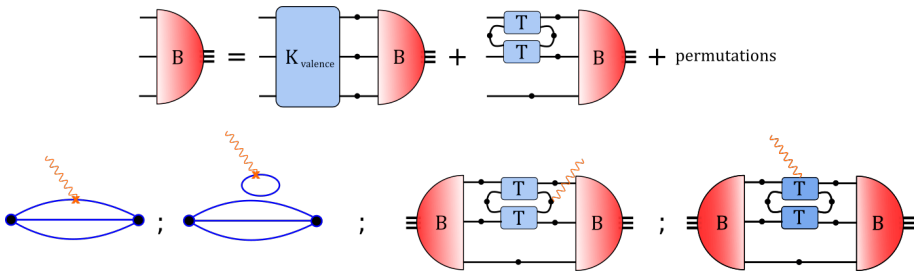


Fig. 1. (Upper panel) Schematic representation of a baryon (B) BSE. The term K_{valence} represents an interaction kernel with only valence quark lines. The last term represents, via the quark-antiquark scattering matrix T , non-valence contributions to the BSE kernel. Lines with blobs are fully-dressed quark propagators. (Lower panel) The first two diagrams show the coupling of an external current via current insertions (crosses) in a LQCD calculation (adapted from [6]), with the first diagram representing the coupling to valence quarks (connected contributions) and the second diagram the coupling to a non-valence quark (disconnected contribution). To the right we show two possible ways how, in a BSE calculation of FFs, an external field would couple to non-valence quarks.

In this work we study a simplification of such a scenario and its effects on the quark-photon interaction vertex. The quark-photon vertex describes the interaction of quarks with photons in quantum field theory. It is, therefore, a crucial ingredient in the study of the electromagnetic interaction of hadrons. Those couplings are described by the spacelike and timelike form factors of hadrons.

It is well known that the strong interactions among quarks generates a structure of the quark-photon vertex much richer than its tree-level component γ^μ . In particular, for timelike photon momentum, the quark-photon vertex must reflect the full excitation spectrum of quantum chromodynamics (QCD) in the vector-meson channel, a fact which is at the heart of the phenomenological success of vector-meson dominance models. The details of such a rich structure of the vertex are, however, not precisely known since they are generated by non-perturbative QCD effects.

We present here the results of a study [1] in which we used an extension of the RL truncation which encodes, to some extent, the above-mentioned non-valence quark effects on the BSE interaction kernel. The truncation studied herein was put forward in [7,8] and keeps the resonant contributions of non-valence terms only, describing them in terms of explicit pionic degrees of freedom. In particular, the new kernel includes a virtual decay channel of e.g. a vector meson into two pions. We have shown that this kernel generates the correct physical picture of the quark-photon vertex on the timelike momentum side, as mentioned above. Moreover, it is reasonable to expect that a calculation of form factors with the kernel used in this work must, to some extent, alleviate the problem of missing meson-cloud effects.

2 Non-valence effects on the quark-photon vertex

The details of this calculation are omitted here and the reader is referred instead to the full publication [1]. Moreover, we focus here on the changes on the timelike structure of the vertex, since it is here that the connection with the resonant structure of QCD becomes clear.

We begin by showing in Fig. 2 the results of the quark-photon vertex using the RL truncation only. Specifically, in what follows we plot the twelve dressing functions describing a non-perturbative quark-photon vertex, as a function of the photon momentum Q . Note that the qualitative features of the solution are the same for any truncation not including non-valence contributions.

As said, we show here the timelike $Q^2 < 0$ only. In this region, the vertex is sensitive to the quark-antiquark bound states with the quantum numbers of the photon $J^{PC} = 1^{--}$, which include the rho meson and its excitations. Because for the RL truncation all hadrons are bound states with no width, this is manifested here in Fig. 2 by the appearance of poles of the vertex dressing functions for the values of Q^2 corresponding to the bound-state masses.

For a realistic interaction kernel, however, those solutions should be resonances and the pole occurs for complex values of Q^2 corresponding to the pole mass $Q^2 = -M^2 + iM\Gamma$, with M and Γ the Breit-Wigner mass and width of the resonance, respectively. That is, the analytic structure of the quark-photon vertex should feature isolated poles. Additionally, the possible decay modes in a given Green's function manifest themselves as the typical multiparticle branch cut, starting at the particle production threshold.

We exemplify this behaviour in Fig. 3 which shows four dressings of the quark-photon vertex, this time with a kernel which includes non-valence degrees

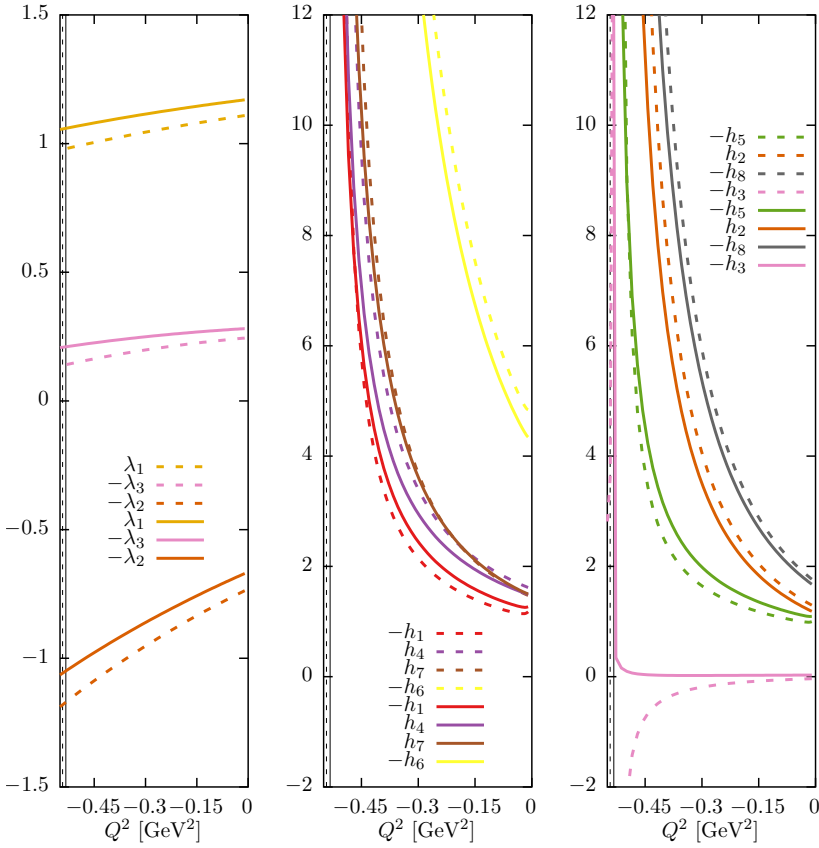


Fig. 2. Dressing functions for the non-transverse (λ_i) and transverse (h_i) components of the quark-photon vertex in the $Q^2 < 0$ region for the RL truncation (solid lines) and with the addition of a t -channel pion exchange (dashed lines). See [1] for further details. The vertical solid and dashed lines indicate the position of the rho mass ($-m_\rho^2$), as obtained from the solution of an homogeneous BSE with the same truncated kernels.

of freedom in the form of the exchange of two pions in the u - and s -channels (see [1]). In this case, the two intermediate pions go on-shell when $Q^2 = -4m_\pi^2$ and thus represent, in particular, the $\rho \rightarrow \pi\pi$ decay channel. The dressings of the transverse components should feature a branch cut starting at the real and negative branch point $Q^2 = -4m_\pi^2$. This is seen in Fig. 3 as a discontinuity in the imaginary part of the dressing functions.

That is, the BSE kernel studied in [1] is capable of partially describing the resonance character of the rho meson as a solution of the homogeneous BSE. In the present context, this simply means that the rho-meson bound-state pole of the transverse dressings of the quark-photon vertex, appearing for real Q^2 values in Fig. 2, moves to the second Riemann sheet of the Riemann surface that is now the domain of the dressing functions.

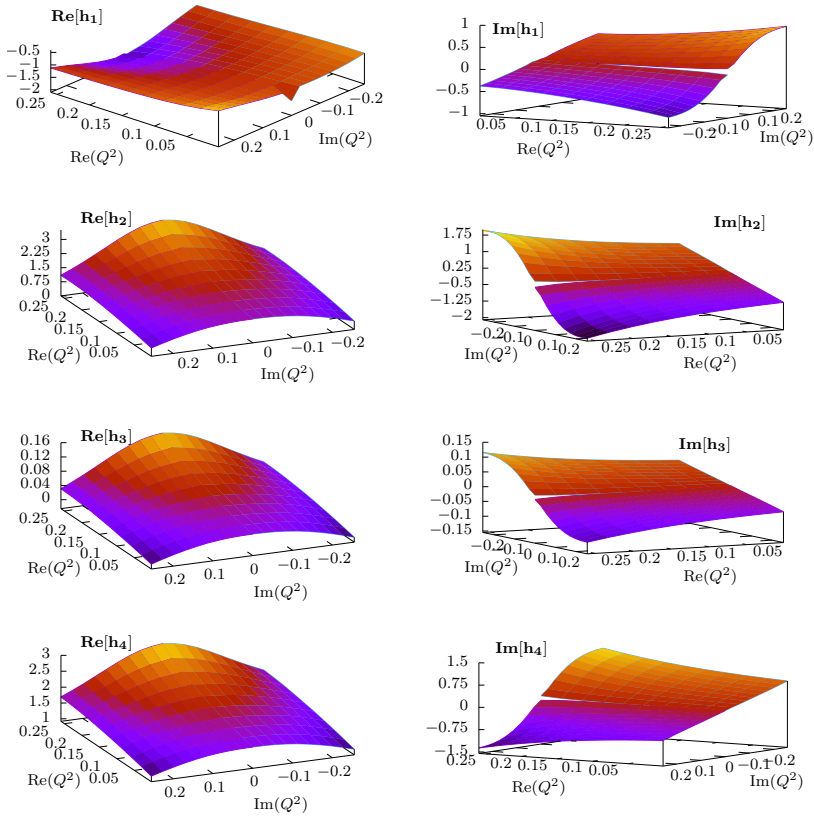


Fig. 3. Real and imaginary parts of four of the transverse dressing functions of the quark-photon vertex in a region of the complex Q^2 -plane with $\text{Re}(Q^2) < 0$ with a truncation including non-valence terms (for details see [1]. Even though not clearly visible in the plots, the branch cut in the imaginary parts begins at $Q^2 = -4m_\pi^2$.

3 Summary

In the work [1] we have studied the non-perturbative structure of the quark-photon interaction vertex in the spacelike photon momentum region $Q^2 > 0$ and in a region of the complex Q^2 -plane with $\text{Re}(Q^2) < 0$, for three different truncations of the inhomogeneous BSE that describes it. To the simple RL truncation we have added quark-pion interactions both as a t-channel pion exchange among quark and antiquark as well as s- and u-channel pion-emission channels. By using explicit pionic degrees of freedom in addition to quarks and gluons, we aim at partially describing *unquenching* effects.

We have seen how the effect of those intermediate particles is to drastically change the analytic structure of the quark-photon vertex. Whilst for the RL truncation, as well as with the inclusion of a t-channel pion exchange, the vertex only has poles for real and negative values of the photon momentum Q^2 , upon inclusion of s- and u-channel pion kernels a multiparticle branch cut starting at

$Q^2 = -4m_\pi^2$ appears and the poles move away of the real axis into the complex plane. Our results for the analytic structure of the vertex are certainly closer to the expected physical picture and, hence, constitute a step forward towards the calculation of timelike hadron form factors in the BSE formalism.

4 Acknowledgments

I would like to thank the organisers and, in particular, Willibald Plessas and Mitja Rosina for the kind invitation and for supporting my participation in the Workshop. This work was supported by the project P29216-N36 and the Doctoral Program W1203-N16 “Hadrons in Vacuum, Nuclei and Stars”, both from the Austrian Science Fund, FWF.

References

1. Á. S. Miramontes and H. Sanchis-Alepuz, *Eur. Phys. J. A* **55** (2019) no.10, 170 doi:10.1140/epja/i2019-12847-6 [arXiv:1906.06227 [hep-ph]].
2. G. Eichmann, H. Sanchis-Alepuz, R. Williams, R. Alkofer and C. S. Fischer, *Prog. Part. Nucl. Phys.* **91** (2016) 1 doi:10.1016/j.pnpnp.2016.07.001 [arXiv:1606.09602 [hep-ph]].
3. H. Sanchis-Alepuz, C. S. Fischer and S. Kubrak, *Phys. Lett. B* **733** (2014) 151 doi:10.1016/j.physletb.2014.04.031 [arXiv:1401.3183 [hep-ph]].
4. R. Williams, C. S. Fischer and W. Heupel, *Phys. Rev. D* **93** (2016) no.3, 034026 doi:10.1103/PhysRevD.93.034026 [arXiv:1512.00455 [hep-ph]].
5. S. x. Qin, C. D. Roberts and S. M. Schmidt, *Few Body Syst.* **60** (2019) no.2, 26 doi:10.1007/s00601-019-1488-x [arXiv:1902.00026 [nucl-th]].
6. C. Alexandrou, S. Bacchio, M. Constantinou, J. Finkenrath, K. Hadjiyiannakou, K. Jansen, G. Koutsou and A. Vaquero Aviles-Casco, *Phys. Rev. D* **100** (2019) no.1, 014509 doi:10.1103/PhysRevD.100.014509 [arXiv:1812.10311 [hep-lat]].
7. C. S. Fischer, D. Nickel and J. Wambach, *Phys. Rev. D* **76** (2007) 094009 doi:10.1103/PhysRevD.76.094009 [arXiv:0705.4407 [hep-ph]].
8. C. S. Fischer, D. Nickel and R. Williams, *Eur. Phys. J. C* **60** (2009) 47 doi:10.1140/epjc/s10052-008-0821-1 [arXiv:0807.3486 [hep-ph]].



Partial Wave Analysis of Pion Photoproduction Data with Fixed- t Analyticity Imposed*

J. Stahov^{a,b}, H. Osmanović^a, M. Hadžimehmedović^a, R. Omerović^a

^a University of Tuzla, Faculty of Natural Sciences and Mathematics, Univerzitetska 4, 75000 Tuzla, Bosnia and Herzegovina

^b European University *Kallos* Tuzla, Maršala Tita 2A - 2B, Tuzla, Bosnia and Herzegovina

Abstract. We present results of an analytically constrained partial wave analysis of π^0 photoproduction data. As an input we used the data on $p(\gamma, \pi^0)p$ and $n(\gamma, \pi^0)n$ reactions from threshold up to $W = 1.95\text{GeV}$.

1 Introduction

In Ref. [1] we have developed a method to impose analyticity of invariant amplitudes in Mandelstam variables s and t on partial wave solution in an iterative procedure. The method consists of two separated analyses, the fixed- t amplitude analysis (Ft AA) and the single-energy partial wave analysis (SE PWA) coupled in such a way that the results from one analysis are used as a constraint in another one. We have applied this method to the η photoproduction $p(\gamma, \eta)p$. It has been shown that iterative procedure converges rapidly. Recently, with minimal changes in computer code, the method was applied to π^0 photoproduction reaction $p(\gamma, \pi^0)p$ [2]. Natural extension of our method, applied to pion photoproduction processes, is to analyze all pion photoproduction processes simultaneously, taking into account more complicated isospin structure of invariant amplitudes and corresponding partial waves (multipoles) (work in progress). As a first step in this direction, in this article we present results of SE PWA using experimental data from two π^0 photoproduction reactions ($p(\gamma, \pi^0)p$, $n(\gamma, \pi^0)n$). Details about the method and formalism are given in references [1], [2].

2 Input data

We used the data on the $p(\gamma, \pi^0)p$ from several collaborations: A2@MAMI, CBELSA/TAPS, DAPHNE/MAMI and GRAAL. The data on the $n(\gamma, \pi^0)n$ are rather old and incomplete. This part of our input will be updated in an ongoing analysis.

Starting from experimental data, input for SE PWA and Ft AA have been prepared using the spline smoothing method [3] as described in references [1], [2].

* Talk presented by J. Stahov

Table 1. Experimental data for $p(\gamma,\pi^0)p$, $n(\gamma,\pi^0)n$ reactions used in our SE PWA.

| $\gamma p \rightarrow \pi^0 p$ | | | | |
|--------------------------------|------|-------------|-------|------------------------|
| Obs | N | W[MeV] | N_E | Reference |
| σ_0 | 5240 | 1075 – 1541 | 262 | A2@MAMI(2013) [4] |
| | 3930 | 1132 – 1895 | 246 | A2@MAMI(2015) [5] |
| Σ | 528 | 1074 – 1215 | 54 | A2@MAMI(2013) [4] |
| | 357 | 1150 – 1310 | 21 | A2@MAMI(2001) [6] |
| | 471 | 1383 – 1922 | 31 | GRAAL(2005) [7] |
| T | 469 | 1295 – 1895 | 34 | A2@MAMI(2016) [8] |
| | 157 | 1462 – 1620 | 8 | CBELSA/TAPS(2014) [9] |
| $T\sigma_0$ | 4500 | 1074 – 1291 | 250 | A2@MAMI(2015) [10] |
| P | 157 | 1462 – 1620 | 8 | CBELSA/TAPS(2014) [9] |
| $E\sigma_0$ | 139 | 1201 – 1537 | 24 | DAPHNE/MAMI(2001) [11] |
| E | 88 | 1481 – 1951 | 5 | CBELSA/TAPS(2014) [12] |
| | 480 | 1129 – 1878 | 40 | A2@MAMI(2015) [13] |
| F | 469 | 1295 – 1895 | 34 | A2@MAMI(2016) [8] |
| $F\sigma_0$ | 4500 | 1074 – 1291 | 250 | A2@MAMI(2015) [10] |
| G | 3 | 1232 | 1 | DAPHNE/MAMI(2005) [14] |
| | 318 | 1430 – 1727 | 19 | CBELSA/TAPS(2012) [15] |
| H | 157 | 1462 – 1620 | 8 | CBELSA/TAPS(2014) [9] |

| $\gamma n \rightarrow \pi^0 n$ | | | | |
|--------------------------------|-----|-------------|-------|-------------|
| Obs | N | W[MeV] | N_E | Reference |
| σ_0 | 42 | 1203 – 1517 | 17 | (1977) [16] |
| | 35 | 1323 – 1535 | 18 | (1972) [17] |
| | 42 | 1318 – 1604 | 17 | (1973) [18] |
| | 29 | 1611 – 1869 | 3 | (1967) [19] |
| Σ | 216 | 1484 – 1912 | 25 | (2009) [20] |

3 Results

In our SE PWA we fitted multipoles up to $L_{\max} = 5$ (40 multipoles). A minimization procedure (80 real parameters) was started at initial values which are randomly distributed in a 30 % range around the starting solution MAID 2007 [21]. The Ft AA was performed at 20 equidistant t -values in the range $-1.00\text{GeV}^2 < t < -0.09\text{GeV}^2$. Resulting multipoles up to $L = 2$ are shown in Figs. 1 and 2. Our SE solutions are poorly determined at energies $W < 1.2\text{GeV}$ and $W > 1.7\text{GeV}$. This is due to the lack of the experimental data. As can be seen from Table 1, in energy range $1.2\text{GeV} < W < 1.7\text{GeV}$ we use as much as eight observables, fitting maximally five of them in the same time. At energies $W > 1.7\text{GeV}$ the number of observables is much smaller. Situation is even worse below 1.2 GeV where only two observables (σ_0, Σ), both from $p(\gamma,\pi^0)p$, were used in our analysis.

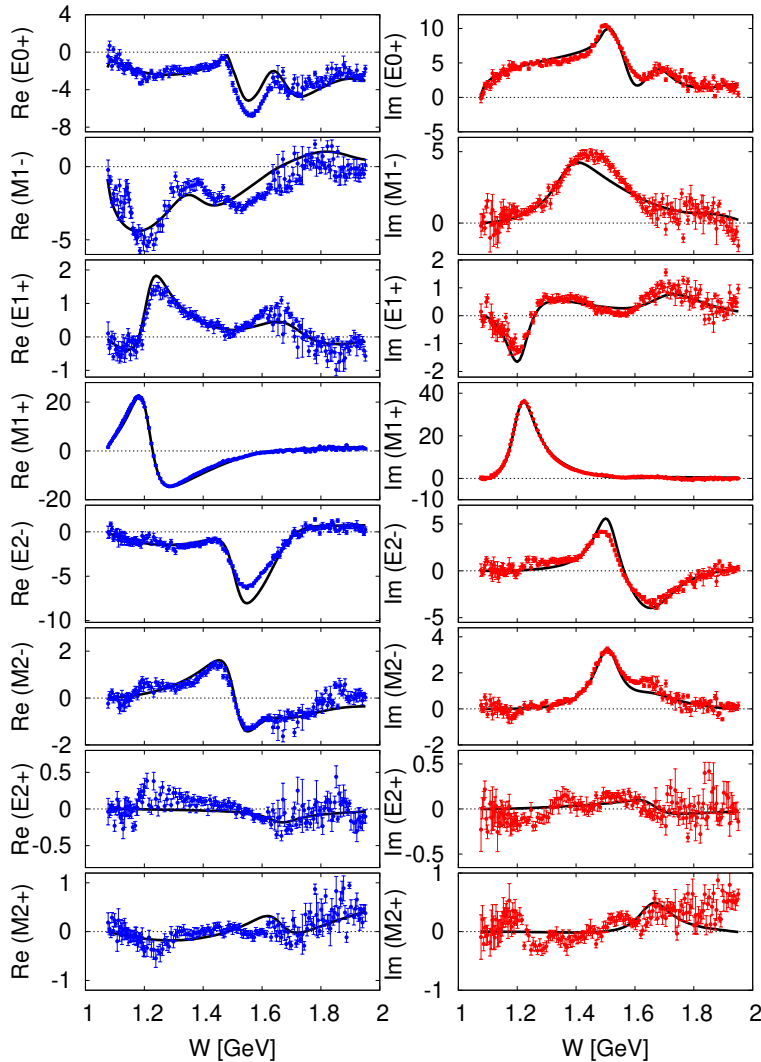


Fig. 1. (Color online) Reaction $p(\gamma,\pi^0)p$. Real and imaginary parts of the S-, P - and D-multipoles obtained with starting solution[21] (black line). Multipoles are in mfm

4 Conclusions

We applied iterative procedure with the fixed- t analyticity constraints to partial wave analysis of π^0 photoproduction experimental data. For both reactions, $p(\gamma,\pi^0)p$ and $n(\gamma,\pi^0)n$, we obtained multipoles up to $L_{\max} = 5$. Improving the quality of SE PWA solutions in our method requires update of the data base in a way that both, the number of observables and the quality of the data, are increased.

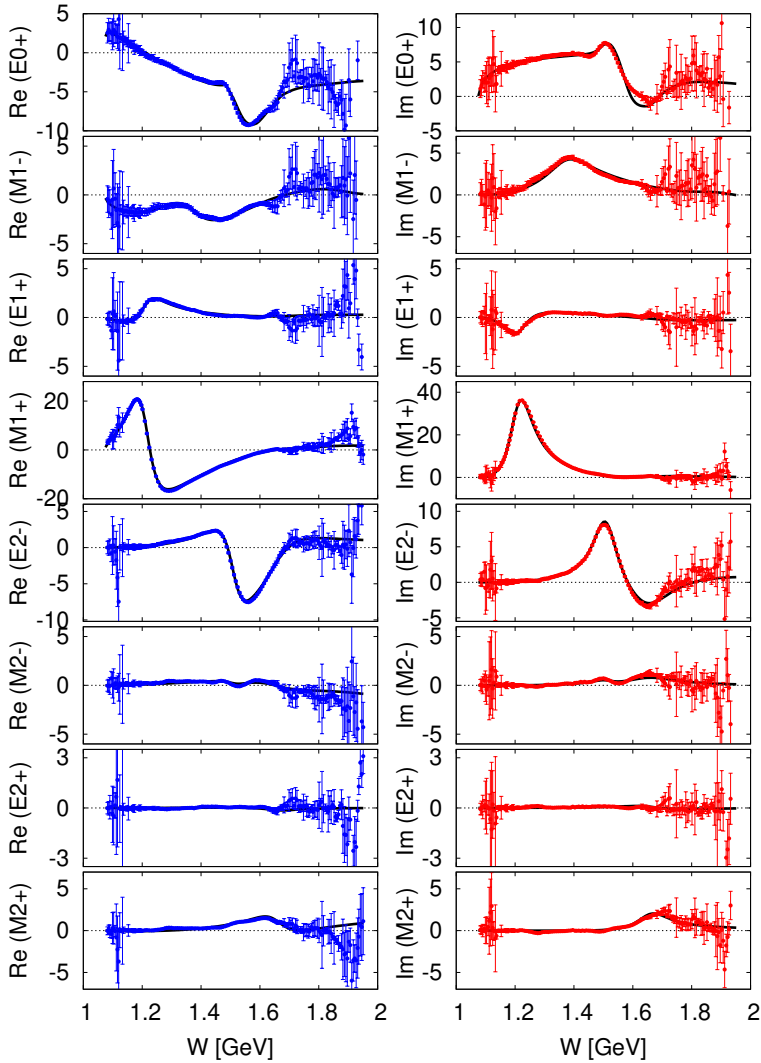


Fig. 2. (Color online) Reaction $n(\gamma, \pi^0)n$. Real and imaginary parts of the S-, P - and D-multipoles obtained with starting solution [21](black line). Multipoles are in mfm

References

1. H. Osmanović, M. Hadžimehmedović, R. Omerović, J. Stahov, V. Kashevarov, K. Nikonov, M. Ostrick, L. Tiator, and A. Švarc, *Phys. Rev. C* **97**, 015207 (2018).
2. H. Osmanović, M. Hadžimehmedović, R. Omerović, J. Stahov, M. Gorchtein, V. Kashevarov, K. Nikonov, M. Ostrick, L. Tiator, and A. Švarc, arXiv:1908.05167 (2019).
3. C. de Boor, *A Practical Guide to Splines*, Springer-Verlag, Heidelberg, 1978, revised 2001.
4. D. Hornidge *et al.* [A2 and CB-TAPS Collaborations], *Phys. Rev. Lett.* **111**, no. 6, 062004 (2013).
5. P. Adlarson *et al.* [A2 Collaboration at MAMI], *Phys. Rev. C* **92**, 024617 (2015).

6. R. Leukel, PhD thesis (2001) Mainz University.
7. O. Bartalini *et al.* Eur. Phys. J. A **26**, 399 (2005).
8. J. R. M. Annand *et al.* [A2 Collaboration at MAMI] Phys. Rev. C **93**, 055209 (2016).
9. J. Hartmann *et al.* [CBELSA/TAPS Collaboration] Phys. Rev. Lett. **113**, 062001 (2014).
10. P. Otte, PhD thesis (2015) Mainz University.
11. I. Preobrajenski, PhD thesis (2001), Mainz University.
12. M. Gottschall *et al.* [CBELSA/TAPS Collaboration] Phys. Rev. Lett. **112**, 012003 (2014).
13. J. Linturi, PhD thesis (2015) Mainz University.
14. J. Ahrens *et al.* Eur. Phys. J. A **26**, 135 (2005).
15. A. Thiel *et al.* [CBELSA/TAPS Collaboration] Phys. Rev. Lett. **109**, 102001 (2012).
16. A. Ando, Physik Daten, Physics Data (Fach-Informationszentrum), Karlsruhe, (1977).
17. C. Bacci *et al.*, Phys. Lett. C **39**, 559 (1972).
18. Y. Hemmi *et al.*, Nucl. Phys. B **55**, 333 (1973).
19. Klimesmith, PhD Thesis (1967) see GWU.
20. R. Di Salvo *et al.*, Eur. Phys. J. A **42**, 151 (2009).
21. D. Drechsel, S. S. Kamalov and L. Tiator, Eur. Phys. J. A **34** (2007) 69; and <https://maid.kph.uni-mainz.de/>.



Structure and transitions of nucleon excitations from lattice QCD^{*}

Finn M. Stokes^{a,b}, Waseem Kamleh^a, Derek B. Leinweber^a

^aSpecial Research Centre for the Subatomic Structure of Matter, Department of Physics, University of Adelaide, South Australia 5005, Australia

^bJülich Supercomputing Centre, Institute for Advanced Simulation, Forschungszentrum Jülich, Jülich D-52425, Germany

Abstract. The recently-introduced Parity Expanded Variational Analysis (PEVA) technique allows for the isolation of baryon eigenstates on the lattice at finite momentum free from opposite-parity contamination. We find that this technique introduces a statistically significant correction in extractions of the electromagnetic form factors of the ground state nucleon. It also allows first extractions of the elastic and transition form factors of nucleon excitations on the lattice. We present the electromagnetic elastic form factors and helicity amplitudes of two odd-parity excitations of the nucleon. These results provide valuable insight into the structure of these states, and allow for a connection to be made to quark-model states in this energy region.

1 Introduction

In lattice QCD, instead of the unstable finite-width resonances of nature, we observe a tower of stable excitations. These eigenstates are associated with the physical resonances in a non-trivial manner. Understanding the structure of the states observed in Lattice QCD will enable predictions of the infinite-volume observables of nature via effective field theory techniques [1,2] or an extension of the Lellouch-Lüscher formalism [3,4].

Investigating the structure of excited states in lattice QCD is recognised as an important frontier in the field. Progress has already been made in the meson sector [5,6]. Here we tackle the more challenging problem of calculating such quantities in the baryon sector.

By using local three-quark operators on the lattice, both the CSSM [7,8] and the Hadron Spectrum Collaboration (HSC) [9,10] observe two low-lying odd-parity states in the resonance regimes of the $N^*(1535)$ and $N^*(1650)$. In the following we summarise our recent results on the elastic form factors of the ground state nucleon, these two odd-parity states, and the lowest-lying even-parity state accessible through the same operators [11,12]. In addition, we present preliminary results on the transition form factors for the two odd-parity states. These results were made possible through the development of the PEVA technique [13].

^{*} Talk presented by Finn M. Stokes

2 Parity Expanded Variational Analysis (PEVA)

The process of extracting elastic form factors of baryonic excited states via the PEVA technique is presented in full in Ref [11]. We provide here a brief summary of this process and the generalisations required to handle transition matrix elements.

We begin with a basis of n conventional spin-1/2 operators $\{\chi_i(x)\}$ that couple to the states of interest. Adopting the Pauli representation, we introduce the PEVA projector $\Gamma_{\pm\mathbf{p}} \equiv \frac{1}{4} (I + \gamma^4) (I \pm i\gamma^5 \gamma^k \hat{\mathbf{p}}^k)$ [13], and construct a set of basis operators

$$\begin{aligned}\chi_{\pm\mathbf{p}i}(x) &\equiv \Gamma_{\pm\mathbf{p}} \chi_i(x), \\ \chi_{\pm\mathbf{p}i'}(x) &\equiv \pm \Gamma_{\pm\mathbf{p}} \gamma^5 \chi_i(x).\end{aligned}$$

We then seek an optimised set of operators $\phi_{\pm\mathbf{p}}^\alpha(x)$ that each couple strongly to a single energy eigenstate α . These optimised operators are constructed as linear combinations of the basis operators by solving a generalised eigenvalue problem as detailed in Ref. [13].

We can then construct the eigenstate-projected two-point correlation function

$$G(\mathbf{p}; t; \alpha) \equiv \text{Tr} \left(\sum_x e^{-i\mathbf{p}\cdot\mathbf{x}} \langle \Omega | \phi_{\pm\mathbf{p}}^\alpha(x) \bar{\phi}_{\pm\mathbf{p}}^\alpha(0) | \Omega \rangle \right),$$

and the three point correlation functions

$$\begin{aligned}\mathcal{G}_{\pm}^3(j_{\text{CI}}^\mu; \mathbf{p}', \mathbf{p}; t_2, t_1; \alpha \rightarrow \beta) \\ \equiv \sum_{x_1, x_2} e^{-i\mathbf{p}'\cdot\mathbf{x}_2} e^{i(\mathbf{p}'-\mathbf{p})\cdot\mathbf{x}_1} \langle \Omega | \phi_{\pm\mathbf{p}'}^\beta(x_2) j_{\text{CI}}^\mu(x_1) \bar{\phi}_{\pm\mathbf{p}}^\alpha(0) | \Omega \rangle,\end{aligned}$$

where $j_{\text{CI}}^\mu(x)$ is the $O(a)$ -improved [14] conserved vector current $j_{\text{CI}}^\mu(x)$ used in Ref. [15], inserted with a three-momentum transfer $\mathbf{q} = \mathbf{p}' - \mathbf{p}$.

For the elastic case, this choice of current gives the matrix element

$$\begin{aligned}\langle \alpha; \mathbf{p}'; s' | j_{\text{CI}}^\mu(0) | \alpha; \mathbf{p}; s \rangle \\ = \sqrt{\frac{m^\alpha}{E^\alpha(\mathbf{p})}} \sqrt{\frac{m^\alpha}{E^\alpha(\mathbf{p}')}} \bar{u}^\alpha(\mathbf{p}', s') \left(\gamma^\mu F_1(Q^2) - \frac{\sigma^{\mu\nu} q^\nu}{2m^\alpha} F_2(Q^2) \right) u^\alpha(\mathbf{p}, s),\end{aligned}$$

where $Q^2 = \mathbf{q}^2 - (E^\alpha(\mathbf{p}') - E^\alpha(\mathbf{p}))^2$, and $F_1(Q^2)$ and $F_2(Q^2)$ are the Dirac and Pauli form factors. The matrix element can be extracted by taking appropriate ratios of the three- and two-point correlation functions. The Sachs electromagnetic form factors

$$G_E(Q^2) \equiv F_1(Q^2) - \frac{Q^2}{(2m^\alpha)^2} F_2(Q^2) \text{ and } G_M(Q^2) \equiv F_1(Q^2) + F_2(Q^2)$$

can then be extracted by taking linear combinations of the matrix elements.

We now move on to the transition form factors. The relevant matrix element is [16]

$$\begin{aligned} \langle \beta^- ; p' ; s' | j_{C1}^\mu(0) | \alpha^+ ; p ; s \rangle &= \sqrt{\frac{m^\alpha}{E^\alpha(\mathbf{p})}} \sqrt{\frac{m^\beta}{E^\beta(\mathbf{p}')}} \\ &\times \bar{u}^\beta(p', s') \left(\left(\delta^{\mu\nu} - \frac{q^\mu q^\nu}{q^2} \right) \gamma^\nu \gamma^5 F_1^*(Q^2) - \frac{\sigma^{\mu\nu} q^\nu}{m^\beta - m^\alpha} \gamma^5 F_2^*(Q^2) \right) u^\alpha(p, s), \end{aligned}$$

where $F_1^*(Q^2)$ and $F_2^*(Q^2)$ are Dirac- and Pauli-like transition form factors. We can then take ratios and linear combinations to obtain the transverse helicity amplitude

$$A_{1/2}(Q^2) \equiv 2\sqrt{\frac{Q^2 + (m^\beta - m^\alpha)^2}{8m^\alpha(m^{\beta 2} - m^{\alpha 2})}} (F_1^*(Q^2) + F_2^*(Q^2)).$$

3 Ground state nucleon

We study the extraction of the elastic form factors of the ground state nucleon in detail in Ref. [11]. This analysis is performed on the PACS-CS (2 + 1)-flavour full-QCD ensembles [17], made available through the ILDG [18]. In the paper we demonstrate the efficacy of variational analysis techniques in general, and PEVA specifically, at controlling excited-state contaminations in the electric form factor. Both the PEVA and conventional variational analysis show clear and clean plateaus, supporting previous work demonstrating the utility of variational analysis in calculating baryon matrix elements [19,20].

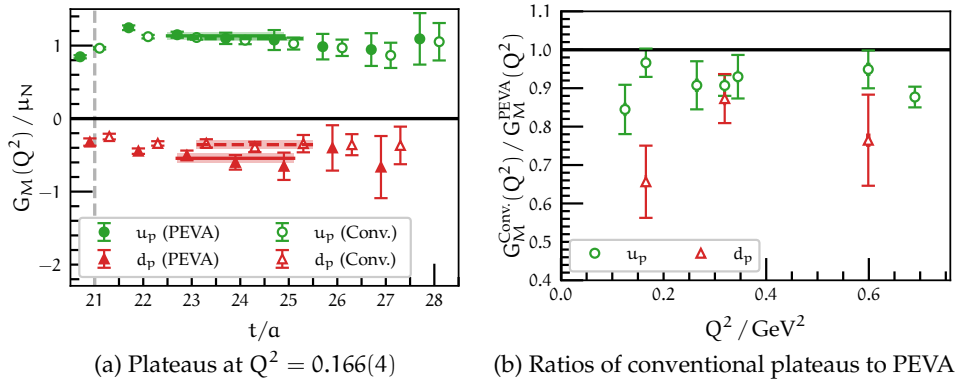


Fig. 1. Comparison of conventional and PEVA extractions of $G_M(Q^2)$ for the ground-state nucleon at $m_\pi = 156$ MeV. Results are contributions for single quarks of unit charge from the doubly represented quark sector (u_p) and the singly represented quark sector (d_p).

Here we focus on the particular case of the magnetic form factor, where we found evidence that the conventional analysis is contaminated by opposite-parity states. In Fig. 1a we plot a comparison of magnetic form factor plateaus produced by a conventional variational analysis (using an initial basis of $n = 8$

operators), with an equivalent extraction via the PEVA technique (with the basis parity-expanded to $2n = 16$ operators). We see a significant difference in the plateaus extracted by the two techniques for the singly represented quark sector. If we take the correlated ratio of the extracted values, as shown for a range of kinematics in Fig. 1b, we see a consistent underestimation of the value by the conventional analysis. This shows $\sim 20\%$ underestimation of the magnitude of the contributions to the magnetic form factor from the singly represented quark flavour in the conventional analysis.

The difference between the two analyses is that the PEVA approach provides additional interpolator degrees of freedom to improve the ground state interpolating field at finite momentum. As such it is clear that the difference between the two extractions is from contaminating states that are present in the conventional analysis but removed by the parity expansion. As such, the PEVA technique is critical for precision measurements of nucleon form factors.

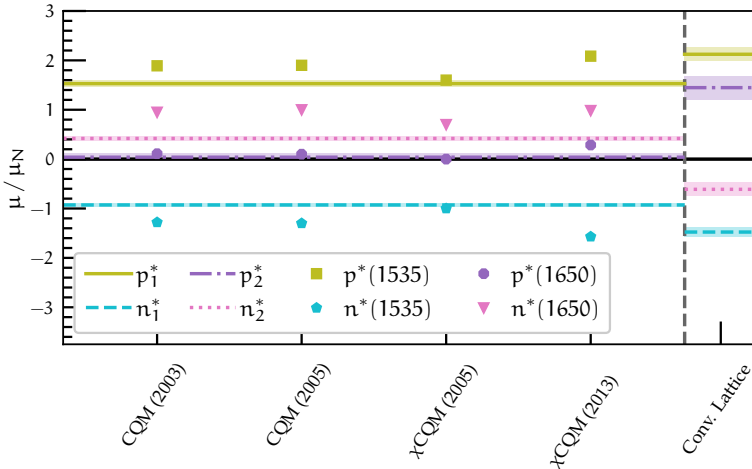


Fig. 2. Comparison between lattice calculations of the magnetic moments of two odd-parity nucleon excitations at $m_\pi = 702$ MeV and quark model predictions [21–23] for the $N^*(1535)$ and $N^*(1650)$ resonances. The shaded bands on the left-hand side of the plot indicate the magnetic moments calculated via the PEVA technique in lattice QCD, and symbols denote the quark model predictions. Lattice calculations of the magnetic moments using conventional parity projection are plotted to the right of the vertical dashed line.

4 Excitations

With our local three-quark operators, we observe two low-lying odd-parity eigenstates in the resonance regimes of the $N^*(1535)$ and $N^*(1650)$. In Ref. [12], we investigate the elastic form factors of these states. There we find that opposite parity contaminations have a large effect on both the electric and magnetic form factors, and the PEVA technique is critical for even a qualitatively correct extraction.

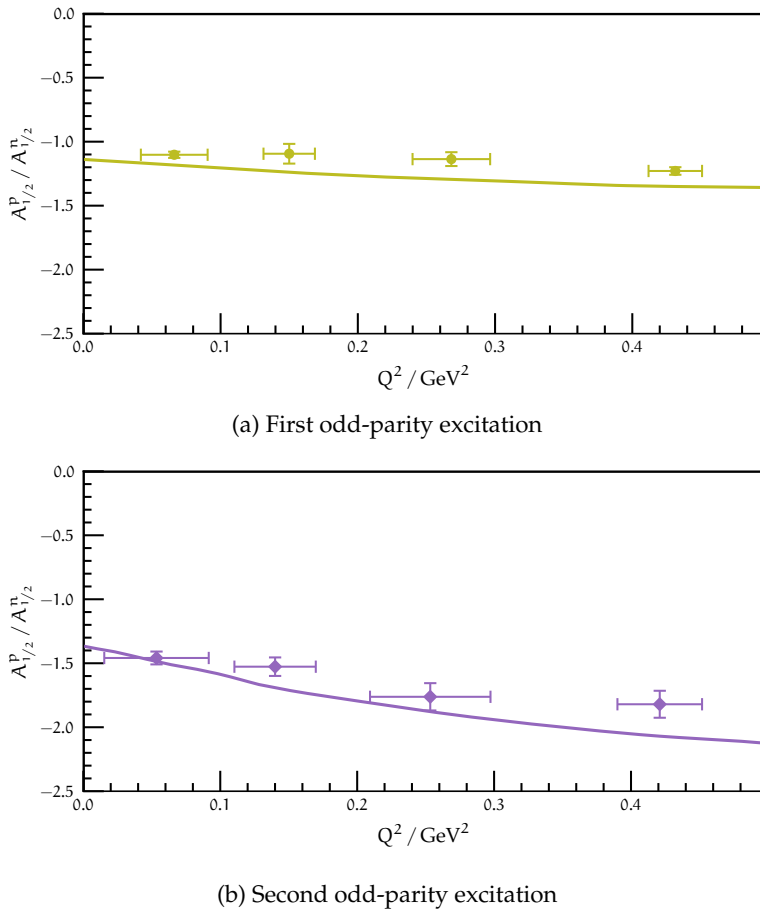


Fig. 3. Constituent quark model predictions [24] (lines) and PEVA extractions (points) of the ratio of proton to neutron helicity amplitudes at $m_\pi = 702$ MeV.

We focus our investigation at heavier pion masses, where these lattice states lie below the relevant two-particle scattering thresholds on the finite volume. At these masses, we find that these states look remarkably similar to constituent quark model predictions for the $N^*(1535)$ and $N^*(1650)$.

We find the size of these lattice eigenstates to be similar to the ground state nucleons. As shown in Fig. 2, their magnetic moments agree well with constituent quark model predictions for the continuum states.

We also present here preliminary results for the transition form factors from the ground state to each of these two lattice eigenstates. These results will be presented in more detail in an upcoming paper. In Fig. 3a we compare the ratio of the transverse helicity amplitudes of the first lattice excitation of the proton and neutron to a constituent quark model prediction for the $N^*(1535)$. Taking this ratio allows us to cancel out some of the model dependence of the constituent quark model result. We once again find good agreement between the structure of the lattice eigenstates at the heavier pion masses and the constituent quark

model prediction. In Fig. 3b we see a similar result for the second lattice excitation compared to the constituent quark model $N^*(1650)$.

We see strong agreement between the lattice eigenstates and constituent quark model predictions at these heavier pion masses. This suggests that while the dynamics are much more complicated at the physical point, and the constituent quark model alone does not appear to give a good description of these resonances in nature, as the pion mass increases the constituent quark model describes the excitations rather well. The agreement of the lighter state with the constituent-quark-model $N^*(1535)$ is consistent with predictions from Hamiltonian Effective Field Theory (HEFT) [25]. However, the agreement of the heavier state with the constituent-quark-model $N^*(1650)$ suggests that future HEFT studies should explore the incorporation of two bare basis states associated with the two different localised states observed herein.

In Ref. [12], we also investigate the lowest-lying even-parity excitation of the nucleon observed on the lattice. We find that it has a charge radius approximately 30% larger than the ground state, and a remarkably similar magnetic moment to the ground state. This is consistent with the state being a radial excitation of the ground-state nucleon as seen in Refs. [26,27].

5 Conclusion

The PEVA technique is critical to correctly extracting the form factors of proton and neutron excitations on the lattice. Such extractions give us insight into the structure of the states seen on the lattice. In addition, even for the ground state, we found evidence that the conventional analysis was contaminated by opposite-parity states. For the kinematics considered here, we observe $\sim 20\%$ underestimation of the magnitude of the contributions to the magnetic form factor from the singly represented quark flavour at the lighter pion masses. All these results make it clear that the PEVA technique is critical for precision measurements of nucleon form factors and for any study of the structure of nucleon excitations.

Acknowledgements

This research was undertaken with the assistance of resources from the Phoenix HPC service at the University of Adelaide, the National Computational Infrastructure (NCI), which is supported by the Australian Government, and by resources provided by the Pawsey Supercomputing Centre with funding from the Australian Government and the Government of Western Australia. These resources were provided through the National Computational Merit Allocation Scheme and the University of Adelaide partner share. This research is supported by the Australian Research Council (ARC) through grants no. DP140103067, DP150103164, LE160100051, and DP190102215.

References

1. J.-J. Wu, T. S. H. Lee, A. W. Thomas, and R. D. Young, *Phys. Rev.*, vol. C90, no. 5, p. 055206, 2014.

2. Z.-W. Liu, W. Kamleh, D. B. Leinweber, F. M. Stokes, A. W. Thomas, and J.-J. Wu, *Phys. Rev.*, vol. D95, no. 3, p. 034034, 2017.
3. M. Luscher, *Nucl. Phys.*, vol. B354, pp. 531–578, 1991.
4. L. Lellouch and M. Luscher, *Commun. Math. Phys.*, vol. 219, pp. 31–44, 2001.
5. B. J. Owen, W. Kamleh, D. B. Leinweber, M. S. Mahhub, and B. J. Menadue, *Phys. Rev.*, vol. D92, no. 3, p. 034513, 2015.
6. R. A. Briceno, J. J. Dudek, R. G. Edwards, C. J. Shultz, C. E. Thomas, and D. J. Wilson, *Phys. Rev. Lett.*, vol. 115, p. 242001, 2015.
7. M. S. Mahhub, W. Kamleh, D. B. Leinweber, P. J. Moran, and A. G. Williams, *Phys. Rev.*, vol. D87, no. 9, p. 094506, 2013.
8. M. S. Mahhub, W. Kamleh, D. B. Leinweber, P. J. Moran, and A. G. Williams, *Phys. Rev.*, vol. D87, no. 1, p. 011501(R), 2013.
9. R. G. Edwards, N. Mathur, D. G. Richards, and S. J. Wallace, *Phys. Rev.*, vol. D87, no. 5, p. 054506, 2013.
10. R. G. Edwards, J. J. Dudek, D. G. Richards, and S. J. Wallace, *Phys. Rev.*, vol. D84, p. 074508, 2011.
11. F. M. Stokes, W. Kamleh, and D. B. Leinweber, *Phys. Rev.*, vol. D99, no. 7, p. 074506, 2019.
12. F. M. Stokes, W. Kamleh, and D. B. Leinweber, arXiv1907.00177, 2019.
13. F. M. Stokes, W. Kamleh, D. B. Leinweber, M. S. Mahhub, B. J. Menadue, and B. J. Owen, *Phys. Rev.*, vol. D92, no. 11, p. 114506, 2015.
14. G. Martinelli, C. T. Sachrajda, and A. Vladikas, *Nucl. Phys.*, vol. B358, pp. 212–227, 1991.
15. S. Boinepalli, D. B. Leinweber, A. G. Williams, J. M. Zanotti, and J. B. Zhang, *Phys. Rev.*, vol. D74, p. 093005, 2006.
16. B. J. Owen, A variational approach to hadron structure in lattice QCD. PhD thesis, Adelaide U., Sch. Chem. Phys., 2015.
17. S. Aoki, K. Ishikawa, N. Ishizuka, T. Izubuchi, D. Kadoh, K. Kanaya, Y. Kuramashi, Y. Namekawa, M. Okawa, Y. Taniguchi, A. Ukawa, N. Ukita, and T. Yoshie, *Phys. Rev.*, vol. D79, p. 034503, 2009.
18. M. G. Beckett, B. Joo, C. M. Maynard, D. Pleiter, O. Tatebe, and T. Yoshie, *Comput. Phys. Commun.*, vol. 182, pp. 1208–1214, 2011.
19. J. Dragos, R. Horsley, W. Kamleh, D. B. Leinweber, Y. Nakamura, P. E. L. Rakow, G. Schierholz, R. D. Young, and J. M. Zanotti, *Phys. Rev.*, vol. D94, no. 7, p. 074505, 2016.
20. B. J. Owen, J. Dragos, W. Kamleh, D. B. Leinweber, M. S. Mahhub, B. J. Menadue, and J. M. Zanotti, *Phys. Lett.*, vol. B723, pp. 217–223, 2013.
21. W.-T. Chiang, S. N. Yang, M. Vanderhaeghen, and D. Drechsel, *Nucl. Phys.*, vol. A723, pp. 205–225, 2003.
22. J. Liu, J. He, and Y. B. Dong, *Phys. Rev.*, vol. D71, p. 094004, 2005.
23. N. Sharma, A. Martinez Torres, K. P. Khemchandani, and H. Dahiya, *Eur. Phys. J.*, vol. A49, p. 11, 2013.
24. S. Capstick and B. D. Keister, *Phys. Rev.*, vol. D51, pp. 3598–3612, 1995.
25. Z.-W. Liu, W. Kamleh, D. B. Leinweber, F. M. Stokes, A. W. Thomas, and J.-J. Wu, *Phys. Rev. Lett.*, vol. 116, no. 8, p. 082004, 2016.
26. D. S. Roberts, W. Kamleh, and D. B. Leinweber, *Phys. Lett.*, vol. B725, pp. 164–169, 2013.
27. D. S. Roberts, W. Kamleh, and D. B. Leinweber, *Phys. Rev.*, vol. D89, no. 7, p. 074501, 2014.



Exotic Baryons in Skyrme Type Models

H. Weigel

Institute for Theoretical Physics, Physics Department, Stellenbosch University,
Matieland 7602, South Africa

Abstract. Skyrme type chiral soliton models suggest low-lying exotic baryons with quantum numbers that cannot be represented by three quarks. In these proceedings I discuss properties of their flavor partners in the nucleon channel.

1 Introduction

The presentation underlying these proceedings contains three parts discussing exotic baryons in Skyrme type chiral soliton models¹. One dealing with light pentaquarks, in particular the extraction of the width from scattering data, the second part discusses the relevance of radial excitations and finally the third part focuses on baryons with a single heavy quark (charm or bottom). The research on the topics covered in parts one and three has distinctively shown that any mean-field treatment is insufficient for a consistent description of exotic baryons. Since I have recently summarized this observation in Ref. [2], I will focus on the radial excitations in present proceedings.

In chiral soliton models exotic baryon states emerge as elements of higher dimensional $SU(3)$ flavor representations; most prominently the anti-decuplet ($\overline{10}$) that, among others, contains the Θ^+ pentaquark [3]. Yet, these representations also contain baryons with quantum numbers of ordinary three quark states. In particular the mass of the nucleon type element of the $\overline{10}$ is predicted [4] in the regime of the Roper and $N(1710)$ resonances, which in the Skyrme model are understood as radial excitations [5]. Strong mixing effects are therefore expected and the comparison with the established spectrum of excited nucleons will give insight on whether or not $\overline{10}$ baryons are mere artifacts.

2 Collective Flavor and Radial Excitations

Skyrme type models are based on effective chiral theories with the basic degree of freedom being the chiral field $U \in SU(N_f)$, where N_f is the number of active flavors, here $N_f = 3$. Baryons are constructed from (static) soliton solutions for the chiral field, $U_0 = U_0(\mathbf{r})$. To generate states with baryon quantum numbers from U_0 , in particular spin and flavor, time dependent collective coordinates,

¹ See Ref. [1] for comprehensive review of these models.

$A(t) \in SU(N_f)$ are introduced via $U_0(\mathbf{r}) \rightarrow A(t)U_0(\mathbf{r})A^\dagger(t)$ and canonically quantized². To facilitate a study of radial excitations the collective coordinate $\lambda(t)$ for the extension of the soliton is added:

$$U_0(\mathbf{r}) \rightarrow A(t)U_0(\lambda(t)\mathbf{r})A^\dagger(t). \quad (1)$$

Canonical quantization produces the Hamiltonian

$$H = H_0 - s(\lambda)D_{88}(A) \quad \text{with} \quad H_0 = V(J^2, C_2; \lambda) - \frac{1}{2m(\lambda)} \frac{\partial^2}{\partial \lambda^2}, \quad (2)$$

where the inertial parameter $m(\lambda)$ is computed numerically from U_0 . The potential V is a sum of terms that are products of coefficients (also computed from U_0) and collective coordinate operators like the spin J and the quadratic Casimir operator C_2 of $SU(3)$ [6]. Diagonalization of the flavor symmetric component, $H_0|\mu, n_\mu\rangle = \epsilon_{\mu, n_\mu}|\mu, n_\mu\rangle$, produces a pertinent basis by finding the radial excitations n_μ for a given $SU(3)$ representation $\mu \in \{\mathbf{8}, \overline{\mathbf{10}} \dots; \mathbf{10}, \mathbf{27}, \dots\}$. That is, the basis states factorize: $|\mu, n_\mu\rangle = |\mu\rangle|n_\mu\rangle$. The flavor symmetry breaking part contains an element of the adjoint representation $D_{ab} = (1/2)\text{tr}[\lambda_a \lambda_b A^\dagger]$ with $\lambda_1, \dots, \lambda_8$ being the Gell-Mann matrices. Computing its matrix elements with respect to the eigenstates of H_0 completes the Hamiltonian matrix

$$\langle \mu, n_\mu | H | \nu, n_\nu \rangle = \epsilon_{\mu, n_\mu} \delta_{\mu, \nu} \delta_{n_\mu, n_\nu} - \langle n_\mu | s(\lambda) | n_\nu \rangle \langle \mu | D_{88}(A) | \nu \rangle. \quad (3)$$

Diagonalization yields the baryon states $|B, m\rangle = \sum_{\mu, m_\mu} C_{\mu, m_\mu}^{(B, m)} |\mu, m_\mu\rangle$ whose eigenvalues are the baryon masses [6]. In figure 1 a typical result for the spectrum relative to the nucleon is compared to models for the excited baryons based on octet-antidecuplet mixing [7,8]. As in Ref. [7] no (new) nucleon type state is seen in the vicinity of 1.6GeV, which is not observed experimentally (so far) but suggested in Ref. [8]. (The models of Refs. [7,8] construct octet and anti-decuplet mixing without specifying the driving dynamics.)

However, there are two nearby structures around 1.8GeV.

Figure 2 sketches the amplitudes $C_{\mu, m_\mu}^{(N, m)}$ in the nucleon channel. Here $m = 0$ refers to the actual nucleon which is dominated by the octet ground state. The Roper resonance would be identified with $m = 1$. Surprisingly, the radial ground state from the octet also has the largest amplitude in this channel, though the first radial excitations from the octet, anti-decuplet and $\mathbf{27}$ -plet contribute similarly. The $m = 2$ state, presumably the $N(1710)$, is mostly composed of the first radial octet and the anti-decuplet ground states.

3 Magnetic Moments

It has been shown some time ago that the transition magnetic moment between pure $\mathbf{8}$ and $\overline{\mathbf{10}}$ protons is zero thereby strongly suppressing photo-excitation of the $\overline{\mathbf{10}}$ proton [9]. It is therefore important to verify or falsify this observation when

² Typically $U_0(\mathbf{r})$ is of hedgehog structure so that spin is given by flavor generators.

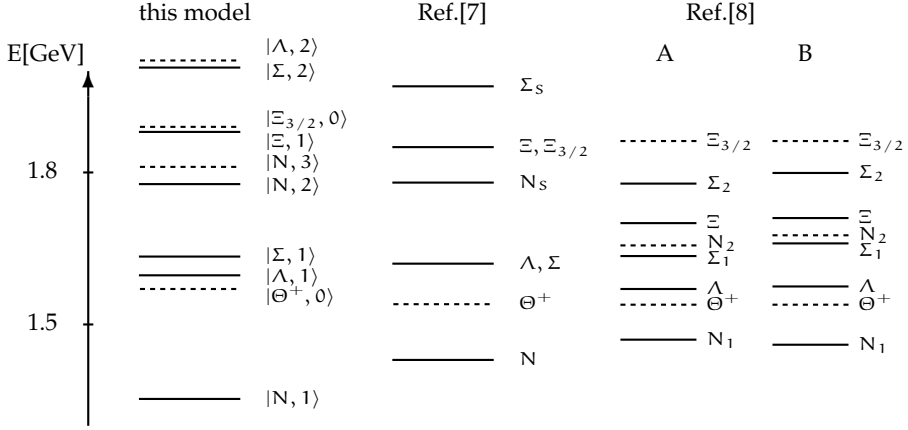


Fig. 1. Model prediction for the spectrum of the positive parity spin $\frac{1}{2}$ and $\frac{3}{2}$ baryons and their radial excitations relative to the nucleon mass. Dashed lines indicate predictions that cannot be (unambiguously) identified with established resonances.

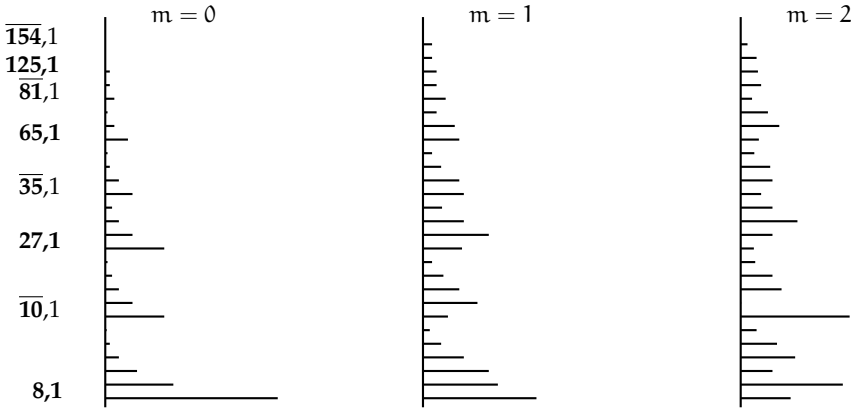


Fig. 2. Typical result for the nucleon expansion coefficients $|C_{\mu, m_\mu}^{(N, m)}|$.

the important radial admixtures are incorporated. Starting point is the electromagnetic current $J_k^{(e.m.)}$ expressed in terms of $AU_0(\lambda r)A^\dagger$ yielding the magnetic moment operator

$$\hat{\mu} = \frac{1}{2} \int d^3r \epsilon_{3jk} \hat{r}_j J_k^{(e.m.)} = \alpha(\lambda) \left[D_{33}(A) + \frac{1}{\sqrt{3}} D_{83}(A) \right] + \dots \quad (4)$$

The (transition) magnetic moments are the matrix elements

$$\begin{aligned} \mu_{B, B'} &= \langle B, m | \hat{\mu} | B', m' \rangle \\ &= \sum_{\substack{\mu, \nu \\ m_\mu, n_\nu}} C_{\mu, m_\mu}^{(B, m)} C_{\nu, m_\nu}^{(B', m')} \langle \mu | D_{33}(A) + \frac{1}{\sqrt{3}} D_{83}(A) | \nu \rangle \langle m_\mu | \alpha(\lambda) | n_\nu \rangle + \dots \end{aligned} \quad (5)$$

In table 1 the resulting data are normalized to the predicted proton magnetic moment in the respective treatments. Here it is $\mu_p = 2.58$. There is distinct improvement over the prediction of the rigid rotator approach (RRA), which is a mean-field treatment that does not include radial excitations and has a significantly smaller $\mu_p = 2.03$ [10] and does not adequately deviate from the U-spin symmetry relations $\mu_{\Sigma^+} \approx \mu_p$ and $\mu_{\Xi^0} \approx \mu_n$. The radial part of the wave-function must be sensitive to flavor symmetry breaking to properly reflect the observed deviation.

| bary. | μ/μ_p | | |
|--------------------------------|-------------|-------|-------|
| | rad.ex. | expt. | RRA |
| n | -0.75 | -0.68 | -0.78 |
| Λ | -0.19 | -0.22 | -0.35 |
| Σ^+ | 0.78 | 0.86 | 0.98 |
| Σ^- | -0.47 | -0.42 | -0.39 |
| Ξ^0 | -0.41 | -0.45 | -0.76 |
| Ξ^- | -0.14 | -0.25 | -0.32 |
| $\Sigma^0 \rightarrow \Lambda$ | -0.60 | -0.58 | -0.68 |

| m | proton | neutron |
|------------|-------------|-------------|
| | μ/μ_p | μ/μ_p |
| 1 (Roper?) | -0.41 | 0.40 |
| 2 (N1710?) | -0.13 | -0.08 |
| 3 (?) | -0.11 | -0.09 |

Table 1. Numerical results for the magnetic moments. Left panel magnetic moments of spin $\frac{1}{2}$ baryons; right panel transition moments in the nucleon channel.

This model result gives good confidence to compute the nucleon channel transition moments. The transition from the first state above the nucleon is of similar magnitude for proton and neutron³. This has to be contrasted to the omission of radial excitations, when the next to leading level in the nucleon channel is a pure anti-decuplet nucleon. In that case the proton transition magnetic moment vanishes [9] while the neutron is of typical size $0.28\mu_p$. Indeed some enhancement of the neutron over the proton channel in η -photoproduction has been reported [11], however, most likely this is caused by a negative negative parity structure [12].

The omission of flavor symmetry breaking produces transition moments to the first excitation of $-0.24\mu_p$ and $0.18\mu_p$ for the proton and neutron channels.

4 Conclusions

In these proceedings I have presented a dynamical mechanism to incorporate radial excitations when describing baryons in Skyrme type models. Only when the mixing of these excitations with members of higher dimensional SU(3) is accounted for, reliable statements on the spectrum of exotic baryons and their flavor

³ The overall signs are subject to the phase conventions on the wave-functions.

partners can be made. The present model calculation does not give evidence for an (additional, presumably narrow) nucleon resonance with a mass between 1.6 and 1.7GeV in contrast to the mean-field approach that omits this mixing [13]. Including radial excitations reverses the mean-field results for the nucleon channel transition magnetic moments of Ref. [9].

Acknowledgment

The author thanks the organizers for providing this worthwhile workshop and the support to cure his broken arm. This work is supported in part by the National Research Foundation of South Africa (NRF) by grant 109497.

References

1. H. Weigel, Lect. Notes Phys. **743** (2008) 1.
2. H. Weigel, Universe **4** (2018) 142.
3. L. C. Biedenharn and Y. Dothan, "Monopolar Harmonics In SU(3)-F As Eigenstates Of The Skyrme-Witten Model For Baryons," Print-84-1039 (DUKE)
4. H. Walliser, Nucl. Phys. A **548** (1992) 649.
5. C. Hajduk and B. Schwesinger, Phys. Lett. **145B** (1984) 171.
6. J. Schechter and H. Weigel, Phys. Rev. D **44** (1991) 2916
H. Weigel, Eur. Phys. J. A **21** (2004) 133
7. R. L. Jaffe and F. Wilczek, Phys. Rev. Lett. **91** (2003) 232003.
8. D. Diakonov and V. Petrov, Phys. Rev. D **69** (2004) 094011.
9. M. V. Polyakov and A. Rathke, Eur. Phys. J. A **18** (2003) 691.
10. H. Weigel, Int. J. Mod. Phys. A **11** (1996) 2419.
11. V. Kuznetsov *et al.*, Phys. Lett. B **647** (2007) 23.
12. F. Miyahara *et al.*, Prog. Theor. Phys. Suppl. **168** (2007) 90
I. Jaegle *et al.*, Phys. Rev. Lett. **100** (2008) 252002
13. G. S. Yang and H. C. Kim, Prog. Theor. Phys. **128** (2012) 397



News from Belle on Hadron Spectroscopy

M. Bračko

University of Maribor, Smetanova ulica 17, SI-2000 Maribor, Slovenia
and Jožef Stefan Institute, Jamova cesta 39, SI-1000 Ljubljana, Slovenia

Abstract. In this contribution, recent results on hadron spectroscopy from the Belle experiment are reviewed. All reported results are based on experimental data sample collected by the Belle detector, which was in operation between 1999 and 2010 at the KEKB asymmetric-energy e^+e^- collider in the KEK laboratory in Tsukuba, Japan. Even a decade after the end of the experiment, the collected data sample is still used for new measurements. Selection of results from recent Belle publications on hadron spectroscopy is presented in this review, reflecting the scope of the workshop and interest of its participants.

1 Introduction

During a decade of successful operation of both Belle detector[1] and KEKB accelerator[2], a large sample of experimental data was collected, corresponding to more than 1 ab^{-1} of integrated luminosity, with energies around the $\Upsilon(4S)$ resonance, but also at other Υ resonances, like $\Upsilon(1S)$, $\Upsilon(2S)$, $\Upsilon(3S)$, $\Upsilon(5S)$ and $\Upsilon(6S)$, as well as in the nearby continuum [3]. The available data has proven to offer excellent opportunities for various measurements, including the ones in hadron spectroscopy, like discoveries of new charmonium(-like) and bottomonium(-like) hadronic states, and studies of their properties.

2 Charmonium and Charmonium-like states

The field of charmonium spectroscopy attracted a lot of interest after the discovery of the state $X(3872)$, decaying to $J/\psi\pi^+\pi^-$ [4], and other so-called “XYZ” states—new charmonium-like states outside of the conventional charmonium picture. Belle continues with studies in this field of research, together with other experiments.

Various experimental studies of the $X(3872)$ state determined its $J^{PC} = 1^{++}$ assignment, and suggested that this state is an admixture of the conventional $2^3P_1 c\bar{c}$ state and a loosely bound $D^0\bar{D}^{*0}$ molecular state. If one wants to better understand the structure of $X(3872)$, further studies of production and decay modes for this narrow exotic state are necessary. An example of these experimental efforts is the recent study [5], where Belle performed searches for $X(3872)$ decaying to $\chi_{c1}\pi^0$. Simultaneously, a poorly understood state $X(3915)$ was also included in the search. No significant signal was found for any of the

two states, since only 2.7 ± 5.5 (42 ± 14) events were observed, with a signal significance of 0.3σ (2.3σ) for the $B^+ \rightarrow X(3872)(\rightarrow \chi_{c1}\pi^0)K^+$ ($B^+ \rightarrow X(3915)(\rightarrow \chi_{c1}\pi^0)K^+$) decay mode. The upper limits on the product branching fractions $\mathcal{B}(B^+ \rightarrow X(3872)K^+) \times \mathcal{B}(X(3872) \rightarrow \chi_{c1}\pi^0) < 8.1 \times 10^{-6}$ and $\mathcal{B}(B^+ \rightarrow X(3915)K^+) \times \mathcal{B}(X(3915) \rightarrow \chi_{c1}\pi^0) < 3.8 \times 10^{-5}$ were determined at 90% confidence level. The null result of the search is compatible with the above mentioned interpretation of the $X(3872)$ state, being the admixture of a conventional charmonium and a $D\bar{D}$ molecular states. Furthermore, the result for the upper limit of the ratio $\mathcal{B}(X(3872) \rightarrow \chi_{c1}\pi^0)/\mathcal{B}(X(3872) \rightarrow J/\psi\pi^+\pi^-) < 0.97$ at 90% confidence level, can be used to constrain the tetraquark/molecular component of the X states.

Another analysis, recently performed by Belle on the data sample corresponding to an integrated luminosity of 711 fb^{-1} and containing $772 \times 10^6 B\bar{B}$ pairs, focused on a search for the decay $B^0 \rightarrow X(3872)(\rightarrow J/\psi\pi^+\pi^-)\gamma$ [6]. Rare decays of B mesons are sensitive probes to study possible new physics beyond the Standard Model, which could significantly modify the branching fraction for the $B^0 \rightarrow J/\psi\gamma$ decay. Non-charmonium components of the exotic $X(3872)$ would make the $B^0 \rightarrow X(3872)\gamma$ branching fraction smaller than that of $B^0 \rightarrow J/\psi\gamma$. The performed search resulted in finding no significant signal, so only an upper limit on the product of the branching fractions $\mathcal{B}(B^0 \rightarrow X(3872)\gamma) \times \mathcal{B}(X(3872) \rightarrow J/\psi\pi^+\pi^-)$ of 5.1×10^{-7} was set at 90% confidence level.

The $Y(4260)$ state, also known as $\psi(4260)$ [7], is another exotic state, which draws much attention. It was first observed in the initial-state radiation (ISR) process $e^+e^- \rightarrow \gamma_{\text{ISR}}Y(4260)$ by the *BABAR* collaboration [8], and due to its production in ISR, its quantum numbers are expected to be $J^{PC} = 1^{--}$. This would make the $Y(4260)$ a natural candidate for a conventional charmonium state with $J^{PC} = 1^{--}$, but its mass and properties are not consistent with those expected for any of the predicted conventional $c\bar{c}$ states in this mass region. Instead, the measured properties indicate the exotic nature of the $Y(4260)$ state—it could be an admixture of charmonium and some other structures, like multi-quark states or mesonic molecules, it could be a hybrid charmonium, or some other exotic object. In order to understand the structure and properties of the $Y(4260)$ (and some other similar 1^{--} states), studies of several decay channels with large data sample are necessary.

The most recent example of such a study performed at Belle, is a search for the $B \rightarrow Y(4260)K$, $Y(4260) \rightarrow J/\psi\pi^+\pi^-$ decays using $B\bar{B}$ pairs collected at the $\Upsilon(4S)$ resonance [9]. The observed signal yields for these decays were $179 \pm 53_{-41}^{+55}$ events and $39 \pm 28_{-31}^{+7}$ events for the charged and neutral $B \rightarrow Y(4260)K$, $Y(4260) \rightarrow J/\psi\pi^+\pi^-$ decays, respectively, from fits to the individual decay samples; the first and second uncertainties are statistical and systematic, respectively. The signal significances are obtained to be 2.1σ and 0.9σ for the charged and neutral decays, respectively, taking into account the systematic uncertainties. The corresponding upper limits on the product of branching fractions, $\mathcal{B}(B^+ \rightarrow Y(4260)K^+) \times \mathcal{B}(Y(4260) \rightarrow J/\psi\pi^+\pi^-) < 1.4 \times 10^{-5}$ and $\mathcal{B}(B^0 \rightarrow Y(4260)K^0) \times \mathcal{B}(Y(4260) \rightarrow J/\psi\pi^+\pi^-) < 1.7 \times 10^{-5}$ determined at the 90% confidence level, are the most stringent to date. However, as these results were already based on the complete Belle data sample, more information about

the nature of the $Y(4260)$ state can only be obtained by improved measurements with a larger data sample, which will only be available at the Belle II experiment [10].

One of the most recent charmonium-related studies from Belle is a search for the decays $B^+ \rightarrow h_c K^+$ and $B^0 \rightarrow h_c K_S^0$ [11]. The decays $B^+ \rightarrow \chi_{c0} K^+$, $B^+ \rightarrow \chi_{c2} K^+$ and $B^+ \rightarrow h_c K^+$ are suppressed by factorization. The decays $B^+ \rightarrow \chi_{cJ} K^+$ have been observed; the current world-average branching fractions are $\mathcal{B}(B^+ \rightarrow \chi_{c0} K^+) = (1.49_{-0.14}^{+0.15}) \times 10^{-4}$ and $\mathcal{B}(B^+ \rightarrow \chi_{c2} K^+) = (1.1 \pm 0.4) \times 10^{-5}$ [7]. While $\mathcal{B}(B^+ \rightarrow \chi_{c0} K^+)$ is smaller than the branching fraction of the factorization-allowed process $\mathcal{B}(B^+ \rightarrow \chi_{c1} K^+) = (4.84 \pm 0.23) \times 10^{-4}$, it is not strongly suppressed. Under the same assumption, the process $B^+ \rightarrow h_c K^+$ was expected to have a similar branching fraction $\mathcal{B}(B^+ \rightarrow h_c K^+) \approx \mathcal{B}(B^+ \rightarrow \chi_{c0} K^+)$. However, the decays $B^+ \rightarrow h_c K^+$ and $B^0 \rightarrow h_c K_S^0$ have not been observed before. The reported analysis, which benefits from the large Belle data sample, but also from improved discrimination between background and signal events due to multivariate analysis, clearly demonstrates the discovery potential at Belle. As a result of this study, evidence for the decay $B^+ \rightarrow h_c K^+$ was found, with a significance of 4.8σ , while no evidence was found for $B^0 \rightarrow h_c K_S^0$. The measured branching fraction for the $B^+ \rightarrow h_c K^+$ decays is $(3.7_{-0.9}^{+1.0} \pm 0.8) \times 10^{-5}$ while the upper limit for $B^0 \rightarrow h_c K_S^0$ branching fraction is 1.4×10^{-5} at 90% confidence level. In addition, a study of the $p\bar{p}\pi^+\pi^-$ invariant mass distribution in the channel $B^+ \rightarrow (p\bar{p}\pi^+\pi^-)K^+$ resulted in the first observation of the decay $\eta_c(2S) \rightarrow p\bar{p}\pi^+\pi^-$ with more than 12σ significance.

3 Results on Charmed Baryons

Almost a decade after the end of data taking at Belle, a lot of effort is now invested into studies of charmed baryons. Many results were obtained recently and many analyses are still ongoing. The list of results is quite long and it probably deserves a separate contribution. Here, we will therefore mention just one of the published results [12]—observation of the excited Ω^- baryon—while other recent publications are only quoted in the reference section ([14], ..., [25]).

In the above mentioned analysis [12], a new hyperon was observed. The observed particle is a candidate for an excited Ω^{*-} baryon. These baryons comprise three strange quarks, and have zero isospin. This means that $\Omega^{*-} \rightarrow \Omega^- \pi^0$ decays are highly suppressed, which restricts possible decays of excited states, so that the largest expected decay modes are ΞK . This behaviour is analogous to the $\Omega_c^0 \rightarrow \Xi_c^+ K^-$ decays recently discovered by the LHCb Collaboration [13] and confirmed soon after by Belle [16]. The observed new resonance, which is identified as an excited Ω^- baryon, was therefore found in the decay modes $\Omega^{*-} \rightarrow \Xi^0 K^-$ and $\Omega^{*-} \rightarrow \Xi^- K_S^0$, as expected. The measured mass of the resonance is $[2012.4 \pm 0.7 \text{ (stat)} \pm 0.6 \text{ (syst)}] \text{ MeV}/c^2$ and its width, Γ , is $[6.4_{-2.0}^{+2.5} \text{ (stat)} \pm 1.6 \text{ (syst)}] \text{ MeV}$. The mass of the new resonance is $340 \text{ MeV}/c^2$ higher than the ground state, which fills the gap in the Ω^- spectrum between the ground state and previously observed excited states. The Ω^{*-} is seen primarily in the decay of the narrow resonances $\Upsilon(1S)$, $\Upsilon(2S)$, and $\Upsilon(3S)$ (1). The corresponding data samples, collected

with the accelerator energy tuned for the production of the three mentioned Υ resonances, correspond to integrated luminosities of 5.7 fb^{-1} , 24.9 fb^{-1} , and 2.9 fb^{-1} , respectively.

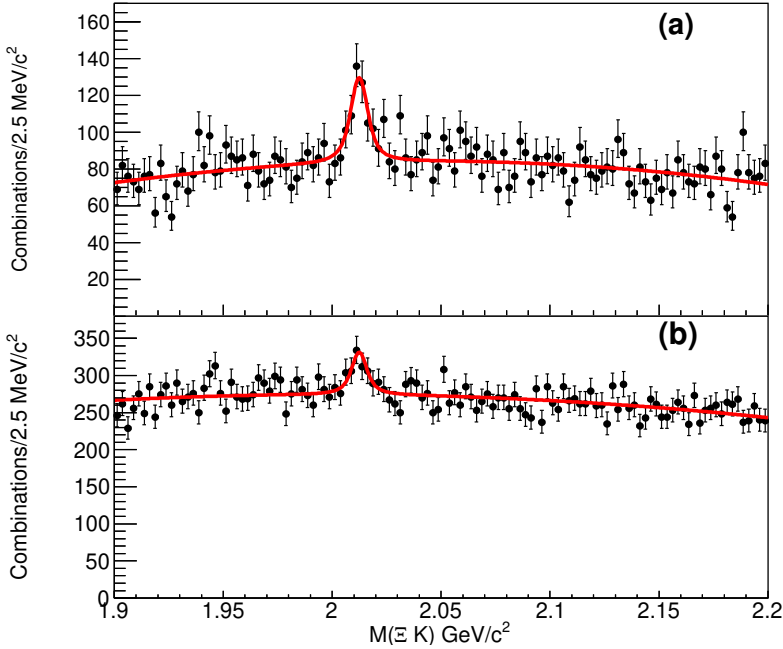


Fig. 1. The (a) $\Xi^0 K^-$ and (b) $\Xi^- K_S^0$ invariant mass distributions in data taken at the energies of $\Upsilon(1S)$, $\Upsilon(2S)$, and $\Upsilon(3S)$ resonances. The curves show the result of a simultaneous fit to the two distributions with a common mass and width.

4 Summary and Conclusions

Many new particles have already been discovered during the operation of the Belle experiment at the KEKB collider, and some of them are mentioned in this report. Although the operation of the experiment finished almost a decade ago, data analyses are still ongoing and consequently more interesting results on charmonium(-like), bottomonium(-like) and baryon spectroscopy can still be expected from Belle in the near future. The results are eagerly awaited by the community and will be widely discussed at various occasions, in particular at workshops and conferences.

Still, the era of the Belle experiment is slowly coming to an end. Further progress towards high-precision measurements—with possible experimental

surprises—in the field of hadron spectroscopy are expected from the huge experimental data sample, which will be collected in the future by the Belle II experiment [10]. Actually, this future has already started, since the completed Belle II detector began its operation at the SuperKEKB collider in March 2019.

References

1. Belle Collaboration, *Nucl. Instrum. Methods A* **479**, 117 (2002).
2. S. Kurokawa and E. Kikutani, *Nucl. Instrum. Methods A* **499**, 1 (2003), and other papers included in this Volume.
3. J. Brodzicka *et al.*, *Prog. Theor. Exp. Phys.*, 04D001 (2012).
4. Belle Collaboration, *Phys. Rev. Lett.* **91**, 262001 (2003).
5. Belle Collaboration, *Phys. Rev. D* **99**, 111101(R) (2019).
6. Belle Collaboration, *Phys. Rev. D* **100**, 012002 (2019).
7. M. Tanabashi *et al.* (Particle Data Group), *Phys. Rev. D* **98**, 030001 (2018).
8. BABAR Collaboration, *Phys. Rev. Lett.* **95**, 142001 (2005); *Phys. Rev. D* **86**, 051102 (2012).
9. Belle Collaboration, *Phys. Rev. D* **99**, 071102(R) (2019).
10. Belle II Collaboration, Belle II Technical design report, [arXiv:1011.0352 [physics.ins-det]].
11. Belle Collaboration, *Phys. Rev. D* **100**, 012001 (2019).
12. Belle Collaboration, *Phys. Rev. Lett.* **121**, 052003 (2018).
13. LHCb Collaboration, *Phys. Rev. Lett.* **118**, 182001 (2018).
14. Belle Collaboration, *Phys. Rev. D* **97**, 012005 (2018).
15. Belle Collaboration, *Phys. Rev. D* **97**, 032001 (2018).
16. Belle Collaboration, *Phys. Rev. D* **97**, 051102 (2018).
17. Belle Collaboration, *Phys. Rev. D* **97**, 072005 (2018).
18. Belle Collaboration, *Phys. Rev. D* **97**, 112004 (2018).
19. Belle Collaboration, *Phys. Rev. D* **98**, 112006 (2018).
20. Belle Collaboration, *Eur. Phys. J. C* **78**, 252 (2018).
21. Belle Collaboration, *Eur. Phys. J. C* **78**, 928 (2018).
22. Belle Collaboration, *Phys. Rev. D* **100**, 032006 (2019).
23. Belle Collaboration, *Phys. Rev. D* **100**, 031101 (2019).
24. Belle Collaboration, *Phys. Rev. Lett.* **122**, 072501 (2019).
25. Belle Collaboration, *Phys. Rev. Lett.* **122**, 082001 (2018).



The enigmatic $\Delta(1600)$ resonance

B. Golli

Faculty of Education, University of Ljubljana and Jožef Stefan Institute, 1000 Ljubljana, Slovenia

Abstract. Our recently proposed model of the $\Delta(1600)$ resonance, in which the dominant component is a quasi-bound state of the $\Delta(1232)$ and the pion, is confronted with a similar model of the $N^*(1440)$ resonance as its counterpart in the P11 partial wave. We stress an essentially different mechanism responsible for generating the two resonances.

The two low-lying resonances in the P11 and P33 partial waves, the Roper resonance ($N^*(1440)$) and the $\Delta(1600)$ resonance, have been attracting special attention due to their relatively low masses compared to the prediction of the quark model in which they figure as the first radial excitations in the respective channel, and have been considered as candidates for dynamically generated resonances. In order to understand the mechanism of their formation we study these two resonances in a chiral quark model, which may produce either a genuine resonance by exciting the quark core, or a dynamically generated resonance involving a baryon-meson quasi-bound state. We use a coupled channel approach involving the πN , $\pi\Delta$, and σN channels which — based on our previous experience — dominate the intermediate energy regime in the P11 and P33 partial waves. The Cloudy Bag Model (CBM) is used to fix the quark-pion vertices while the s -wave σ -baryon vertex is introduced phenomenologically with the coupling constant g_σ as a free parameter. Labeling the channels by α, β, γ , the Lippmann-Schwinger equation for the meson amplitude $\chi_{\alpha\gamma}$ for the process $\gamma \rightarrow \alpha$ can be cast in the form

$$\chi_{\alpha\gamma}(k_\alpha, k_\gamma) = \mathcal{K}_{\alpha\gamma}(k_\alpha, k_\gamma) + \sum_\beta \int dk \frac{\mathcal{K}_{\alpha\beta}(k_\alpha, k) \chi_{\beta\gamma}(k, k_\gamma)}{\omega(k) + E_\beta(k) - W}. \quad (1)$$

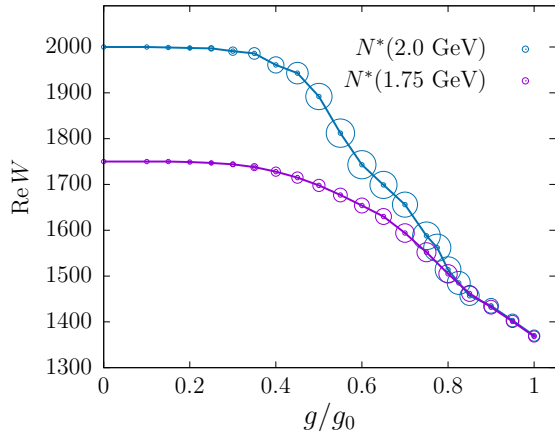
The half-on-shell pion amplitude consists of the resonant and non-resonant part,

$$\chi_{\alpha\gamma}(k, k_\gamma) = c_{\gamma R} \mathcal{V}_{\alpha R}(k) + \mathcal{D}_{\alpha\gamma}(k, k_\gamma), \quad (2)$$

with the non-resonant part $\mathcal{D}_{\alpha\gamma}(k, k_\gamma)$ satisfying the same Lippmann-Schwinger equation, while the dressed vertex $\mathcal{V}_{\alpha R}(k)$ satisfies the Lippmann-Schwinger equation with the same kernel and the bare vertex for the non-homogeneous part. Approximating the kernel \mathcal{K} by a separable form, the integral equations reduce to a system of linear equations which can be solved exactly. The resulting amplitude is proportional to the K matrix which, in turn, determines the scattering T matrix. The Laurent-Pietarinen expansion is finally used to extract the information about the S-matrix poles in the complex energy plane.

The formation of the Roper resonance ($N^*(1440)$) is studied in Ref. [1], confronting two mechanisms for resonance formation: the explicit inclusion of a resonant three-quark state in which one quark is promoted to the $2s$ state, and the dynamical generation in the absence of the resonant state. In both cases the nucleon pole is explicitly included. While the p -wave πN interaction is repulsive in the P_{11} channel, the s -wave σN interaction is attractive, and is able to support a (quasi) bound state for sufficiently strong g_σ . The resulting mass of the resonance is close to the PDG value in a relatively wide interval of g_σ , while its width is smaller than the PDG value and drops with increasing g_σ . Including a three-quark resonant state, the mass of the resonance remains almost the same, while its width increases and comes very close to its PDG value (see Table III in [1]). The result is rather insensitive to the mass of the three-quark resonant state, which allows us to use a value around 2 GeV, in agreement with the quark-model ordering of the $2s$ and $1p$ states, as well as with the recent results of the lattice calculations [2,3] which have not found a sizable three-quark component below ~ 1.7 GeV. We conclude that while the mass of the S -matrix pole is determined by the dynamically generated state, its width and modulus are strongly influenced by the three-quark resonant state. This conclusion is further supported by a smooth evolution of the S -matrix pole in the complex energy plane as the coupling of the σ as well as of the pion to the quark core is gradually increased on (see Fig. 1). Starting with two bare masses of 1750 MeV and 2000 MeV, both curves end up almost at the same point with the mass and width consistent with the PDG values.

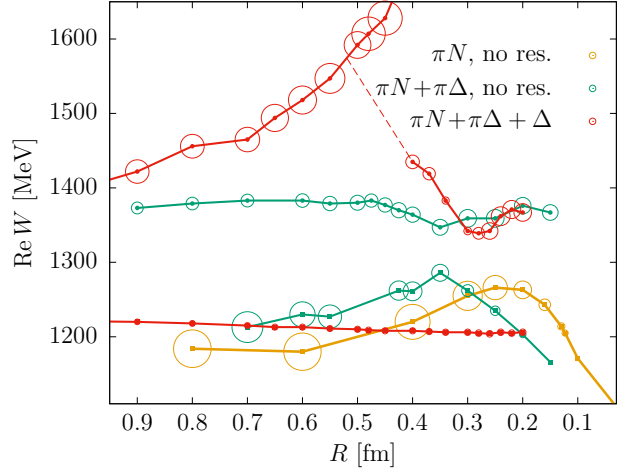
Fig. 1. Evolution of the $N^*(1440)$ mass ($\text{Re } W$) and the width (proportional to the radius of the circle) as a function of the interaction strength for two bare masses of the three-quark configuration, 1750 MeV and 2000 MeV; g/g_0 denotes the reduction factor, equal for each coupling constant. The radius at $g/g_0 = 1$ corresponds to $\text{Im } W = 180$ MeV.



Though we might expect that, because of apparently the same three-quark configuration, the situation with the $\Delta(1600)$ is similar to that with the $N^*(1440)$ resonance, this is not the case. One important difference is the nature of the p -wave πN interaction which is attractive in the P_{33} partial wave, in contrast to its repulsive character in the P_{11} , P_{13} , and P_{31} waves. Furthermore, the analog of the σN system, the $\sigma\Delta(1232)$ system, turns out to make a sizable contribution to the scattering amplitude only above 1700 MeV, and hence the σ plays a minor role in the formation of the $\Delta(1600)$ resonance. In [5] we therefore consider only the

πN and the $\pi\Delta$ channels. Since the πN coupling constant is fixed by the behavior of the scattering amplitudes near the threshold, the only free parameter in the underlying model (CBM) is the bag radius R which is inversely proportional to the cutoff energy; for the value of $R = 0.8$ fm, leading to the most consistent results for the nucleon as well as for the low lying resonances, it corresponds to ≈ 550 MeV.

Fig. 2. Evolution of the poles as a function of the bag radius in the P33 partial wave in three different approximations: (i) including only the nucleon and the pion (orange curve and circles), (ii) including the nucleon and the Δ but without a resonant state (green), (iii) with the Δ resonant states (red). The width of the resonance $-2\text{Im}W$ is proportional to the radius of the circle.



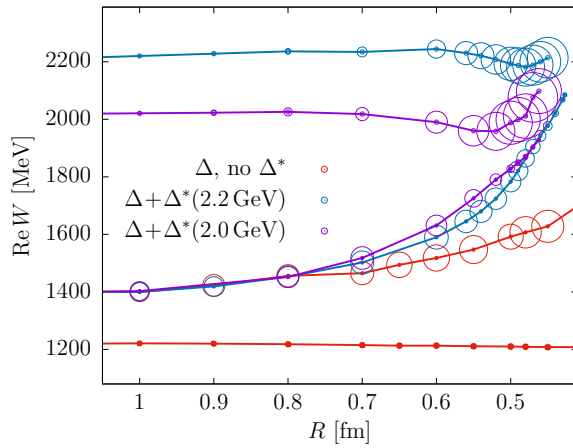
Already a few years after the discovery of the $\Delta(1232)$ resonance, it was conjectured that this resonance arises as a consequence of the attraction in the πN system at sufficiently strong cutoff [6]. In our model we do observe a resonance in the πN system manifesting itself as a pole in the complex energy plane at a mass around 1200 MeV, with a width that decreases with increasing interaction strength (decreasing R) (orange curve in Fig. 2). For $R = 0.123$ fm the mass and the width reach the values which agree well with the PDG values, and for $R = 0.050$ fm the system becomes bound. We next include the Δ (in addition to the nucleon) as the u -channel exchange particle in the kernel, and solve (1) for the nonresonant amplitude \mathcal{D} . Besides the pole at around 1200 MeV another pole slightly below 1400 MeV emerges (green curves in Fig. 2). The second pole is dominated by the $\pi\Delta$ configuration and can be interpreted as a progenitor of the $\Delta(1600)$ resonance.

We next include a three-quark state corresponding to the $\Delta(1232)$ in the s -channel and fix its bare mass such that the resulting Breit-Wigner mass (i.e., the zero of $\text{Re} T$) appears at 1232 MeV. With decreasing R the resonant state mixes more and more strongly with the lower dynamically generated state, forming the physical $\Delta(1232)$. The latter component dominates below $R = 0.2$ fm, nonetheless, the mass and the width of the resonance pole remain constant (red curves in Fig. 2) and stay close to the PDG value. The upper dynamically generated resonance is pushed toward a slightly higher mass and acquires a larger width. In the physically sensible region around $R \approx 0.8$ fm, the mass and the width come close to the PDG values for the $\Delta(1600)$ resonance. The attribution of this pole to the

$\Delta(1600)$ resonance is, however, not justified for smaller R , where its mass keeps increasing, and, in addition, another branch emerges, approaching the upper dynamically generated resonance.

We finally add a bare $(1s)^2(2s)$ configuration representing the first radial excitation of the $\Delta(1232)$. In the harmonic oscillator model, its mass is expected to lie ~ 1 GeV above the $(1s)^3$ configuration, so we fix its (bare) mass at 2.2 GeV, while its coupling is taken from the CBM. Apart from the two resonances discussed above, the third resonance emerges with a mass ($\text{Re } W$) close to the bare value. Increasing the strength of the interaction (decreasing R) we notice that it stays almost constant and — at least in the physically relevant regime of R 's — well separated from the other two resonances.

Fig. 3. Evolution of the poles in the model including two resonant states with the second state at the bare mass of 2.2 GeV (blue curves) and at 2.0 GeV (violet), respectively, compared with the model involving Δ alone (red, the same curve as in Fig. 2).



We can therefore conclude that the radially excited quark state plays a very minor role in the formation of the $\Delta(1600)$ resonance, which in our model turns out to be primarily a quasi-bound state of $\Delta(1232)$ and the pion. This mechanism is therefore fundamentally different from that responsible for the formation of the $N^*(1440)$ resonance, discussed above, and originates in the different nature of the pion interaction in the two partial waves.

This work has been done in collaboration with H. Osmanović (Tuzla) and S. Širca (Ljubljana).

References

1. B. Golli, H. Osmanović, S. Širca, and A. Švarc, *Phys. Rev. C* **97**, 035204 (2018).
2. C. B. Lang, L. Leskovec, M. Padmanath, S. Prelovšek, *Phys. Rev. D* **95**, 014510 (2017).
3. A. L. Kiratidis et al., *Phys. Rev. D* **95**, 074507 (2017).
4. M. Tanabashi et al. (Particle Data Group), *Phys. Rev. D* **98**, 030001 (2018).
5. B. Golli, H. Osmanović, S. Širca, *Phys. Rev. C* **100**, 035204 (2019).
6. G. F. Chew and F. E. Low, *Phys. Rev.* **101**, 1570 (1956).



A phenomenological lower bound for the Ξ_{cc}^{++} mass

Mitja Rosina

Faculty of Mathematics and Physics, University of Ljubljana, Jadranska 19, P.O. Box 2964, 1001 Ljubljana, Slovenia and J. Stefan Institute, 1000 Ljubljana, Slovenia

Abstract. We show that a simple interpolation between mesonic binding energies can give a good semiquantitative binding energy of the cc diquark and the Ξ_{cc}^{++} baryon. The mass of the Ξ_{cc}^{++} baryon is almost insensitive to widely different choices of the constituent quark masses.

1 Introduction

After the discovery of the Ξ_{cc}^{++} baryon at LHCb, there is a strong interest to verify whether the quark models which have been successful for light and single-heavy hadrons apply also to double-heavy hadrons; in particular, how rich spectrum we can expect. It is important to check whether we may use the same effective quark-quark interaction (apart from the colour factor and the mass-dependent spin-spin term): $V_{uu} = V_{cu} = V_{cc} = V_{c\bar{c}} = V_{bu} = V_{bb} = V_{b\bar{b}}$. For this purpose it is instructive to study some phenomenological models even if the results are only semiquantitative.

The present study is based on two assumptions:

(1) The quark-quark interaction in colour-triplet state is half the quark-anti-quark interaction in colour-singlet state.

(2) The ccu baryon can be treated as a two-body system, the cc diquark plus the u quark, similar to the $c\bar{u}$ or $b\bar{u}$ meson.

These assumptions have been made already by several authors, for example [1,2]. The purpose of this presentation is to show a nice trick how to obtain easily the binding energies of meson-like systems by a simple interpolation between mesonic data [3].

2 The cc diquark interpolated between mesons

We compare the nonrelativistic Schrödinger equations for an $(a\bar{b})$ meson in the colour singlet state and for an (ab) diquark in a colour antitriplet state (with twice weaker interaction):

$$\left[\frac{p^2}{2m_{a\bar{b}}} + V_{a\bar{b}} \right] \psi = E_{a\bar{b}} \psi \equiv F(m_{a\bar{b}}) \psi,$$

$$\begin{aligned} \left[\frac{p^2}{2m_{ab}} + V_{ab} \right] \psi &= \left[\frac{p^2}{2m_{ab}} + \frac{1}{2}V_{a\bar{b}} \right] \psi = \frac{1}{2} \left[\frac{p^2}{2(m_{ab}/2)} + V_{a\bar{b}} \right] \psi \\ &= E_{ab}\psi \equiv \frac{1}{2}F\left(\frac{1}{2}m_{ab}\right)\psi. \end{aligned}$$

Here the reduced masses are $m_{a\bar{b}} = m_a m_{\bar{b}}/(m_a + m_{\bar{b}})$ and $m_{ab} = m_a m_b/(m_a + m_b)$, respectively. The binding energy $F(m)$ is a smooth function of m as illustrated in Fig. 1.

Phenomenological binding energies of mesons are obtained from experimental meson masses M and model values of constituent quark masses: $E_{a\bar{b}} = M_{a\bar{b}} - m_a - m_{\bar{b}}$. The diquark masses are then predicted (Table 1). The trick is to take for the diquark binding energy $\frac{1}{2}F(\frac{1}{2}m_{ab})$, according to the above Schrödinger equation.

The constituent quark masses in Fig. 1 and Table 1 are taken from Bhaduri [4]: $m_{u,d,s,c,b} = 337, 337, 600, 1870, 5259$ MeV, and in Table 1 also from Karliner and Rosner [1]: $m_{u,d,s,c,b} = 310, 310, 483, 1663, 5004$ MeV.

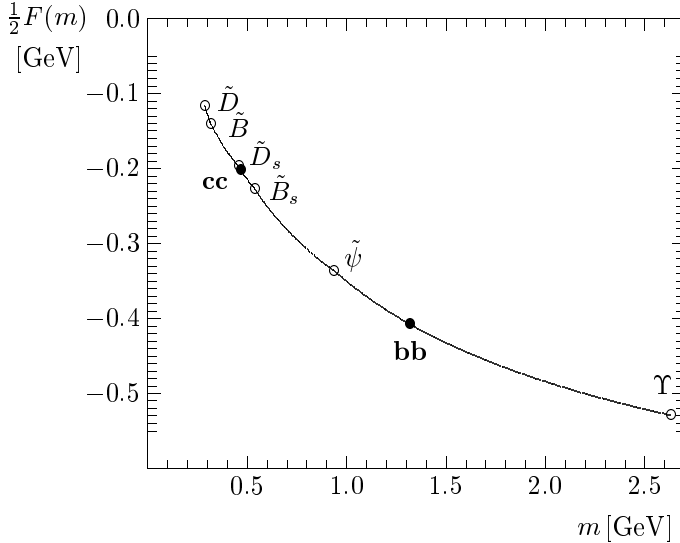


Fig. 1. The meson binding energy $F(m)$, multiplied by $\frac{1}{2}$, as a function of the reduced mass $m = m_{a\bar{b}}$. The diquark binding energies $\frac{1}{2}F(\frac{1}{2}m_{ab})$ are then predicted by interpolation. (From [3]).

3 The binding of the Ξ_{cc}^{++} baryon

The $(cc)u$ baryon is treated as a two-body system. The reduced mass is $m = m_u M_{cc}/(m_u + M_{cc})$, where $M_{cc} = 2m_c + \frac{1}{2}F(\frac{1}{2}m_{cc})$ and the binding energy between the u quark and the (cc) diquark $E_{(cc)u} = F(m)$ is obtained by interpolation in Fig. 1 or Table 1. The mass of the Ξ_{cc}^{++} baryon is then $M_{(cc)u} = M_{cc} + m_u + E_{(cc)u} = 3605$ (3596) MeV for the choice of constituent masses of Bhaduri (or Karliner-Rosner).

Table 1. The interpolation between mesons.

The tilde means spin average, Δ is the difference between the vector and scalar mesons, m is the reduced mass for mesons and half the reduced mass for diquarks; F is the meson or baryon binding energy and twice the diquark binding energy. Reduced masses refer to the constituent quark masses of Bhaduri [4] or Karliner-Rosner [1], respectively. Energies and masses are in MeV. In the 6th and 9th column are predictions for the diquark and double heavy baryons.

| Meson | mass | Δ | m | F | mass | m | F | mass |
|------------------------|------|----------|------|-------|---------|---------|------|---------|
| | | | Bha | | predict | Kar-Ros | | predict |
| \widetilde{D} | 1973 | 141 | 286 | -234 | | 261 | 0 | |
| \widetilde{B} | 5314 | 46 | 317 | -282 | | 292 | 0 | |
| \widetilde{D}_s | 2076 | 144 | 454 | -394 | | 374 | -70 | |
| \widetilde{B}_s | 5403 | 48 | 539 | -456 | | 440 | -84 | |
| $\widetilde{\psi}$ | 3069 | 113 | 935 | -671 | | 832 | -257 | |
| $\widetilde{\Upsilon}$ | 9445 | 61 | 2630 | -1073 | | 2502 | -563 | |
| \widetilde{cc} | | | 467 | -405 | 3538 | 416 | -80 | 3286 |
| \widetilde{bb} | | | 1315 | -819 | 10108 | 1251 | -383 | 9817 |
| $\widetilde{(cc)u}$ | | | 308 | -268 | 3605 | 283 | 0 | 3596 |
| $\widetilde{(bb)u}$ | | | 317 | -282 | 10163 | 301 | -4 | 10123 |

4 The hyperfine correction

So far, spin averages were taken for the diquark and baryon binding energies. The hyperfine splitting is obtained from the experimental differences between vector and scalar mesons. The cc diquark ($S = 1$) is therefore heavier by $(1/4)\Delta(\psi)/2 = 113 \text{ MeV}/8 = 14 \text{ MeV}$. (The extra $(1/2)$ comes from the fact, that the potential in cc colour triplet state is twice weaker than in mesons.) On the other hand, the $(cc)u$ ($S = \frac{1}{2}$) baryon is lighter by $\approx \Delta(D) (1870/3552) = -74 \text{ MeV}$. (The latter factor takes into account that the spin-spin interaction is inversely proportional to both masses, so instead of the u quark mass in the D meson one takes the (cc) mass. Also, it is convenient that the reduced mass of $(cc)u$ is close to that of D and D_s mesons, so the interpolation is trivial.)

The result for the Ξ_{cc}^{++} mass is then 3545 MeV (Bhaduri quark masses) or 3539 MeV (Karliner-Rosner quark masses).

5 A note on the binding energy of the DD^* dimeson

We cannot estimate the binding energy of the DD^* dimeson in the same way since the $(cc)\bar{u}\bar{b}$ ("tetraquark" or "atomic" or "He-like") configuration is about 100 MeV above the $D+D^*$ threshold [3]. This is then only a minor configuration, the main configuration is a DD^* "molecule", with a covalent bond like the H_2

molecule. In the restricted 4-body space with the two c quarks far apart and a general wavefunction of \bar{u} and \bar{d} the energy is also above the $D+D^*$ threshold, as presented by several authors.

Only combining both types of configurations brings the energy below the threshold, as shown by Janc and Rosina [5–7]. In the nonrelativistic calculation with the one-gluon exchange potential (including the chromomagnetic term) plus the linear confining potential they obtain the binding energy $(DD^*) - (D + D^*) = -2.7$ MeV. The model parameters (Grenoble AL1) [8] fitted all relevant mesons and baryons and a rich 4-body space was used (Gaussian expansion at optimized distances, with 3 types of Jacobi coordinates).

We pose an important question (“to be discussed at the next Bled Workshop”) whether the pion and sigma clouds between the u and d antiquarks can increase binding, in analogy with the deuteron. Is there a double counting? Would it be necessary to refit the model parameter so much that this extra binding would be compensated? If, however, the binding really becomes much stronger, at least below -6 MeV, the $DD\pi$ decay channel would be closed, the DD^* system would live longer and would be easier to be recognized in experiment.

6 Conclusion

The phenomenological binding energies of the cc diquark and the Ξ_{cc}^{++} baryon can be obtained by interpolation between the mesonic data. The mass of the Ξ_{cc}^{++} baryon is a lower bound, further corrections (eg. the Coulomb energy and the finite size of the cc diquark) would raise it, possibly close to the experimental value.

It is instructive to see that the final result depends only very weakly on the choice of quark constituent masses. In the binding energy, larger constituent masses (larger by as much as 200 MeV) are compensated by a stronger attractive potential.

References

1. M. Karliner and J. L. Rosner, *Phys. Rev. D* **90** (2014) 094007.
2. M. Karliner and J. L. Rosner, *Bled Workshops in Physics* **20**, No. 1 (2019), these Proceedings; also available at <http://www-f1.ijs.si/BledPub>.
3. D. Janc and M. Rosina, *Few-Body Systems* **31** (2001) 1-11; also available at arXiv:hep-ph/0007024v3.
4. R. K. Bhaduri L. E. Cohler, Y. Nogami, *Nuovo Cim.* **A65** (1981) 376.
5. D. Janc and M. Rosina, *Few-Body Systems* **35** (2004) 175-196; also available at arXiv:hep-ph/0405208v2.
6. M. Rosina and D. Janc, *Bled Workshops in Physics* **5**, No. 1 (2004) 74; also available at <http://www-f1.ijs.si/BledPub>.
7. M. Rosina, *Bled Workshops in Physics* **18**, No. 1 (2017) 82; also available at <http://www-f1.ijs.si/BledPub>.
8. B. Silvestre-Brac, *Few-Body Systems* **20** (1996) 11.



Measurement of G_A and the GDH sum rule at high energies at Jefferson Lab: two proposals

S. Širca^{a, b}

^a Faculty of Mathematics and Physics, University of Ljubljana, Jadranska 19, 1000 Ljubljana, Slovenia

^b Jožef Stefan Institute, Jamova 39, 1000 Ljubljana, Slovenia

Abstract. We present two developing experimental proposals for measurements to be performed by using electron scattering, with TJNAF (Jefferson Lab) as the most likely facility: a clean measurement of the nucleon axial form-factor, G_A , and a measurement of the high-energy contribution to the Gerasimov-Drell-Hearn (GDH) sum rule. The work on G_A is done in collaboration with A. Deur (Jefferson Lab) and C. M. Camacho (IPN-Orsay), and the GDH effort is pursued in collaboration with A. Deur, M. Dalton (Jefferson Lab) and J. Stevens (College of William & Mary).

1 Clean measurement of G_A

The nucleon electro-magnetic form-factors, $G_E(Q^2)$ and $G_M(Q^2)$, parameterize the (nucleon) electro-magnetic current operator, and they are well known over a range of Q^2 from $e-p$ and $e-n$ scattering. With certain approximations, they can be considered as Fourier transforms of spatial distributions of nucleon charge and magnetization. On the other hand, the *axial* and *pseudoscalar* form-factors, $G_A(Q^2)$ and $G_P(Q^2)$, entering the axial current,

$$\left\langle N(p') \left| \bar{q} \gamma_\mu \gamma_5 \frac{\tau^\alpha}{2} q \right| N(p) \right\rangle = \bar{u}(p') \left[\gamma_\mu G_A(Q^2) + \frac{(p' - p)_\mu}{2M} G_P(Q^2) \right] \gamma_5 \frac{\tau^\alpha}{2} u(p),$$

are less well known. The axial form-factor, in particular, can be thought to probe the spatial distribution of the nucleon spin, as can be seen from the terms containing σ appearing upon a non-relativistic reduction of the axial current:

$$\sigma, \quad \frac{\sigma \cdot p}{E + M}, \quad \frac{\sigma \cdot p'}{E' + M}, \quad \frac{\sigma \cdot p}{E + M} \sigma \frac{\sigma \cdot p'}{E' + M}.$$

The axial form-factor is conventionally parameterized in the so-called “dipole” form, i. e. by using the same traditional functional form as used in the electro-magnetic form-factors:

$$G_A(Q^2) = \frac{G_A(0)}{\left(1 + \frac{Q^2}{M_A^2}\right)^2}, \quad G_A(0) = g_A \approx 1.27, \quad (1)$$

where g_A is the axial coupling constant and $M_A \approx 1$ GeV is an adjustable “axial mass” (cut-off parameter). Different (and better justified) parameterizations exist, e. g. based on axial-vector dominance, large N_c and high-energy-QCD constraints:

$$G_A(Q^2) = g_A \sum_n c_n \frac{1}{1 + Q^2/m_n^2}.$$

Such a representation uses a sum of “monopole” forms, with the index n running over isovector/axial-vector mesons (a_1, a'_1, \dots), and $c_n = f_n g_{nNN}/g_A$, where f_n is the vacuum amplitude of meson n and g_{nNN} its coupling to the nucleon [1].

1.1 Existing determinations of G_A

Thus far $G_A(Q^2)$ has been extracted by using two methods: elastic or quasi-elastic neutrino scattering, and electron scattering. In the first case one measures the cross-sections for the processes $\nu n \rightarrow l^- p$ and $\bar{\nu} p \rightarrow l^+ n$ (in nuclei),

$$\frac{d\sigma}{dQ^2} = \frac{G_F^2 M^2 \cos^2 \theta_c}{8\pi E_\nu^2} \left[A(Q^2) \mp B(Q^2) \frac{s - M^2}{M^2} + C(Q^2) \frac{(s - M^2)^2}{M^4} \right],$$

where $A(Q^2)$, $B(Q^2)$ and $C(Q^2)$ are known functions of $G_E(Q^2)$, $G_M(Q^2)$ and $G_A(Q^2)$. The axial form-factor is then determined by fitting the Q^2 -dependence of the cross-section; the cut-off parameter M_A is then typically extracted by assuming the dipole form of $G_A(Q^2)$ (see [2] and references therein).

In the second case, one exploits the $p(e, e'\pi^+)n$ process near threshold [3], for which the cross-section can be written as

$$\frac{d\sigma}{dE'_e d\Omega'_e d\Omega_\pi^*} = \Gamma_\nu \frac{d\sigma_\nu}{d\Omega_\pi^*}, = \Gamma_\nu \left[\frac{d\sigma_T}{d\Omega_\pi^*} + \varepsilon_L^* \frac{d\sigma_L}{d\Omega_\pi^*} \right],$$

where Γ_ν is the virtual photon flux. The longitudinal part of the cross-section probes $F_\pi(Q^2)$, while its transverse part is sensitive to $G_A(Q^2)$ and, in turn, to the axial RMS radius,

$$\langle r_A^2 \rangle = -\frac{6}{G_A(0)} \left. \frac{dG_A(Q^2)}{dQ^2} \right|_{Q^2=0} = \frac{12}{M_A^2}.$$

It is well known from χ PT [4] that the axial radius picks up a correction due to pion loops, such that the “true” axial radius (measured in neutrino scattering) becomes modified in electro-production experiments:

$$\langle r_A^2 \rangle \rightarrow \langle r_A^2 \rangle + \frac{3}{64f_\pi^2} \left(1 - \frac{12}{\pi^2} \right). \quad (2)$$

As suggested by the extractions shown in Fig. 1, this indeed seems to be the case: the neutrino experiments yield a world average of $\langle M_A \rangle = (1.026 \pm 0.009)$ GeV, while the pion electro-production experiments give $\langle M_A \rangle = (1.062 \pm 0.015)$ GeV. There is an $\approx 2.5 \sigma$ difference in $\langle M_A \rangle$ between the two extraction methods, but one should not overlook the large statistical and systematic uncertainties and possible data inconsistencies. In particular, the MiniBooNE collaboration, performing a state-of-the-art neutrino scattering experiment, has reported values as high as $M_A \approx 1.35$ GeV!

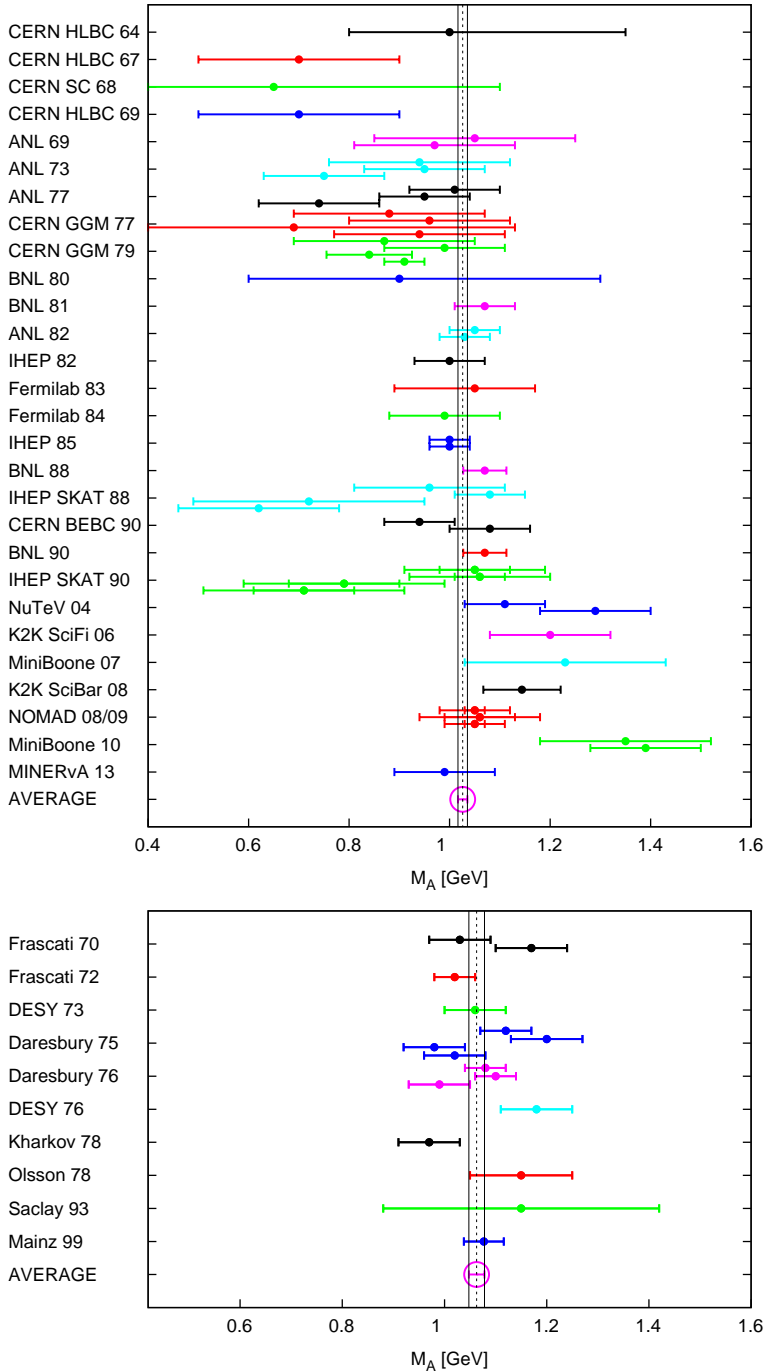


Fig. 1. Extractions of the axial mass parameter from neutrino experiments (top panel) and electron scattering experiments (bottom panel). The difference in their averages, $\langle M_A \rangle = (1.026 \pm 0.009)$ GeV and $\langle M_A \rangle = (1.062 \pm 0.015)$ GeV, respectively, may have their origin in the chiral correction (2) — but may also hint at a limitation of the dipole parameterization.

1.2 Proposed measurement of G_A by using inverse β decay

Clearly our knowledge of the axial form-factor would benefit from a third, independent and ideally cleaner, way to access G_A . The theoretically cleanest way to access G_A (but, as it turns out, experimentally very challenging) is through the weak interaction, as in neutrino experiments — but it can also be probed in weak electron scattering, i. e. in inverse β decay shown in Fig. 2:

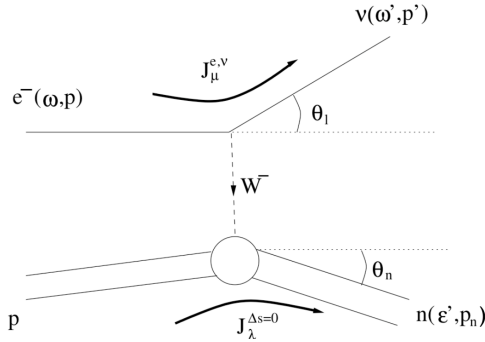


Fig. 2. Kinematics of inverse β decay used to access G_A in an electron scattering experiment, with detection of neutrons the final state.

The weak charged-current cross-section is given by

$$\frac{d\sigma}{d\omega'} = M \frac{G_F^2 \cos^2 \theta_c}{\pi} \frac{\omega'}{\omega} \left[\cos^2 \left(\frac{\theta_l}{2} \right) f_2 + \left(2f_1 + \frac{\omega + \omega'}{M} f_3 \right) \sin \left(\frac{\theta_l}{2} \right) \right],$$

where the structure functions f_1 , f_2 and f_3 are known functions of the electromagnetic form-factors and G_A . In contrast to pion electro-production experiments, the extraction of G_A from this purely weak process is model-independent, and with recent advances in polarized beams high precision is possible.

The main experimental challenges are: tiny cross sections (on the order of $\approx 10^{-40}$ cm²/sr), neutron detection with accurate kinematics; and (very) large electro-magnetic backgrounds. The strategies to deal with these challenges are presently being developed, but we will certainly wish to exploit the available high-intensity polarized electron beams at either JLab or MAMI, in conjunction with a long LH2 target; we would wish to remain at low beam energy (less than ≈ 120 MeV) in order to stay below the pion production threshold; and design a suitable backward kinematics to enhance the weak cross-section (forward neutrons). The beam must be polarized and pulsed so that the electro-magnetic background can be cleanly removed: the weak process has a 100% asymmetry while the electro-magnetic process has a vanishing asymmetry, and they can be separated on a pulse-by-pulse basis.

So far several facilities have been considered where this experiment could take place: MESA at Mainz, FEL at JLab, Hall D tagger at JLab, at the JLab injector, or at Cornell. Each has its particular instrumental constraints, its own pros and cons regarding beam conditions and available infrastructure. Regardless of

the peculiarities of the setup, we will need to remove the scattered electrons (Møller, nuclear scattering) by means of a sweeper magnet; reduce the prompt electro-magnetic radiation (γ -flash, electrons) by timing cuts; reduce the background from the target cell window by minimizing window thickness and using a backwards veto detector. We do possess preliminary background estimates, and a detailed Monte Carlo simulation is underway. Assuming 100% efficiency and no further backgrounds, the precision of the extracted G_A that we could achieve in about 2 months of running (order of magnitude estimate) is indicated in Fig. 3.

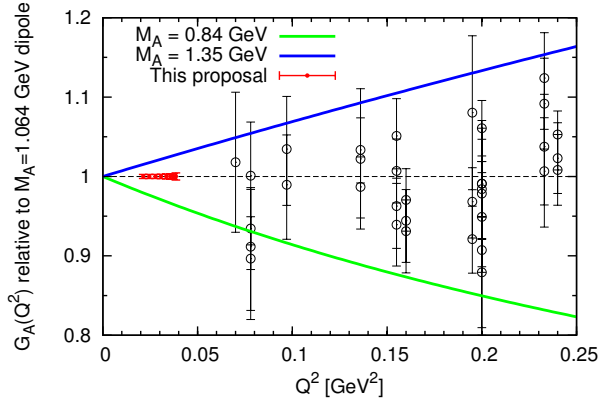


Fig. 3. The expected precision of the extracted G_A with ≈ 2 months runtime at a typical high-luminosity facility. The $M_A = 0.84$ GeV and $M_A = 1.35$ GeV curves correspond to the dipole parameterization (1) with the two rather extreme axial masses (one far below and one far above the world average). If nothing else, with the shown precision we should be able to reject or confirm the dipole form itself.

2 Ascertaining the high-energy behavior of the GDH integrand

The Gerasimov-Drell-Hearn (GDH) sum rule is a sum rule that relates the energy-weighted difference of the spin-dependent cross-section for photo-production off a given target to the spin (S) and anomalous magnetic moment (κ) of that target:

$$\int_{\nu_{\text{thr}}}^{\infty} (\sigma_{3/2} - \sigma_{1/2}) \frac{d\nu}{\nu} = \frac{4\alpha S \pi^2 \kappa^2}{M^2},$$

where α is the fine-structure constant. This is a generic QFT prediction valid for any type of target. In its derivation, one relies on causality, unitarity, Lorentz and gauge invariances. In addition, one assumes that in the forward Compton scattering amplitude,

$$\frac{1}{8\pi M} T(\nu, \theta = 0) = f(\nu) \boldsymbol{\varepsilon}'^* \cdot \boldsymbol{\varepsilon} + i g(\nu) \boldsymbol{\sigma} \cdot (\boldsymbol{\varepsilon}'^* \times \boldsymbol{\varepsilon}),$$

the spin-dependent amplitude $g(\nu)$ vanishes at large ν to derive the dispersion relation, and that $\text{Im} g(\nu)$ decreases fast enough with ν (faster than $\sim 1/\log \nu$) for

the integral to converge. Note that the integral of the unpolarized cross-section, $\int(\sigma_{3/2} + \sigma_{1/2}) dv$, *without* the $1/v$ weight, *does not* converge.

Looking at Fig. 4 which shows a prediction of the running GDH integral to very high energies one could claim that the sum rule is saturated already at $\nu \approx 3 \text{ GeV}$ but in fact no measurements exist above that energy: all existing experiments (at LEGS, MAMI and ELSA) were performed below it. The polarized cross-section at large ν is *unknown*, yet it is usually expected to be described by Regge theory: it considers isoscalar ($p + n$) and isovector ($p - n$) contributions to $\sigma_{3/2} - \sigma_{1/2}$ as coming from different meson families: $f_1(1285)$ and $\alpha_1(1260)$, respectively, resulting in the parameterization

$$\Delta\sigma^{(p\pm n)} = \sigma_{3/2} - \sigma_{1/2} = c_2 s^{\alpha_{f_1}-1} \pm c_1 s^{\alpha_{\alpha_1}-1},$$

where $s = 2M\nu + M^2$, α_{f_1} and α_{α_1} are the Regge intercepts of $f_1(1285)$ and $\alpha_1(1260)$ trajectories, respectively, and c_1 and c_2 are parameters.

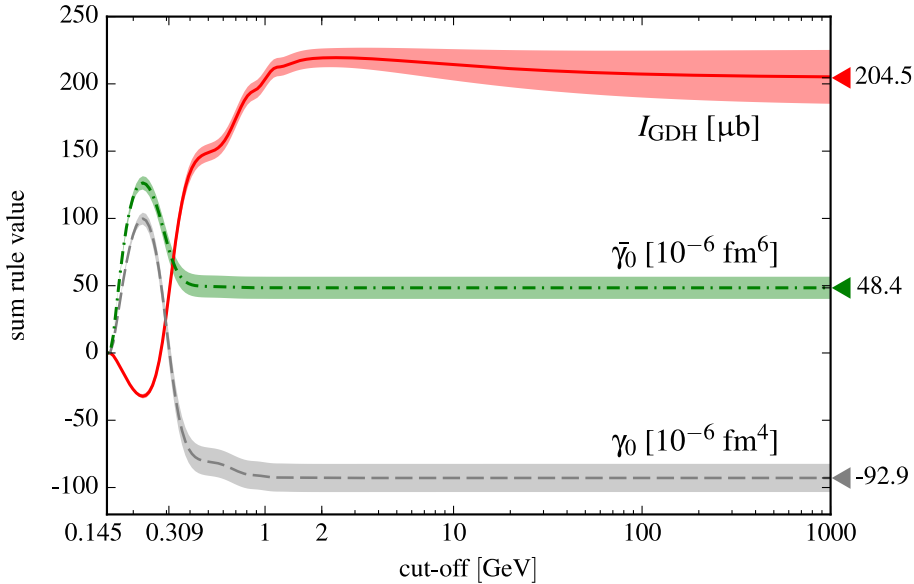


Fig. 4. The value of the GDH integral on the proton as a function of the upper integration bound. (Figure taken from [5].)

If the sum rule fails, its derivation implies that this would occur at high energies, and there are several conceivable violation mechanisms [6]. For instance, the appearance of a fixed $J = 1$ pole of the Compton amplitude in the complex angular-momentum plane or the existence of an anomalous charge-density commutator, i. e. $[J^0(x), J(y)]_{\text{e.t.}} \neq 0$ would both cause the sum rule to fail; other, more exotic possibilities have been proposed.

2.1 Experimental strategy

The main task of the experiment currently being devised is to measure the energy dependence of the GDH integrand at high energies for both proton and neutron (deuteron) to allow for isospin separation. Assuming

$$\sigma_{3/2} - \sigma_{1/2} = \alpha \nu^b$$

(for a given target), the primary goal is to get b , without a need to extract an accurate a . Initially, we would measure only the *yield difference*, $N_{3/2} - N_{1/2}$, and consider proper normalization (absolute cross-sections) later on. The ideal facility to run the proposed experiment would be Hall D at JLab with a circularly polarized tagged photon beam, longitudinally polarized target and large solid-angle ($\approx 4\pi$) detector: this setup would allow us to measure $\Delta\sigma(\nu)$ at high ν where no data exist, and to cover four times the existing ν range (3 GeV \rightarrow 12 GeV).

2.2 Impact of the proposed experiment

Intercept of the α_1 Regge trajectory

The high-energy behaviors of the isovector (non-singlet) and isoscalar (singlet) cross-section differences are driven by the $\alpha_1(1260)$ and $f_1(1285)$ Regge trajectories,

$$\Delta\sigma^{(p-n)} \sim s^{\alpha_{\alpha_1} - 1}, \quad \Delta\sigma^{(p+n)} \sim s^{\alpha_{f_1} - 1}.$$

From DIS data one typically extracts $\alpha_{\alpha_1} \approx 0.4$, $\alpha_{f_1} \approx -0.5$, while a recent fit [7] yields $\alpha_{\alpha_1} \approx 0.45$, $\alpha_{f_1} \approx -0.36$. A naive Regge expectation gives $\alpha_{\alpha_1} \approx -0.27$, $\alpha_{f_1} \approx -0.32$, so there appears to be a discrepancy in the α_1 intercept between the two extractions. Measuring $\Delta\sigma$ at high ν for both proton and neutron targets would help to remove this uncertainty.

Spin-dependent Compton amplitude

Figure 5 shows the real and imaginary parts of the spin-dependent Compton amplitude g . The imaginary part is measured directly in a GDH experiment as

$$\text{Im } g(\nu) = -\frac{\nu}{8\pi} \Delta\sigma(\nu).$$

The real part, however, is given by a dispersion relation,

$$\text{Re } g(\nu) = -\frac{\nu}{4\pi^2} \mathcal{P} \int_0^\infty \frac{\nu' \Delta\sigma(\nu')}{\nu'^2 - \nu^2} d\nu',$$

and is therefore very sensitive to the quality of the integrand.

If both $\text{Re } g(\nu)$ and $\text{Im } g(\nu)$ were known precisely enough (and given $f(\nu)$ which is well measured), the two complex amplitudes could be used to determine the forward-scattering ($\theta = 0$) quantities

$$\left. \frac{d\sigma}{d\Omega} \right|_{\theta=0} = |f|^2 + |g|^2, \quad \Sigma_{2z}|_{\theta=0} = -\frac{fg^* - f^*g}{|f|^2 + |g|^2}.$$

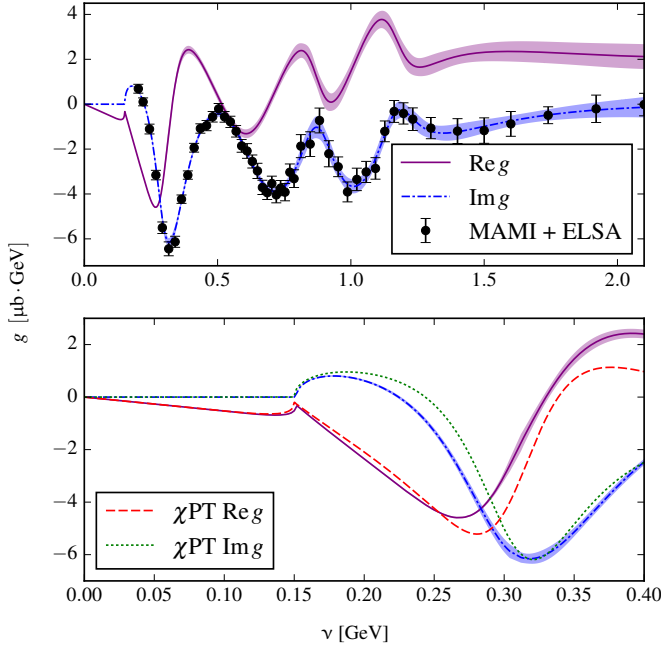


Fig. 5. The spin-dependent Compton amplitude $g(\nu)$. Top: real and imaginary parts, the latter fitted to GDH data, the former calculated via dispersion relations. Bottom: χ PT calculation. Figure from [5].

The asymmetry for circularly polarized photons and nucleons polarized along the z axis,

$$\Sigma_{2z} = \frac{d\sigma_{3/2} - d\sigma_{1/2}}{d\sigma_{3/2} + d\sigma_{1/2}},$$

as well as its counterpart Σ_{2x} (with transverse polarization of the nucleons), can provide information on all four spin polarizabilities appearing in Compton scattering. In addition, Σ_{2z} (in particular its behavior near $\theta = 0$) is very sensitive to chiral loops. Moreover, the uncertainty of the product of the unpolarized XS and Σ_{2z} for $\theta = 0$ increases rapidly for $\nu > 2$ GeV, hence a precise measurement of $\Delta\sigma(\nu)$ in the ν range up to about 10 or 12 GeV could significantly reduce the uncertainty on Σ_{2z} .

Polarizability correction to hyperfine splitting in muonic hydrogen

The third impact of the proposed measurement is related to the “proton radius puzzle”, specifically to the effect of proton structure on the hyperfine splitting of the nS levels in muonic hydrogen,

$$E_{\text{HFS}}(nS) = [1 + \Delta_{\text{QED}} + \Delta_{\text{weak}} + \Delta_{\text{structure}}] E_{\text{Fermi}}(nS).$$

The proton-structure correction can be split into three terms: the Zemach radius, the recoil contribution, and the polarizability contribution,

$$\Delta_{\text{structure}} = \Delta_Z + \Delta_{\text{recoil}} + \Delta_{\text{pol}}.$$

At present, the relative uncertainties of the three terms are 140 ppm, 0.8 ppm and 86 ppm, respectively, which need to be put into the perspective of the forthcoming PSI measurement of the hyperfine splitting whose precision is expected to be as low as 1 ppm. Our proposed measurement can contribute to the uncertainty reduction in the third correction term. It can be written as

$$\Delta_{\text{pol}} = \frac{Z\alpha m}{2\pi(1+\kappa)M} [\delta_1 + \delta_2],$$

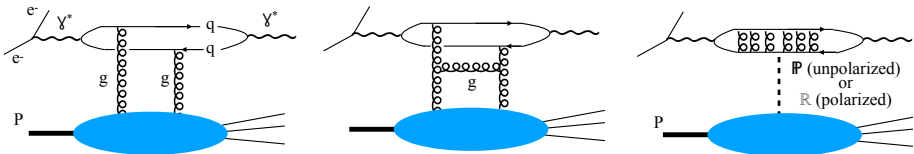
where m is the electron mass. Here δ_1 involves an integral of the polarized distribution function $g_1(x, Q^2)$ over both x and Q , while δ_2 involves a similar integration of $g_2(x, Q^2)$: see [8] for explicit formulas. Since g_1 at low Q is essentially the GDH integrand,

$$\sigma_{1/2} - \sigma_{3/2} = \frac{4\pi\alpha^2}{m\mathcal{F}} \left(g_1 - \frac{Q^2}{\nu^2} g_2 \right),$$

a precise measurement of $\Delta\sigma$ would constrain δ_1 . To calculate δ_1 , one indeed needs the Q^2 dependence of g_1 , but *the integrand is weighted by $1/Q^3$* , thus knowing the value at $Q^2 = 0$ would stabilize the integration. This is badly needed, as the above mentioned 86 ppm uncertainty needs to be brought down to the 1 ppm level, and this implies that our knowledge of g_1 needs to be improved by two orders of magnitude!

Transition from polarized DIS to diffractive regime

The proposed experiment would also have the capability to explore the transition between DIS and low- x regime of diffractive scattering. This regime has been investigated e. g. at HERA, but only in the unpolarized case. Such processes are traditionally described in terms of a diquark picture: a hard γ^* hadronizes into a $\bar{q}q$ pair of coherence length $1/(xM)$, with high Q^2 dominated by gluon exchange and low Q^2 dominated by Pomeron/Reggeon exchange as shown in the Figure:



The spin-0 Pomeron couples to the proton components irrespectively of their helicity, i. e. controls unpolarized diffractive scattering, while double-polarized $\vec{e}\vec{p}$ scattering filters out Pomeron exchange to reveal the non-singlet Reggeon exchange. This is relevant for the physics of the envisioned Electron-Ion-Collider (EIC), and a measurement of $\Delta\sigma$ would provide a $Q^2 = 0$ baseline for the study of the transition from hard partonic picture to soft Reggeon exchange picture.

2.3 The physics goals in brief

The primary physics goal is to determine the α_{f_1} and α_{a_1} intercepts (in case $N_{3/2} - N_{1/2}$ follows Regge) and thus validate the convergence of the GDH integral. We intend for instance, acquire the data precise enough to result in uncertainties $\Delta\alpha_{a_1} = \pm 0.008$, $\Delta\alpha_{f_1} = \pm 0.016$ as compared to $\Delta\alpha_{a_1} = \pm 0.23$,

$\Delta\alpha_{f_1} = \pm 0.22$ from ELSA: see Fig. 6. The secondary physics goal is to improve the current experimental accuracy of the GDH integral by $\approx 25\%$ (with reasonable assumptions on ΔP_e , ΔP_t , and absolute normalization). Finally, regardless of the convergence and sum rule validity, we would be able to explore the region of diffractive QCD relevant to EIC physics.

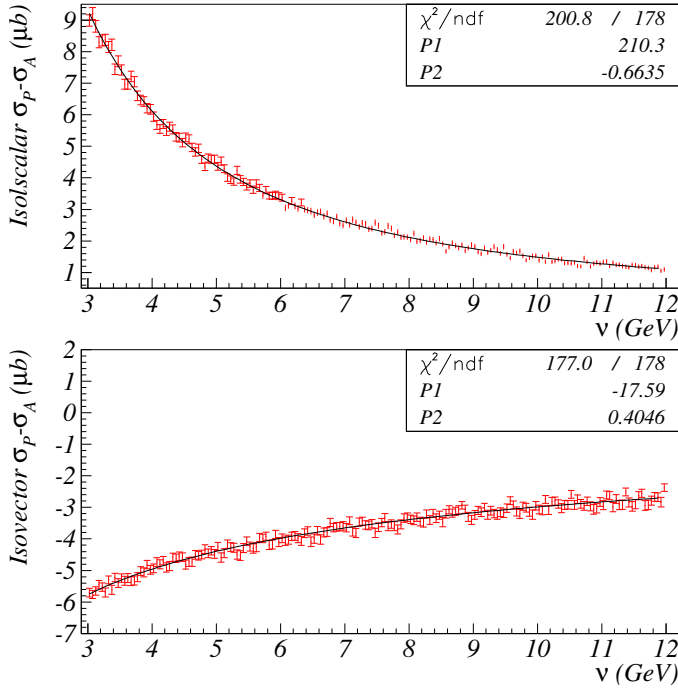


Fig. 6. The expected precision of the isoscalar (top panel) and isovector (bottom panel) polarized cross-section differences (plotted on a Regge curve).

References

1. J. E. Amaro, R. Ruiz Arriola, Phys. Rev. D **93**, 053002 (2016).
2. J. A. Formaggio, G. P. Zeller, Rev. Mod. Phys. **84**, 1307 (2012).
3. A. Liesenfeld et al. (A1 Collaboration), Phys. Lett. B **468**, 20 (1999).
4. V. Bernard, N. Kaiser, U.-G. Meißner, Phys. Rev. Lett. **69**, 1877 (1992); see also comment in Phys. Rev. Lett. **72**, 2810 (1994).
5. O. Gryniuk, F. Hagelstein, V. Pascalutsa, Phys. Rev. C **94**, 034043 (2016).
6. R. Pantförder, *Investigations on the Foundation and Possible Modifications of the Gerasimov-Drell-Hearn Sum Rule*, arXiv:hep-ph/9805434.
7. M. Vanderhaeghen, private communication.
8. F. Hagelstein, R. Miskimen, V. Pascalutsa, Prog. Part. Nucl. Phys. **88** (2016) 29.

Povzetki v slovenščini

Elektromagnetna sklopitev pentakvarkov

Roelof Bijker in Emmanuel Ortiz-Pacheco

Instituto de Ciencias Nucleares, Universidad Nacional Autónoma de México, A.P. 70-543, 04510 Ciudad de México, México

V tem prispevku razpravljava o elektromagnetni sklopitvi pentakvarkovskih stanj, ki imajo skrito kvantno število *čar*. To delo so vzpodbudili nedavni eksperimenti v Evropskem centru CERN (kolaboracija LHCb) in tekoči eksperimenti v laboratoriju JLab (ZDA) z namenom, da s fotoprodukcijo potrdijo obstoj čarobno nevtralnih pentakvarkovskih stanj.

Resonance in deformacije konture

Gernot Eichmann

CFTP, Instituto Superior Técnico, Universidade de Lisboa, 1049-001 Lisboa, Portugal

Dajemo zgled, kako iz vrednotiti lastnosti resonanc iz integralnih enačb z Lorenzovo invarianco. V ta namen rešimo Bethe-Salpetrovo enačbo in in sipalne enačbe za skalarni model in določimo lege resonančnih polov ter fazne premike. Izkaže se, da skalarni model ne da resonančnih polov v kompleksni ravnini, temveč da virtualna stanja na realni osi druge Riemannove ploskve.

Mešanje okusov, nevtrinske oscilacije in mase nevtrinov

Harald Fritzsch

Department für Physik, Universität München, Theresienstraße 37, D-80333 München, Germany

Predstavim masne matrike z vzorcem s štirimi ničlami za kvarke in leptone. Trije koti pri mešanju okusov za kvarke so funkcije kvarkovih mas in se dajo izračunati. Rezultati se skladajo z eksperimentalnimi podatki. Za leptone uporabim masne matrike z vzorcem z ničlami ter mehanizem "guncnice", da izračunam matrične elemente leptonske mešalne matrike kot funkcije leptonskih mas. Izračunane vrednosti nevtrinskih mas so $m_1 \approx 1.4$ meV, $m_2 \approx 9$ meV, $m_3 \approx 51$ meV. Razpravljam o breznevtrinskem dvojnem razpadu beta. Efektivna Majoranova masa nevtrinov, ki opisuje dvojni razpad beta, se da izračunati - znaša okrog 5 meV. Sedanja eksperimentalna zgornja meja je 140 meV.

Pentakvarki kot molekule s skritim čarom: nekaj odprtih vprašanj

Marek Karliner

School of Physics and Astronomy, Tel Aviv University, Tel Aviv 69978, Israel

Pri detektorju LHCb (CERN, Ženeva) so nedavno poročali o treh ozkih stanjih pri razpadih bariona $\Lambda_b^0 \rightarrow J/\psi pK^-$, in sicer $P_c(4312)$, $P_c(4440)$ in $P_c(4457)$, ki razpadajo v $J/\psi p$. Torej imajo minimalno vsebino kvarkov cčuud. Dve stanji sta za malenkost pod pragom za $\Sigma_c \bar{D}^*$ in eno stanje je za malenkost pod pragom za $\Sigma_c \bar{D}$. To močno namiguje na hadronske molekule in neposredno odpira nekaj mamljivih vprašanj, ki iz tega sledijo.

Poenoteni pristop k zgradbi lahkih in težkih barionov

Hyun-Chul Kim

Department of Physics, Inha University, Incheon 22212, Republic of Korea,
School of Physics, Korea Institute for Advanced Study (KIAS), Seoul 02455,
Republic of Korea

V tem prispevku podajam pregled nedavnih del o zgradbi lahkih in težkih barionov, osnovanih na kiralnem solitonskem modelu s kvarki. Pregled je namenjen kot kratek vodnik po modelu. Podrobnosti so na voljo v navedeni literaturi.

Izboljšana pionska povprečna polja

June-Young Kim^a, Hyun-Chul Kim^{a,b}

^a Department of Physics, Inha University, Incheon 22212, Republic of Korea

^b School of Physics, Korea Institute for Advanced Study (KIAS), Seoul 02455,
Republic of Korea

V tem prispevku podajava rezultate z izboljšanimi pionskimi povprečnimi polji v okviru kiralnega solitonskega modela s kvarki. Raziskujeva učinke zmanjšanja števila valenčnih kvarkov od N_c do $N_c - 1$ in $N_c - 2$ na pionska povprečna polja in razpravljava o njihovih fizičnih implikacijah.

Odvisnost lastnosti mezona $\rho(770)$ od mas lahkih in čudnih kvarkov

R. Molina^a, J. Ruiz de Elvira^b

^a Departamento de Física Teórica II, Plaza Ciencias, 1, 28040 Madrid, Spain and Institute of Physics of the University of São Paulo, Rua do Matão, 1371 -Butantã, São Paulo -SP, 05508-090

^b Albert Einstein Center for Fundamental Physics, Institute for Theoretical Physics, University of Bern, Sidlerstrasse 5, 3012 Bern, Switzerland

Upoštevamo analizo nedavnih faznih premikov pri trku $\pi\pi$ ($I=J=1$) ter podatke z računov na mreži za razpadno konstanto psevdoskalarnih mezonov na dveh različnih trajektorijah, pri katerih je fiksirana bodisi vsota mas kvarkov u, d in s , bodisi masa kvarka s . Iz tega izpeljemo odvisnost parametrov mezona ρ od mas lahkih in čudnega kvarka in napovemo parametre na kiralnih trajektorijah, ki privzemajo lažje mase, kot je fizična masa čudnega kvarka. Ugotovimo, da lahko postane masa mezona ρ lahka vse do 700 MeV, če vzamemo maso čudnega kvarka nič in fizične mase pionov. Pri tem je razmerje sklopitev pri kanalih $\pi\pi$ in $K\bar{K}$ enako $\sqrt{2}$ na SU(3) simetrični kiralni trajektoriji.

Elektromagnetni oblikovni faktorji nukleona, bariona Δ in hiperonov

Willibald Plessas

Theoretical Physics, Institute of Physics, University of Graz, A-8010 Graz, Austria

Obravnavamo elektromagnetno zgradbo barionov v okviru poenotene relativističnega modela iz konstituentnih kvarkov. Potem ko ponovimo kovariantne elastične oblikovne faktorje nukleonov vključno z njihovo sestavo glede okusov, nadaljujemo po isti poti proti oblikovnim faktorjem barionov Δ, Λ, Σ in Ω . Izpostavimo značilne lastnosti elastičnih elektromagnetnih faktorjev barionov, ki pripadajo bodisi oktetnim, bodisi dekupletnim multipletom glede okusa.

Eksotična stanja iz težkih kvarkov

Jonathan L. Rosner

Enrico Fermi Institute, University of Chicago, 5640 Ellis Avenue, Chicago, IL 60637

Težki kvarki c in b stabilizirajo eksotične mezone ($qq\bar{q}\bar{q}$) in barione ($qqqq\bar{q}$). Predstavim delo z M. Karlinerjem o molekulah, ki vsebujejo ($c\bar{c}$) in ($b\bar{b}$); prvi dvojno čarobni barion; izospinske razcepe; mase barionov $\Xi_{cc}^+ = ccd$ in $\Omega_{cc} = ccs$; življenske čase; tetrakvarke, ki so stabilni glede na močni in elektromagnetni razpad; vzbujena stanja Ω_c ; in vzbuditvene energije v valu P.

Vpliv vmesnih resonanc na sklopitev kvarkov s fotonom

Hèlios Sanchis-Alepuz

University of Graz, A-8010 Graz, Austria

Predstavimo glavne rezultate našega članka z leta 2019, v katerem proučujemo učinke vmesnih hadronskih resonanc v interakcijskem jedru kvarka z antikvarkom na vozlišče kvarka s fotonom. To je prvi korak na dolgi poti do vključitve nevalenčnih prispevkov v Bethe-Salpetrovem pristopu k hadronskim lastnostim.

Analiza delnih valov pri podatkih o fotoprodukciji pionov z zahtevo po analitičnosti pri fiksni spremenljivki t

J. Stahov^{a,b}, H. Osmanović^a, M. Hadžimehmedović^a, R. Omerović^a

^a University of Tuzla, Faculty of Natural Sciences and Mathematics, Univerzitetska 4, 75000 Tuzla, Bosna in Hercegovina

^b European University *Kallos* Tuzla, Maršala Tita 2A - 2B, Tuzla, Bosna in Hercegovina

Predstavimo rezultate analitično omejene analize delnih valov pri fotoprodukcijskih podatkih za mezon π^0 . Vhodne podatke smo dobili iz reakcij $p(\gamma, \pi^0)p$ in $n(\gamma, \pi^0)n$ od praga vse do energije $W = 1.95$ GeV.

Zgradba in prehodi vzbujenih stanj nukleona pri kromodinamiki na mreži

Finn M. Stokes^{a,b}, Waseem Kamleh^a in Derek B. Leinweber^a

^a Special Research Centre for the Subatomic Structure of Matter, Department of Physics, University of Adelaide, South Australia 5005, Australia

^b Jülich Supercomputing Centre, Institute for Advanced Simulation, Forschungszentrum Jülich, Jülich D-52425, Germany

Nedavno vpeljana variacijska analiza z razvojem po parnosti (PEVA) omogoča ločevanje barionskih lastnih stanj na mreži pri končni gibalni količini brez primesi z nasprotno parnostjo. Pokažemo, da ta metoda vpelje statistično pomembne popravke pri izvednotenju elektromagnetnih oblikovnih faktorjev nukleona v osnovnem stanju. Omogoča tudi prvo izvednotenje elastičnih in prehodnih oblikovnih faktorjev vzbujenih stanj nukleona na mreži. Predstavimo elektromagnetne elastične oblikovne faktorje in vijačnostne amplitude dveh vzbujenih stanj nukleona z negativno parnostjo. Te rezultati nudijo nazoren vpogled v zgradbo teh stanj in omogočajo povezavo s stanji iz kvarkovega modela v tem energijskem območju.

Eksotični barioni v modelih Skyrmovega tipa

Herbert Weigel

Institute for Theoretical Physics, Physics Department, Stellenbosch University,
Matieland 7602, South Africa

Kiralni solitonski modeli Skyrmovega tipa predvidevajo nizko ležeče eksotične barione s kvantnimi števili, ki se ne dajo sestaviti s trem kvarki. V tem prispevku razpravljam o lastnostih njihovih partnerjev z drugačnim okusom v nukleonskem kanalu.

Novice z eksperimenta Belle: hadronska spektroskopija

Marko Bračko

Univerza v Mariboru, Smetanova ulica 17, 2000 Maribor
in Institut Jožef Stefan, Jamova cesta 39, 1000 Ljubljana

V tem prispevku so predstavljeni izbrani novejši rezultati spektroskopije hadronov pri eksperimentu Belle. Meritve so bile opravljene na vzorcu izmerjenih podatkov, ki ga je v času svojega delovanja – med letoma 1999 in 2010 – zbral eksperiment Belle, postavljen ob trkalniku elektronov in pozitronov KEKB, ki je obratoval v laboratoriju KEK v Cukubi na Japonskem. Zaradi velikosti vzorca in kakovosti izmerjenih podatkov lahko raziskovalna skupina Belle še sedaj, ko je od zaključka delovanja eksperimenta minilo že skoraj desetletje, objavlja rezultate novih meritev. Izbor opisanih meritev in njihovih rezultatov odraža interese udeležencev delavnice, kjer so bili rezultati predstavljeni.

Enigmatična resonanca $\Delta(1600)$

Bojan Golli

Pedagoška fakulteta, Univerza v Ljubljani in Institut Jožef Stefan, 1000 Ljubljana, Slovenija

Soočimo opisa dveh vzbujenih stanj nukleona, ki imata v kvarkovskem modelu enako strukturo: Roperjevo resonanco $N(1440)$ v parcialnem valu P11 in resonanco $\Delta(1600)$ v parcialnem valu P33. Medtem ko pri prvi resonanci igra pomembno vlogo kvazivezано stanje mezona sigma in nukleona, pa pri drugi resonanci dominira kvazivezано stanje piona in resonančnega stanja $\Delta(1232)$.

Fenomenološka spodnja meja za maso bariona Ξ_{cc}^{++}

Mitja Rosina

Fakulteta za matematiko in fiziko, Univerza v Ljubljani,
Jadranska 19, P.O.Box 2964, 1001 Ljubljana, Slovenija
in Institut Jožef Stefan, 1000 Ljubljana, Slovenija

Predstavim preprosto interpolacijo med mezonskimi vezavnimi energijami, ki lahko da dobro semikvantitativno vezavno energijo za dikvark cc in potem še za barion Ξ_{cc}^+ . Masa bariona Ξ_{cc}^+ je zelo malo občutljiva na zelo različne izbire mas konstituentnih kvarkov.

Meritev G_A in vsotnega pravila GDH pri visokih energijah v centru Jefferson Lab: dva predloga

Simon Širca

Fakulteta za matematiko in fiziko, Univerza v Ljubljani,
Jadranska 19, P.O.Box 2964, 1001 Ljubljana, Slovenija
in Institut Jožef Stefan, 1000 Ljubljana, Slovenija

Predstavljena sta bila dva eksperimentalna predloga (proposals) za meritvi z elektronskim sipanjem, kjer bi bil center TJNAF (Jefferson Lab) bržkone najprimernejši za njuno izvedbo: modelsko čisto meritev nukleonskega aksialnega oblikovnega faktorja, G_A , in meritev visokoenergijskega prispevka k Gerasimov-Drell-Hearnovemu (GDH) vsotnemu pravilu. V obeh primerih je ključno odstranjevanje elektromagnetnega ozadja, zato poleg optimizacije eksperimentalne postavitve (zlasti polarizirane tarče) že potekajo podrobne simulacije Monte-Carlo.

BLEJSKE DELAVNICE IZ FIZIKE, LETNIK 20, ŠT. 1, ISSN 1580-4992

BLED WORKSHOPS IN PHYSICS, VOL. 20, NO. 1

Zbornik delavnice 'Elektrošibki procesi pri hadronih',
Bled, 15. – 19. julij 2019

Proceedings of the Mini-Workshop 'Electroweak Processes of Hadrons',
Bled, July 15 – 19, 2019

Uredili in oblikovali Bojan Golli, Mitja Rosina, Simon Širca

Članki so recenzirani. Recenzijo je opravil uredniški odbor.

The articles are peer reviewed by the Editorial Board

Izid publikacije je finančno podprla Javna agencija za raziskovalno dejavnost RS iz sredstev državnega proračuna iz naslova razpisa za sofinanciranje domačih znanstvenih periodičnih publikacij.

Tehnični urednik Matjaž Zaveršnik

Založilo: DMFA – založništvo, Jadranska 19, 1000 Ljubljana, Slovenija

Natisnila tiskarna Itagraf v nakladi 70 izvodov

Publikacija DMFA številka 2104

Brezplačni izvod za udeležence delavnice
